ABSTRACT

CONVERSION-ELECTRON AND γ-RAY EXPERIMENTS WITH THE DECAY OF BROMINE-82 AND STRONTIUM-83

By Robert C. Etherton

The energy levels of ^{82}Kr populated by the beta decay of ^{82}Br have been studied. The internal conversion electron spectra were recorded with permanent magnet electron spectrometers and the singles and coincidence spectra were recorded using both NaI(Tl) and Ge(Li) detectors. A total of 21 transitions have been identified. Excited states in ^{82}Kr have been placed at 772, 1475, 1821, 2094, 2429, 2560, 2648, 2652, and 2832 keV. Angular correlation measurements for eight of the prominent gamma-gamma cascades were made and the results used to make unique spin assignments for the 777, 1475, 1821, 2094, and 2648 keV states. Transitions from the 2832, 2652, and 2560 keV states and log ft values were used to place limits on the possible spin assignments for these states. The level structure of ^{82}Kr was used to test some of the predictions of the Davydov-Filippov asymmetric rotor model.

Similar experiments as those described for the investigation of ^{82}Br were performed with the decay of ^{83}Sr. An M2 isomeric transition was identified at 42.3 keV. Some sixty transitions were identified enabling the placement of excited states at 5.0, 42.3, 295.2, 389.2, 423.5, 736.8, 804.8, 994.2,

1043.7, 1053.7, 1103.0, 1202.0, 1242.6, 1273.1, 1324.6, 1653.1, 1756.9, 1783.5, 1916.7, 1952.2, 2014.8, 2090.0, 2147.8, 2179.3 keV. Limits on the spins and parities of these states were placed on the basis of gamma ray branching and log ft values.

An attempt was made to correlate the level structure of ^{83}Rb to that of ^{82}Kr with the core-coupling model. No simple relationship was found.

CONVERSION-ELECTRON AND γ-RAY EXPERIMENTS WITH THE DECAY OF BROMINE-82 AND STRONTIUM-83

By

Robert C. Etherton

A THESIS

Submitted to
Michigan State University
in partial fulfillment of the requirements
for the degree of

DOCTOR OF PHILOSOPHY

Department of Physics

1967

ACKNOWLEDGMENTS

I wish to thank Dr. W. H. Kelly for the suggestion of this thesis project. His guidance and helpful discussions during the various phases of this investigation are deeply appreciated.

Dr. R. L. Auble, Dr. L. M. Beyer, Dr. G. Berzins, Mr. A. Bisson, and Mr. D. Beery were of great assistance with the acquistion of the data.

I am grateful to Dr. M. L. Wiedenbeck and Dr. R. Woods for making available the University of Michigan permanent magnet electron spectrometers for the investigation of the conversion-electron spectra of ^{82}Br.

Dr. G. Berzins and Dr. L. Kull were of assistance in the analysis of the data with the computer.

Dr. D. Horan contributed many valuable discussions.

Mr. N. Mercer and his staff were of assistance in the fabrication of some of the apparatus used in this investigation.

I appreciate the financial support contributed by Michigan State University and the National Science Foundation.

Finally, I wish to thank my wife Jean and my children Michael, Kathy and Cindy for their encouragement and patience and for the sacrifice of many vacations during the long course of this study.

TABLE OF CONTENTS

Chapter

Page

LIST OF TABLES

LIST OF FIGURES

Figure

INTRODUCTION

A vast amount of experimental data have been collected over the years in studies of the radioactive decay of unstable isotopes by means ob beta and gamma ray spectroscopy to provide information on the properties of a large number of nuclei (1). Even so, large gaps in the data still exist which hinder the nuclear theorist in the construction of, and the testing of, consistent nuclear models. This is partly the result of the fact that only a few of the available states are populated in beta and gamma decay because of the energy available and the selection rules governing the decays (2). However, in a number of cases, nuclear reaction experiments have complemented these results, often giving information on the high energy excited states not available to beta decay. But more important, much of the data have been incomplete or erroneously interpreted because the limited instrumentation available to the experimentalist did not provide the required energy resolution. This is particularly the case for spherical nuclei (i.e., nuclei with small quadrupole moments) in the medium mass region ($70 \leq A \leq 150$) where the level structure has proved to be quite complex and energy spacings very small (1).

In the deformed nucleus region of $150 \leq A \leq 190$ and $A > 220$, it has been possible to formulate a nuclear model which has had spectacular success (3) in predicting the level schemes for these nuclei. More accurate experimental data have been available here, chiefly because the highly converted nature of the transitions has enabled their energy measurement with precision electron spectrometers. Moreover, because of the success of the model, it has been used as a guide in the construction of new decay schemes for nuclei in this region.

For most of the isotopes, in the medium mass region, the decay schemes are unknown beyond the first one or two excited states. This is especially true for those nuclei whose half-lives were $\lesssim$ 1 day. Partly because of this, very few model calculations have been performed for nuclei in this region. Fortunately, the recent development of the Ge(Li) detector and improved multi-channel analyzers have wrought a great change in the situation for the beta and gamma ray spectroscopist. Data can be recorded relatively rapidly with energy resolutions that are nearly an order of magnitude better than those previously attainable. In addition, more particle accelerators capable of accelerating a larger variety of particles to higher energies are becoming available. Hence, more complete and more accurate systematic experimental studies can now be made.

Davydov and Filippov have proposed an asymmetric rotor model of the nucleus to predict the level spacings and transition probabilities of the excited states in certain even-even nuclei (4). They have tested their predictions with those medium and heavy mass nuclei for which experimental data were available (4). In the regions of deformed nuclei $150 \leq A \leq 190$, and $A \geq 222$, their calculations were found to be in good agreement with the experimental data (4). In addition, good agreement with experimental data was obtained for some nuclei in the region $70 \leq A \leq 130$, a region where nuclei are normally considered to be spherical.

Marshalek, Person, and Sheline have shown theoretically that this region has islands of deformed nuclei (5). The regions are $74 \leq A \leq 80$ (isotopes of arsenic and selenium) and $120 \leq A \leq 134$ (isotopes of barium, cerium, and neodymium). In addition, they suggest that the isotopes having $82 \leq A \leq 88$ and $100 \leq A \leq 112$ are approaching regions of deformation.

In these mass regions, Davydov and Chaban have shown (6) that the asymmetric rotor model predictions of energy and gamma transition probabilities are in good agreement with experimental data for ^{76}Se, ^{100}Ru, ^{106}Pd, ^{110}Cd, ^{122}Te, ^{126}Te, and ^{128}Xe. It is possible then that the D-F model may apply to other nuclei near these mass regions. In this study, ^{82}Kr, which is near one of the regions of possible permanent deformation suggested by Marshalek *et al.* (5)

was chosen to test the D-F model. The excited states of this nucleus are strongly populated in the decay of ^{82}Br.

Of further interest in this study is the examination of the relationship between the level structures of the nuclei ^{82}Kr and ^{83}Rb, which differ by one proton. A simple relationship should exist if the excited states arise from the coupling of the single proton states to states of excitation of the even-even ^{82}Kr core. The excited states in ^{83}Rb are populated by the positron and electron capture decay of ^{83}Sr.

In addition, Talmi and Unna have made shell model calculations (7) to predict the energy levels and spins of the first few excited states of several Z = 38 or N = 50 isotopes, including ^{83}Sr. Since the experimental results of the level structure of ^{83}Rb should imply, at least, the ground state spin of ^{83}Sr, it should be possible to partially test the calculations of Talmi and Unna for ^{83}Sr.

The transitions from the decay of these two isotopes have been studied with high resolution beta and gamma ray spectrometers which are described briefly in Chapter 2. The decay schemes constructed from these data are discussed in Chapters 3 and 4.

Since comparisons of these decay schemes are made with the predictions of the asymmetric rotor model of Davydov and Filippov (4) and the shell model calculations

of Talmi and Unna (7), qualitative discussions of these models and, for completeness, of the collective model (8) are presented in Chapter 1. Also, the core-coupling model is included as a guide in the comparison of the ^{82}Kr and ^{83}Rb level structures.

CHAPTER I

NUCLEAR MODELS

One of the primary goals in physics is to be able to correlate theoretical formalisms with experimental data. In the case of nuclear physics, the inadequate knowledge of the nuclear force has rendered this a formidable task. Nevertheless, a number of the properties of nuclei, such as binding energy, level structures, magnetic moments and quadrupole moments have been explained, at least qualitatively, by some semi-phenomenological models (2). Those models that are most pertinent to the present study will be discussed very briefly here.

1.1. The Shell Model

Stimulated by the appearance of the so-called "magic nucleon numbers" (Z or N equal to 20, 8, 20, 28, (40), 50, 82, and 126) where large discontinuities in nuclear binding energy occurred, M. Goeppert-Mayer (9) and Haxel, Jensen, and Suess (10) independently constructed a nuclear model analogous to the atomic electron shell structure. In this model, each nucleon is assumed to be moving independently in an average potential due to all of the remaining nucleons. This potential was picked to be intermediate between that of an isotropic harmonis oscillator and a square well. In order

to generate the nuclear orbital energy spacings to give shell closure at the "magic numbers" a strong spin-orbit coupling term had to be added to the Hamiltonian. This had the effect of splitting each harmonic oscillator level into two $j = \ell + 1/2$ and $j = \ell - 1/2$ levels which are $(2j + 1)$- fold degenerate. It was found empirically that the $j = \ell + 1/2$ levels lie lower in energy than the $j = \ell - 1/2$. This then leads to the required energy level spacings consistent with the "magic numbers." The filling of the levels inside the shell must be in accord with the Pauli principle for protons and neutrons independently.

In the ground states, the nucleons are paired so that the nuclear properties are determined by the last unpaired nucleon. This has been found to be the case for odd mass nuclei having one nucleon just outside a closed shell. The model has failed to predict correctly the spins, magnetic moments, and quadrupole moments for nuclei that have several nucleons (holes) outside a closed shell, i.e., those nuclei with only partially filled shells. This is caused, in part, by the fact that the model cannot predict the order of the level filling inside a closed shell because the strengths of the spin-orbit coupling and residual interactions cannot be determined accurately. However, Mayer and Jensen have extended the application of the model to include j-j coupling with some very simple coupling rules (11). These rules require that: even-even

nuclei have zero spin and positive parity; in odd mass nuclei, the ground state spin and parity are determined by the odd numbered nucleons only; and these odd numbered nucleons usually will couple their spins in such a way that the total spin, J, of the nucleus is that of the last partially filled orbit j.

It was found that most of the nuclei followed these rules with a few exceptions in odd A nuclei where spins of $J = j - 1$ have been observed. Exceptions have been reported (1) for ^{77}Ge, ^{79}Si, and ^{81}Kr, all of which have 45 neutrons. It will be shown later that ^{83}Sr, one of the nuclei studied in this thesis, is another exception to the rule. ^{83}Sr also has 45 neutrons.

1.2. Residual Interactions

The fact that Mayer and Jensen had to supplement their independent particle model with coupling rules to determine the ground state angular momentum for a given nucleus indicates that nucleon interactions cannot be completely specified by a potential well and spin-orbit coupling. The energy degeneracy of the nucleons with the same (nlj) quantum numbers can be partially removed by extending the independent particle model to include short range nucleon-nucleon residual interactions. When this interaction is included, the Hamiltonian becomes

$$H = H_o + a \sum_i \bar{l}_i \cdot \bar{s}_i + \sum_{i>k} V_{ik}$$

where V_{ik} is the residual interaction potential. All the single particle configurations determined from the first two terms in the Hamiltonian are couplied to give a set of all the possible resultant angular momenta. The set of wave functions so generated are, in general, too many to allow an easy calculation to diagonalize the total Hamiltonian. In lieu of this, the residual interaction has been determined empirically for low mass nuclei.

The model has had some success in explaining the features of the level structure of some light and medium mass nuclei. For example, Kurath, using an interaction potential determined from ^{6}Li, has shown (12) that the model is in good agreement with experiment for ^{10}B. Also, Sweet, Bhatt, and Ball have made calculations (13) for ^{92}Nb using a residual interaction determined from ^{92}Zr and ^{93}Nb which are in excellent agreement with the experimental data. However Elliot and Flowers, in extending the model to ^{19}F have shown (14) that the E2 lifetime of the 5/2+ state calculated from the model is longer than that measured experimentally by a factor of 4.

1.3. The "Talmi-Unna Model"

The residual interaction calculations have been extended to other heavier nuclei which have a few nucleons outside a closed shell. One such treatment has been performed by Talmi and Unna (7) for nuclei having $N = 50$ or $Z = 38$. Since one aim of this work is to test

some of their calculations, a summary of their treatment of the shell model with residual interaction is presented here.

In their analysis, a nuclear potential due only to two-body effective interactions between nucleons is assumed. The unknown matrix elements, including those from configuration interaction, which were taken to be the same for all nuclei in the same subshell being filled, were determined from experimental data.

Nine experimental energy differences which were used were obtained from ^{89}Y, ^{87}Sr, ^{86}Sn, ^{85}Sr, ^{91}Nb, ^{93}Te, and ^{90}Zr to give nine equations involving six parameters to be fit. These parameters were:

$$\beta = E_{p_{1/2}} - E_{g_{9/2}}$$

the difference between the single-proton energies in the $p_{1/2}$ and $g_{9/2}$ orbits,

$$\beta' = E_{\left(g_{9/2}\right)^{-1}} - E_{\left(p_{1/2}\right)^{-1}}$$

which are the single neutron hole energy differences in the $p_{1/2}$ and $g_{9/2}$ orbits. The other parameters arise from the effective two body mutual interaction and are taken to be the same for the proton configurations and the neutron hole configurations. These then are: the energy difference between $J = 2$ and $J = 0$ states of $g^2_{9/2}$ (or $g^{-2}_{9/2}$), expressed by

$$\gamma = V\,(g^2_{9/2},\ J = 0) - V\,(g^2_{9/2},\ J = 2);$$

the interaction energy difference of the unperturbed $J = 0$ states of $g^2_{9/2}$ and $p^2_{1/2}$ configurations given by

$$\delta_2 = V\,(g^2_{9/2},\ J = 0) - V\,(p^2_{1/2},\ J = 0);$$

the non-diagonal matrix element of the effective mutual interaction between the $p^2_{1/2}$ and $g^2_{9/2}$ states expressed by

$$V = \langle p^2_{1/2},\ J = 0 | V | g^2_{9/2},\ J = 0 \rangle;$$

and finally the interaction energy difference in the three particle configuration $g^3_{9/2}$ or $p_{1/2}\ g^2_{9/2}$ expressed by

$$\delta_3 = V\,(p_{1/2}\ g^2_{9/2},\ J = 1/2) - V\,(g^3_{9/2},\ J = 9/2,\ v = 1)$$

where v is the seniority number.

The difference in the single particle energies taken from ^{89}Y and ^{87}Sr were set equal to β and β' respectively. The two and three particle configuration parameters, given above, were determined from the diagonalization of two by two matrices. For example, for ^{86}Sr, the ground state energy shift due to configuration interaction was obtained from diagonalizing the matrix

$$\begin{pmatrix} 2\beta' + \delta_2 & V \\ V & 0 \end{pmatrix}$$

The calculated energies thus determined from this analysis were in good agreement with the experimental data. These energies are listed in Table 1 which is taken from Talmi and Unna's paper (7).

The experimental investigation of the states of ^{85}Sr by Horen and Kelly (15) indicates that the T-U level predictions for this isotope are not in complete agreement with the experimental data for those levels above the first excited state. Experimentally, there appears to be a preponderance of $7/2^+$ and $9/2^+$ levels. This discrepancy could, in part, be due to insufficient experimental data from which an insufficient number of interaction parameters were determined. These results may also indicate that the nuclear states are due to different types of interactions.

1.4. The Unified Model

The experimental observation of large quadrupole moments for some nuclei could not be explained by the shell model. This is not surprising since the large quadrupole moment could only arise from the collective motions of several nucleons and departure from spherical symmetry, both of which were ignored in the shell model. To account for these motions and the possibility of nuclear deformation, the "collective model" was proposed by Bohr (16) and later extended by Bohr and Mottelson (8).

In this model, the nucleus is considered in two parts, the filled "core" and the nucleons in the unfilled

TABLE 1

Experimental and Calculated Energy Differences

Nucleus	Spins of Levels Considered		Energy Difference in MeV Experimental	Calculated
$^{89}_{50}Y_{39}$	1/2 −	9/2 +	0.915	0.99
$^{87}_{49}Sr_{38}$	9/2 +	1/2 −	0.388	0.37
$^{86}_{48}Sr_{38}$	0 +	2 +	1.079	1.1
$^{90}_{50}Zr_{40}$ (ground st.)	0 +	2 +	2.182	2.09
$^{90}_{50}Zr_{40}$ (first excited)	0 +	2 +	0.430	0.46
$^{91}_{50}Nb_{41}$	9/2 +	1/2 −	0.105	0.11
$^{85}_{47}Sr_{38}$	9/2 +	1/2 −	0.233	0.27
	9/2 +	7/2 +	0.255	0.27
$^{93}_{50}Tc_{43}$	9/2 +	1/2 −	0.39	0.44

shell. The core is considered to be a deformable liquid drop in interaction with the nucleons in the unfilled shell. The motions of the nucleons can now be treated in much the same way as the surface motion of a classical liquid drop--except, of course, the nucleon motion must be quantized. A brief summary of the development is presented here which follows the more detailed treatment by Preston (2).

1.4.1. The Collective Model

The nuclear surface of any general shape may be represented by

$$R = R_o \left[1 + \sum_{\lambda=o}^{\infty} \sum_{\mu=-\lambda}^{\lambda} \alpha_{\lambda\mu} Y_\lambda^\mu \ (\theta,\phi)\right]$$

where θ and ϕ are polar angles with respect to arbitrary axes. The collective motions are determined by letting $\alpha_{\lambda\mu}$ vary with time. The kinetic energy is of the form

$$T = (1/2) \sum_{\lambda\ \mu} B_\lambda \ | \ \dot{\alpha}_{\lambda\mu}|^2$$

where B_λ is $B_\lambda = \frac{\rho R_o^5}{\lambda}$, the mass parameter. The potential energy, in terms of the $\alpha_{\lambda\mu}$ is

$$V = (1/2) \sum_{\lambda\mu} C_\lambda \ |\alpha_{\lambda\mu}|^2$$

where C_λ is related to the surface tension by

$$C_\lambda^{(1)} = S\ R_o^2\ (\lambda - 1)\ (\lambda + 2).$$

If the liquid contains electric charge, the Coulomb energy is reduced by the distortion so that

$$C_\lambda = C_\lambda^{(1)} - C_\lambda^{(2)}$$

where

$$C_\lambda^{(2)} = \frac{3}{2\pi} \frac{Z^2 e^2}{R_o} \frac{\lambda - 1}{2\lambda + 1}$$

The frequency of oscillation associated with the $\alpha_{\lambda\mu}$ is

$$\omega_\lambda = \left(\frac{C_\lambda}{B_\lambda}\right)^{1/2}$$

The values of $\lambda = 0$ or 1 are of no interest here since ω would be zero. The collective states will have the excitation energies $\sum_\lambda n_\lambda \hbar\omega_\lambda$, where n_λ is the number of phonons of order λ. The state with $n_\lambda = 1$ is $(2\lambda + 1)$ fold degenerate. Only low values of λ need to be considered since $\hbar\omega_\lambda$ is a rapidly increasing function of λ. The first excited vibrational state would correspond to one $\lambda = 2$ phonon and therefore be a 2^+ state. The 3^- state formed by one $\lambda = 3$ phonon would have about the same energy as the degenerate 0^+, 2^+, or 4^+ state formed by two $\lambda = 2$ phonons.

An easy test to see if nuclei exhibit collective vibrational levels would be to compare the ratio of the energies of the first and second 2^+ states, which should be about 2. A large number of nuclei, particularly those with $40 \leq N \leq 80$, do display vibrational characteristics (2).

Negative parity states can arise from the combination of a $\lambda = 2$ and $\lambda = 3$ phonon which would give five states from 1- to 5-. These states lie above the 3^- state formed by the $\lambda = 3$ phonon.

1.4.2. Axially symmetric nuclei

For quadrupole shapes ($\lambda = 2$) the expression for the nuclear surface may be rewritten as

$$R = R_o \left[1 + \sum_{\mu} a_{2\mu} Y_2^{\mu} (\theta' \ \phi')\right]$$

where θ' and ϕ' are the polar angles with respect to the body axes.

Then

$$\Sigma a_{2\mu} Y_2^{\mu} (\theta', \phi') = \sum_{\nu} \alpha_{2\nu} Y_2^{\nu} (\theta, \phi).$$

Since the products of the moments of inertia are zero, $a_{21} = a_{2-1} = 0$ and $a_{22} = a_{2-2}$. Two distortion parameters, β and γ, are defined such that

$$a_{20} = \beta \cos \gamma$$

and

$$a_{22} = \sqrt{\frac{1}{2}} \beta \sin \gamma$$

The quantity β is the measure of the total nuclear deformation since

$$\sum_{\mu} |\alpha_{2\mu}|^2 = \sum_{\mu} a_{2\mu}^2 = \beta^2$$

Hence the potential energy becomes

$$V = (1/2)\ C\beta^2.$$

The deviation, δR_k, from spherical symmetry in terms of β, and γ is

$$\delta R_k = \sqrt{\frac{5}{4\pi}}\ R_o\ \beta\ \cos\ (\gamma - k\ \frac{2\pi}{3}\ )$$

where R_o is the undeformed nuclear radius and k equals 1, 2, or 3 and refers to the body axes. For fixed γ and a time varying β (β-vibrations) the nucleus maintains its symmetry axis; however, for a varying γ (γ-vibration) the nucleus loses its axial symmetry. The kinetic energy can be put in terms of β and γ, and becomes

$$T = \left(1/2\right)B\ (\dot{\beta}^2 + \beta^2\ \dot{\gamma}^2) + 1/2 \sum_{k=1}^{3} \mathfrak{I}_k\ \omega_k^2$$

which is separated into vibrational and rotational parts. The Hamiltonian is

$$H = H_\beta + H_\gamma + \sum_{k=1}^{3} \frac{L_k^2}{2\mathfrak{I}_k} + 1/2\ C\ \beta^2$$

where L_k is the component of angular momentum along the k axis. There are three rotational constants of the motion, J, M, and K determined by

$$L^2 = J(J+1)$$
$$L_z = M$$
$$L_3 = K$$

The motion separates into a vibrational part, $f(\beta)$, $g(\gamma)$ and a rotational part and the energy correspondingly to $E_{vib} + E_{rot}$. The rotational part is

$$E_{rot} = \hbar^2 \frac{[J(J+1) - K^2]}{2\mathcal{I}_1} + \frac{\hbar^2 K^2}{2\mathcal{I}_3}$$

For axial symmetry, $\mathcal{I}_3 = 0$ and hence $k = 0$ and

$$E_{rot} = \frac{\hbar^2}{2\mathcal{I}} J(J+1)$$

Only states of even J are possible for the axially symmetrical case since the wave function $|JMK\rangle = 0$ vanishes for $K = 0$.

The model predicts spins of 0, 2, 4, 6, etc. of even parity for the first few excited states with energies proportional to $J(J+1)$ for the rotational band. The energy ratios are $E_4/E_2 = 3.33$ and $E_6/E_2 = 7$. Many nuclei in the region $150 \leq A \leq 190$ and $A > 220$, where large nuclear deformations are known to exist as evidenced by the large quadrupole moments, exhibit level structures in agreement with these spin sequence and level spacings (1).

In this treatment of the collective motion, the condition that $K = 0$ requires that the expectation value, β_o, of β is large and that $\langle(\beta-\beta_o)\rangle^2$ is small. Also the expectation value of γ is zero. This means that the nucleus possesses a permanent axially symmetric deformation and, as mentioned previously, excludes odd spin values in

the rotational band. Yet, the level structures of many nuclei in these regions have been found (1) to have odd spin states which may arise by a γ vibration to an unsymmetrical excited state or by unsymmetrical ground states.

1.4.3. The Asymmetric Rotor Model

The asymmetric rotor model proposed by Davydov and Filippov (4) differs from the collective model in the following way. They use the general Hamiltonian with three unequal moments of inertia. However, these moments are considered to be constant for an intrinsic state through the use of the adiabatic approximation. In this approximation, the motion of the outer nucleons is assumed to be much faster than the motion connected to the changes in β and γ. Hence, these parameters are treated as fixed with the values of γ restricted to $0° \leq \gamma \leq 30°$. The parameters β and γ are the same as defined in section 1.4.2.

The level structure predicted by this model now includes odd spin states. The states predicted are 0+, 2+ (two states), 3+, 4+ (three states), 5+ (two states), 6+ (four states), etc.

The expressions for the level energies in units of $\frac{\hbar^2}{4B\beta^2}$ are, for $J = 2$

$$E_1(2) = \frac{9(1 - \sqrt{1 - 8/9 \sin^2 3\gamma})}{\sin^2 3\gamma}$$

$$E_2(2) = \frac{9(1 + \sqrt{1 - 8/9 \sin^2 3\gamma})}{\sin^2 3\gamma}$$

for which $\frac{E_2(2)}{E_1(2)} \geq 2$ depending upon γ.

For $J = 3$

$$E(3) = \sum_{\lambda=1}^{3} \frac{2}{\sin^2(\gamma - \frac{2\pi}{3}\lambda)} = \frac{18}{\sin^2 3\gamma}$$

Comparisons of the energies for $J = 2$ to the energy for $J = 3$ gives

$$E_1(2) + E_2(2) = E(3)$$

The three energy levels for spin 4 are determined by the roots of the cubic equation

$$E^3 - \frac{90}{\sin^2 3\gamma} E^2 + \frac{48}{\sin^4 3\gamma} (27 + 26 \sin^2 3\gamma) E - \frac{640}{\sin^4 3\gamma} \times (27 + 7 \sin^2 3\gamma) = 0$$

and for $J = 5$, the two energy levels are

$$E(5) = \frac{(45 + 9\sqrt{9 - 8 \sin^2 3\gamma})}{\sin^2 3\gamma}$$

For γ equal to zero degrees, the energy levels are the same as those for the permanently deformed axially symmetric nuclei described in section 1.4.2.

A good test of this model is to compare the reduced transition probabilities for the transitions between the two spin 2+ states and the ground state. Other models have assumed that these spin 2+ states are one and two phonon oscillations of the nuclear surface which make the transition between the 2nd spin 2+ to the ground state hard to explain unless there is a breakdown in the oscillator approximation. As was shown in section 1.4.2., the matrix elements for $\alpha_{2\mu}$ will be non-zero for only those states that differ by one phonon. Hence, the transition between the 2+, 2 phonon state to the ground state would be forbidden. If, however, the two states are assumed to be rotational levels, the reduced transition probabilities can be expressed in terms of the parameter, γ.

For the various transitions, these are given by,

$$B\ (E2;\ 21 \longrightarrow 0) = \left(1/2\right)\left(1 + \frac{3-2\ \sin^2 3\gamma}{\sqrt{9-8\ \sin^2 3\gamma}}\right)$$

$$B\ (E2;\ 22 \longrightarrow 0) = \left(1/2\right)\left(1 - \frac{3-2\ \sin^2 3\gamma}{\sqrt{9-8\ \sin^2 3\gamma}}\right)$$

$$B\ (E2;\ 22 \longrightarrow 21) = \left(10/7\right)\ \frac{\sin^2 3\gamma}{9-8\ \sin^2 3\gamma}$$

$$B\ (E2;\ 3 \longrightarrow 22) = \left(25/28\right)\left(1 + \frac{3-2\ \sin^2 3\gamma}{\sqrt{9-8\ \sin^2 3\gamma}}\right)$$

$$B\ (E2;\ 3 \longrightarrow 21) = \left(25/28\right)\left(1 - \frac{3-2\ \sin^2 3\gamma\ )}{\sqrt{9-8\ \sin^2 3\gamma}}\right)$$

expressed in units of $\frac{e^2 Q_o^2}{16 \pi}$, where $Q_o = \frac{3ZR^2\beta}{\sqrt{5 \pi}}$ is the intrinsic quadrupole moment.

The ratios of the reduced transition probabilities can be easily obtained from the experimental data.

The model has had mixed success when compared to experimental data for those nuclei where it is expected to be applicable. For example, the level spacings and reduced transition ratios predicted (4) by the model are in good agreement with those determined from experimental data for ^{114}Cd, ^{152}Sm, ^{182}W, ^{192}Pt, and ^{238}Pu. Yet, for some nuclei, such as ^{76}Se, ^{122}Te, and ^{126}Te the reduced transition ratios predicted (4) by the model are not in agreement with experimental data. Davydov and Filippov interpret these discrepancies as arising from a breakdown of the adiabatic approximation for these nuclei (4).

Davydov and Chaban (6) have extended the model to allow for violations of the adiabatic condition with the introduction of a "non-adiabaticity" parameter, μ. This parameter is defined such that

$$\mu^2 = \frac{\hbar}{\sqrt{CB}\,\beta_o^2}$$

where C is the elasticity constant, B is the mass parameter and β_o is the equilibrium value of β. As a result, the parameters β_{KJ} and C_{KJ} contained in the

potential energy operator of the Hamiltonian are now functions of μ. The energies thus determined depend only upon the "non-axiality" parameter γ, and the "non-adiabaticity" parameter, μ. The reduced E2 transition probabilities are

$$B(E2;\ JK \longrightarrow J'K') = B_a(E2;\ JK \longrightarrow J'K')\ S$$

where $B_a(E2;\ JK \longrightarrow J'K')$ are the reduced transition probabilities computed in the adiabatic approximation and S is the correction factor which accounts for coupling between rotation and vibration of the nuclear surface. This correction factor, S, is expressed by

$$S = \beta^{-2}\ |(JK_\mu|\beta|J'K'_\mu)|^2$$

Davydov and Chabin show (6) that for $\mu \leq 0.5$ the factor S is approximately unity. Hence, the reduced E2 transition probabilities are essentially the same as for those nuclei which have $\mu \leq 0.5$.

Klema, Mallmann and Day (17) have evaluated the energy state predictions of this model for a number of nuclei, including ^{82}Kr. The predictions for those nuclei for which $\mu \leq 0.5$ were found to be in good agreement with the experimental energies.

1.4.4. The Core Coupling Model

The core coupling model may be thought of as an extension of the collective model to odd A nuclei. In

this scheme, the motion of the odd particle is coupled to the collective motion of the even-even core. As a result of this coupling, it is expected that the resulting level structure should exhibit characteristics similar to the even-even core, but modified by the single particle motion. In other words, one would expect the low lying single particle states to have collective states built upon them.

The core, for simplicity, is considered to be all of the paired nucleons. The strength of the particle-core interaction will certainly be a function of the nuclear deformation, weak for small β, γ deformations near spherical nuclei, and strong for large nuclear deformations.

1.4.4.A. Weak Coupling, Spherical Nuclei.--For nuclei near closed shells the interaction can be treated by perturbation methods. The Hamiltonian is written as

$$H = H_c + H_p + H_{int}$$

where H_c is the collective Hamiltonian of the core, H_p is the spherical single particle Hamiltonian. The interaction term, H_{int} is

$$H_{int} = - k(r) \sum_{\lambda\mu} \alpha_{\lambda\mu} Y_\lambda^\mu \quad (\theta\Phi)$$

where $\alpha_{\lambda\mu}$ are the distortion parameters described in section 1.4.1, and k (r) is the coupling parameter.

The states of the uncoupled systems are formed by the vector addition of the single particle state $|jm\rangle$ of angular momentum j with the collective state $|NR\rangle$ of N phonons and angular momentum R. The Hamiltonian is then diagonalized to determine the states as a result of the coupling.

In order for the perturbation to be applicable it is necessary that

$$\left(\frac{5}{16\ \pi}\right)^{1/2} \quad \frac{k}{(\hbar\omega C)^{1/2}} \quad << 1$$

where $\hbar\omega$ is the phonon energy. If as in section 1.4.2., we restrict the nucleus to quadrupole shapes, the quadrupole terms $\alpha_{2\mu}$ restrict the coupling of the ground state to only those states with one 2+ phonon present. The matrix elements involving the second order harmonics Y_2^{μ} will be non-zero only if $\Delta j \leq 2$ and no parity change. Hence only the single particle states of the same parity and $\Delta j \leq 2$ will mix. Lawson and Uretsky have shown (18) that the center of gravity of a multiplet of core-particle states in odd mass nuclei should occur at the same energy as the corresponding collective state in the adjacent even-even nucleus.

DeShalet has made calculations (19) for the core-particle interactions for $j = 1/2$ particle states coupled to 2+ phonon level for nuclei in the medium and heavy mass region. His calculations, in general, are in good

agreement with the experimental data for those nuclei used to test the model.

1.4.4.B. Strong Coupling, Deformed Nuclei.--For nuclei with large deformations, the perturbation method described in section 1.4.4.A. can no longer be applied. The procedure is to use the single-particle Schrödinger equation,

$$H_p \psi_\alpha = [T + V(\beta,\gamma; \hat{r}, \hat{\ell}, \hat{s}] \psi_\alpha = E_\alpha (\beta,\gamma) \psi_\alpha$$

where α represents the appropriate quantum numbers. The values of the parameters of β and γ are determined which minimize the total particle energy. The calculations may be simplified some what with certain assumptions. These are: that the adiabatic approximation is applicable; that the nucleus maintains axial symmetry; and that there is only one nucleon outside the core.

Nilsson has made extensive calculation (20) for the single particle states in deformed nuclei.

1.5. The Experimental Determination of the Properties of Nuclear States

The nuclear models described in the previous sections of this chapter predict the energies of nuclear levels as well as their spins, parities, and transition probabilities between states. Transition probabilities, internal conversion coefficients, and gamma-gamma directional correlation coefficients are all functions of

the change in angular momentum carried off by the radiation and, in the case of transition probabilities and internal conversion coefficients, also upon the change in parity. Hence, the spins and parities of the states producing the transition may be determined, though not always uniquely, from these properties provided the spins of one of the states is known from other experiments.

Since the transition probabilities, internal conversion coefficient, and directional correlation coefficients have such an important role, a brief description of the selection rules and other properties governing them will be presented here.

1.5.1. Beta Selection Rules

The transition probability for the beta decay from an initial state, i, to a final state f, in the daughter nucleus is given by

$$W(i \longrightarrow f) = g^2/\pi^3 \int_0^{p_{max}} p^2 \, q^2 \, F_o(\pm Z, A, P) \, x \, S_n \left(\frac{1}{n!}\right)^2 dp$$

where g is a coupling constant, p is the electron momentum, q is the neutrino momentum, F_o is the Fermi function, A and Z are the mass and charge numbers of the daughter nuclide, S_n is a shape factor, and n is the order of forbiddeness. The plus sign is used for negatrons and the negative sign for positrons. For most cases, the

shape factor may be set equal to one. A quantity independent of the coupling constant is easy to determine experimentally. This quantity is the reduced half-life, ft where f is given by

$$f = \int_0^{p_m} p^2 \, q^2 \, F_o \, dp$$

and t is the half life of the decay. The reduced half life, ft, should be approximately the same for the same degree of forbiddeness, independent of the decay energy and of the nuclear charge.

Nomographs have been prepared (21) from which the value of log ft can be determined from the beta decay end-point energies and the half-life of the decay. The degrees of forbiddeness associated with the log ft values have been determined empirically. The accepted (22) values are: for odd A, if log ft $\leq$ 4.0 then $\Delta J = 0$, $\Delta\pi = 0$; for $Z < 80$, if log ft $\leq$ 5.8, the transition is allowed ($\Delta J = 0, 1$ $\Delta\pi = 0$); if 5.8 $\leq$ log ft $\leq$ 10.6, the transition is allowed or 1st forbidden ($\Delta J = 0$, or 1, $\Delta\pi$ = yes); if 10.6 $\leq$ log ft $\leq$ 15 the transition is allowed, first forbidden or second forbidden ($\Delta J = 2$, or 3 $\Delta\pi$ = no); a beta transition is unique ($\Delta J = 2$, $\Delta\pi$ = yes) if log ft $\geq$ 7.6 and if the Fermi plot has appreciable curvature corresponding to a shape factor $(p^2 + q^2) = S_1$.

1.5.2. Gamma Ray Transition Probabilities

The transition of a nucleus in a state, i, to a state, f, may occur through the emission of a photon with an angular momentum, L (≥ 1). This angular momentum can be any of the values

$$|j_i - j_f| \leq L \leq j_i + j_f,$$

however, only those gamma rays with the lowest possible L value are usually observed. In addition, gamma rays with admixtures of angular momentum of L, and L + 1 have also been observed. The character of the radiation will be magnetic or electric 2^L pole order depending upon whether $\Delta\pi$ is yes or no.

The transition probability for the gamma emission is given by

$$W(\sigma,L) = \frac{8\pi(L+1)}{L[(2L+1)!!]^2} \frac{E^{2L+1}}{\hbar} B(\sigma L)$$

where σ, represents the electric or magnetic character of the transition. The quantity, $B(\sigma L)$ is the reduced transition probability, and is predicted by the various nuclear models.

1.5.3. Gamma-Gamma Angular Correlations

The angular distributions of the emitted gamma rays are functions of the multipole order characterizing the transition. Unfortunately, the nuclei are randomly

oriented and, unless some means is available to align the nuclei, the measured distribution will be isotropic.

When gamma rays are found to be in cascade, coincidence counting techniques, which are described in Chapter 2, can be used to measure only those gamma rays from similarly aligned nuclei. The nuclei must be placed in an environment which will not perturb the orientation of the nuclei during the emission of the gamma rays. For life-times of $T \leq 10^{-12}$secs this condition is always fulfilled. For life-times greater than 10^{-12}secs the nuclei can be placed in liquid solution to fulfill this requirement.

In this method, the angular distribution function can be expressed (23) as

$$W(\theta) = \sum_{k=0}^{k_{max}} A_k P_k (\theta)$$

where the coefficients A_k are functions of the spins of the initial, intermediate, and final states and the multipole order of both gamma rays. They can be expressed as a product.

$$A_k = A_{k1} (J_i, J, L_1, \delta_1) A_{k2} (j, J_f, L_2, \delta_2)$$

Only even values of k occur k_{max} = min (2J, $2L_1$, 2L2) and is usually never greater than 4. A_{k1} is the coefficient for the first gamma ray whereas A_{k2} is the coefficient for the second. Since its not unusual to have

admixtures of L, and L + 1 multipole transitions, the δ_i in the coefficient is the mixing ratio of the admixture.

It is possible that there may be an unobserved transition intermediate to the gamma rays of interest. In this case, a correction (24) must be made for the attenuation of the distribution in the form of

$$A_k = A_k\ (1)\ U_k\ (2)\ .\ .\ .\ .\ U_k\ (n-1)\ A_k\ (n)$$

for n gamma rays. The U_k's are the coefficients for the unobserved gamma rays. If the unobserved transition is not pure then, in terms of the mixing ratio, δ, for the unobserved transition,

$$U_k' = \frac{U_k(L) + \delta^2\ U_k\ (L + 1)}{1 + \delta^2}$$

The theoretical A_k coefficients can be calculated from parameters that have been tabulated (21,23). In some cases, the theoretical coefficients, A_k have been tabulated (25) for various combinations of spin sequences and mixing ratios. However, in comparisons of the experimentally determined coefficients with the theoretical ones, it is not always possible to determine uniquely the multipole order of the transition as there can be considerable overlap depending upon the mixing ratio. Some of the ambiguity can be removed if the mixing ratios are independently determined.

1.5.4. Internal Conversion Coefficients

The internal conversion of an orbital electron is in competition with the gamma emission for the transition of the nucleus from state i, to state f. The branching ratio between the two processes is defined as the internal conversion coefficient. These coefficients are functions of the change in angular momentum and parity in the transition, the nuclear charge, and the energy available for the transition. The theoretical coefficients for given ΔJ and $\Delta\pi$ as a function of Z and energy have been tabulated (26) for K, L, and M shells. Here again it is possible to determine ΔJ and δ through the comparison of experimental values with those of theory. These determinations, used in conjunction with the angular correlation data and transition probabilities, help to remove some of the ambiguities introduced through a single measurement.

The values of ΔJ and $\Delta\pi$ determined in this way are model independent. Hence they supply valuable information with which to test the success of a particular model.

CHAPTER II

APPARATUS AND EXPERIMENTAL PROCEDURES

2.1. The Gamma-Ray Spectrometer

2.1.1. Singles Experiments

In the early stages of this investigation, the gamma ray spectra of both ^{82}Br and ^{83}Sr were recorded with 7.6 cm by 7.6 cm NaI(Tl) scintillation detectors mounted on EMI 9578S photomultiplier tubes. The pulses from these tubes were electronically coupled through Cosmic Model 901 linear amplifiers to a Nuclear Data 150FM 1024 channel multi-parameter pulse height analyser. The energy resolutions of these detectors were each $\simeq$ 9% for the 661 keV photon from ^{137}Cs.

Later, the NaI(Tl) detectors were replaced by the newly developed lithium drifted germanium detectors [Ge(Li)] with sensitive volumes of 1 to 7 cm^3. A Tennelec Model 100C preamplifier and this system gave resolutions from 3 keV to 4.5 keV for the 661 keV photon from ^{137}Cs. This greatly improved resolution facilitated gamma ray energy measurement giving precisions which vary from $\pm$ 0.5 to $\pm$ 1.0 keV. The energies were measured from calibration curves determined from least squares fitting the peak centroids of well known gamma ray transitions

to a quadratic equation after the background had been subtracted. The background was determined by making a third order fit to counts in channels adjacent to the high and low energy sides of the peaks. The MSU CDC 3600 computer was used to make these calculations. The calibration gamma ray energies (27) are listed in Table 2.

The relative intensities of the gamma rays were determined from experimentally determined efficiency curves (28).

2.1.2. Coincidence Experiments-- NaI(Tl) Detectors

Knowledge of the gamma ray energies and relative intensities alone is not sufficient information with which to construct a decay scheme. Coincidence experiments were used to determine those gamma rays that were in cascade. For these studies, a conventional fast-slow transistorized multiple coincidence unit, Cosmic Model 801, was used to provide the coincidence gate to the multichannel analyser. The resolving times were variable, but were usually set to $2T \simeq 50$ nsec.

Two 7.6 cm by 7.6 cm NaI(Tl) detectors, each enclosed in a graded lead cylinder, were used as the gamma detectors. Each crystal was usually placed 10 cm from the source with the crystal axes at 90°. This minimized coincidences due to crystal to crystal scattering.

Table 2.--Gamma ray calibration energies[a].

Source	Energy, keV
^{131}I	80.164
^{123m}Te	159.000
^{131}I	284.307
^{131}I	364.467
^{83}Sr	511.006
^{137}Cs	661.595
^{60}Co	1173.226
^{60}Co	1332.483
ThC''(DE)	1592.46
^{88}Y	1836.2
ThC''	2614.47

[a]Reference 27.

[b]Errors in these energies are $\leq$ 0.1 keV except for ^{88}Y which is $\pm$ 0.3 keV.

The entire detection system was enclosed in a Styrofoam box where the temperature was controlled to ± 0.5° C. This facilitated control of the gain stability to better than ± 0.25%.

The multi-parameter feature of the multi-channel analyser was employed in a 32 x 32 channel mode to record gamma-gamma coincidences and directional correlation spectra. This enabled the correlations and coincidence spectra of several gamma rays to be recorded simultaneously.

The equivalent chance spectra were simultaneously subtracted by utilizing a second identical (except delayed) coincidence circuit in parallel with the first (29). The delayed coincidence output was coupled to the external subtract input of the 1024 channel analyser. The resolving times for both coincidence circuits were monitored and matched to within 1%.

For the directional correlation measurements on the ^{82}Br decay, an additional graded lead cone was placed over the front of each NaI(Tl) detector. The source, in liquid form, was contained in a thin wall Teflon cup that was symmetrically located 11 cm from each crystal. The dimensions of the Teflon cup were 0.3 cm diameter by 1 cm with a wall thickness 0.08 cm. The coincidence counting rates were measured in 45° increments from 90° to 270° with 100 minute time intervals at each angle. It has been shown by Reich *et al.* (30) that this

method can give as accurate correlation functions as those determined with smaller angle increments. The singles counting rates in the moveable detector were measured before and after the coincidence runs at each angle. As a result of measuring the coincidence counting rate in the symmetrical angular sequence, and the division of the coincidence counting rate by the sum of the singles counting rates, a first order correction is obtained for source decay and geometrical asymmetries. Comparisons of the singles counting rates at 90° with the counting rates at 270°, and the counting rates at 135° with the counting rates at 225°, indicate that this correction is good to within $\pm$ 0.5%. Each directional correlation measurement was repeated; and, in one case, the measurement was repeated with 30° increments. The correlation functions determined from the data taken at 45° increments were in excellent agreement with those determined from the data taken in 30° increments.

2.1.3. Coincidence Experiments-- NaI(Tl) and Ge(Li)

The energy spacings between many of the gamma rays from the decay of ^{83}Sr were very small. Because of this, the coincidence data recorded for this isotope with the NaI(Tl) detectors were next to impossible to interpret. Therefore, all of the coincidence experiments for ^{83}Sr were repeated using the 7 cm^3 Ge(Li) detector in place of

one of the NaI(Tl) detectors. This did not completely solve the problem since the coincidence gate provided by the NaI(Tl) detector necessarily included two or more gamma rays and many underlying Compton photons. However, a consistent interpretation could be obtained by quantitative comparisons of the different coincidence spectra.

2.1.4. Anti-Coincidence Experiments

The small volume of the Ge(Li) detector and the low Z of the germanium give rise to a relatively larger Compton background in the gamma ray spectra recorded with these detectors than in those spectra recorded with NaI(Tl) detectors. Therefore, it is possible that low intensity, low energy transitions are masked by the large number of Compton photons from the more intense higher energy gamma rays. In order to reduce this large Compton background in the gamma ray singles spectra, an anti-Compton spectrometer (31) was utilized. For this purpose, the 7 cm^3 Ge(Li) detector was inserted into a large split annulus NaI(Tl) detector. The annulus was two and one half inches thick and eight inches long with an outside diameter of eight inches. Each half of the annulus was optically isolated from the other half. Three RCA 8053 photo tubes were optically coupled to each half of the annulus. The Compton scattered photons from the Ge(Li) detector are very efficiently detected by the annular

NaI(Tl) detector. The output pulses from this detector are then used to provide an anti-coincidence gate to the multichannel analyser. Therefore, those gamma ray events detected in the Ge(Li) detector that are in coincidence with those detected in the annular NaI(Tl) will not be stored by the analyser.

The split annulus NaI(Tl) detector was also used to provide some of the coincidence gates for coincidence experiments with ^{83}Sr.

2.2. The Permanent Magnet Beta-ray Spectrometer

Three flat-field 180° permanent-magnet beta-ray spectrometers were used to record the internal-conversion electron spectrum for ^{82}Br. The magnetic field strengths of these spectrometers provided energy ranges 0 to 150 keV, 0 - 900 keV, and 0 to 2000 keV, respectively (32).

The source was lined onto aluminized mylar film with a standard drawing pen. The source strength of those used in the high energy spectrometer were estimated to be several millicuries. Photographic plates were exposed to the sources in the spectrometer from four to eight hours in the low-energy spectrometers, and for one to two half-lives in the high-energy spectrometer. The source in each spectrometer was followed for five half-lives.

The electron lines on the photographic plates were measured with a low-power traveling microscope. The least count of the vernier scale was 0.001 cm. Each plate was read by three different persons. The energies of the internal-conversion electrons were then determined from the average scale reading made by the three individuals.

CHAPTER III

TRANSITIONS IN ^{82}Kr

The transitions in ^{82}Kr following the beta decay of ^{82}Br have been studied by several investigators over the past decade (33-38). Lu, Kelly, and Wiedenbeck (33), using NaI(Tl) detectors and single channel pulse height analyzers, identified gamma rays of 555, 619, 698, 762, 1040, 1320, and 1475 keV as belonging to ^{82}Kr. They constructed a decay scheme for ^{82}Br from the results of gamma ray summing experiments. Later, Waddell and Jensen (34) reported gamma rays from the decay of ^{82}Br essentially in agreement with Lu et al.; however, their decay scheme that was constructed from gamma-gamma coincidence measurements was an inversion of the one proposed by Lu et al. The decay scheme proposed (34) by Waddell and Jensen is shown in Figure 1. The location of the first excited state at 777 keV has since been substantiated (39) by Coulomb excitation experiments by Heydenberg. The spins and parities shown on the decay scheme were assigned as a result of gamma-gamma angular correlation and internal conversion electron measurements (34). The electron data were recorded (34) with an intermediate image electron spectrometer for which the resolution was nominally 3%.

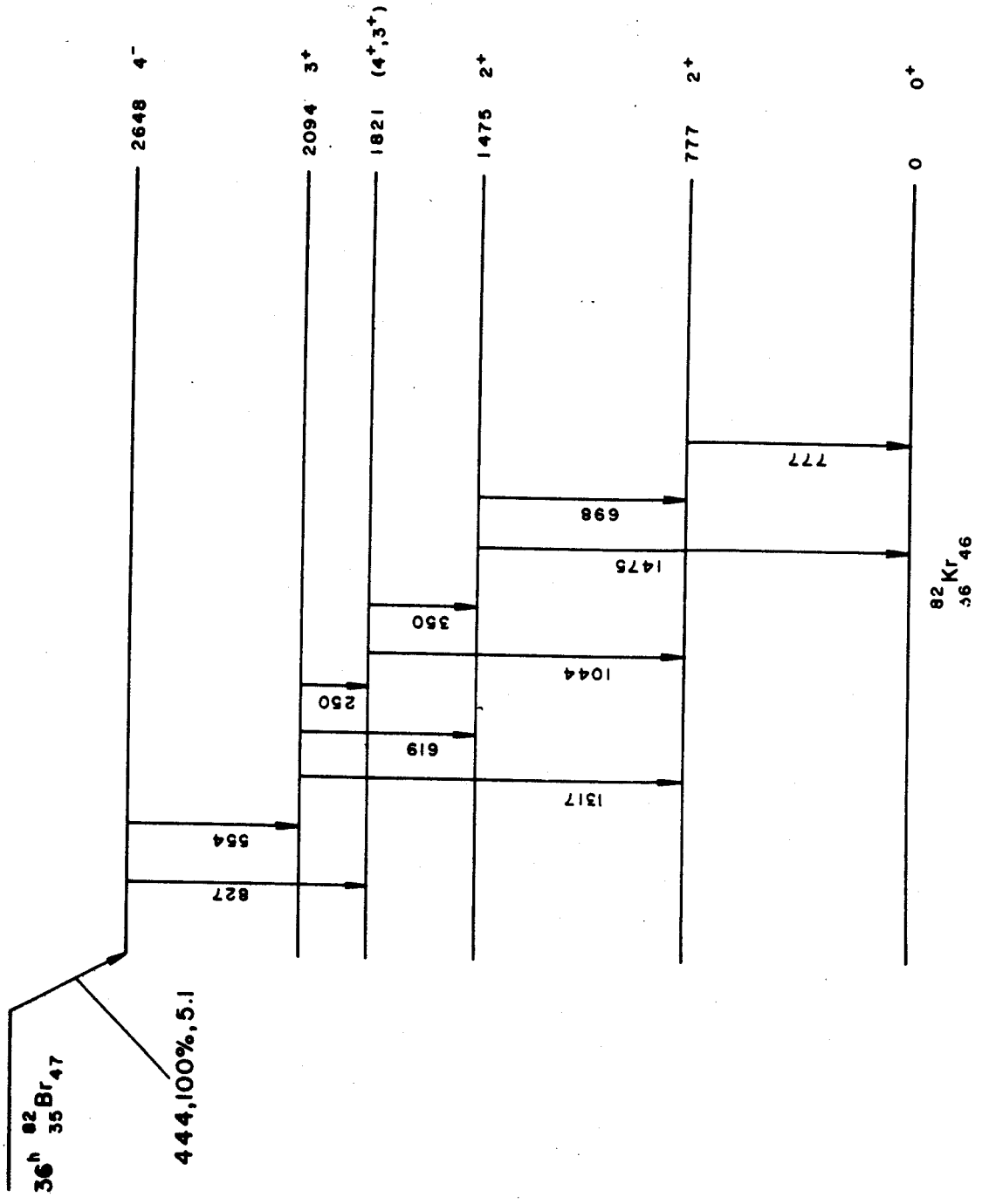

Figure 1.--Presently accepted decay scheme of ^{82}Br.

N. Benczer-Koller (35) later repeated the angular correlation and internal conversion measurements. These results are in agreement with those of Waddell and Jensen. Hultberg and Hedgran (38), using an iron core $\pi\sqrt{2}$ electron spectrometer, have reported the accurate measurement of the transition energies. Dzhelepov, Eliseev Prikhodtseva and Kholnov (37) made use of an external converter to measure the high energy portion of the gamma ray spectrum with an electron spectrometer. In addition to all the previously reported transitions, they found transitions at 1648 and 1780 keV but were not able to place them in the decay scheme.

The ordering of the 828-1044 keV cascade in this decay scheme had been ambiguous with the only supporting evidence for the placing of the state at 1821 keV being the observation of weak coincidences of two gamma rays at 250 and 350 keV with the 1475 and 554 keV photons. These results were reported by Duby, Mandeville, and Rothman (36). More recently, Simons, Bergström, and Anttila have reported angular correlation coefficients (40) for 832-1044, 1044-777, and 832-777 keV gamma ray cascades and conclude that the ordering of the 828-1044 keV gamma ray cascade is such that the placement of a state at 1821 keV is correct.

In addition, Kennett, Webster and Prestwich have reported (41) finding coincidences between the 1648-777

and 1648 -- 220 keV gamma rays and thereby place a state at 2429 keV.

The present investigations were undertaken to test the above energy level diagram and spin assignments and to examine the characters of some of the excited states prior to the reports of Simons et al., (40), and Kennett et al., (41). Of special interest was the 4^- state at 2648 keV. No corresponding state has been observed in adjacent even-even nuclei. The results of the present investigation confirm many of the above described results. Several additional weak transitions have been identified which allow the placing of additional excited states in ^{82}Kr.

3.1. Experimental Results

The ^{82}Br sources for these investigations were obtained from the Oak Ridge National Laboratory in the form of KBr in water. The specific activities were approximately 20,000 mc/gm at the start of the experiments.

3.1.1. The Internal Conversion Electron and Gamma-ray Singles Spectra

Examination of the internal conversion electron spectra revealed several new, weak transitions in addition to the previously reported strong transitions. The energies of the corresponding gamma transitions that

were observed are summarized in Table 3. Also given are the gamma-ray energies as determined from the measurements using the Ge(Li) detector. These latter measurements are discussed below. In addition to the K internal conversion lines, L internal conversion lines were observed for the 92.1, 554.1, 618.6, and 698.4 keV transitions. The high energy transitions were observed using a source of several millicuries that was exposed in the spectrometer for approximately one half-life.

A typical gamma-ray singles spectrum measured with the Ge(Li) detector is shown in Figure 2A, 2B, and 2C. Portions of this spectrum are shown with linear scales in Figures 3A, 3B, and 3C. A stripped singles spectrum taken with a 7.6 cm by 7.6 cm NaI(Tl) crystal is shown in Figure 4 for comparison. The resolution of the NaI(Tl) detector was approximately 8.8% for the ^{137}Cs photon. All of the transitions that were observed in the internal conversion electron spectrum, except that at 183.9 keV, are resolved in the spectrum from the Ge(Li) detector. This gamma-ray could have been easily masked by the high back-scatter peaks from the strong transitions. The singles spectra from the Ge(Li) detector also revealed weak peaks at 274, 602, 952, 1085, and 1823 keV which were not observed in the internal conversion electron spectra. These weak transitions were observed to decay with the same half-life as the strong transitions.

Table 3.--Energy and intensity measurements of gamma rays emitted in the decay of ^{82}Br.

Gamma Transition Energies		Relative Photon Intensities		Previously Reported Results[a]	
Ge(Li) E in keV	Internal Conversion Electrons E in keV	Ge(Li)	NaI(Tl)	Photon Energy	Photon Relative Intensity
96.3[b]	92.1 ± 0.2	0.6			
	183.9 ± 0.3	?			
222.9[b]	221.4 ± 0.3	2.8			
274.2 ± 1.0		1.2			
452.0 ± 1.0	451.1 ± 1.0	0.5			
554.0 ± 1.0	554.1 ± 0.5	88.2	73	554.1 ± 0.2	80
602.0 ± 1.0		1.5			
618.9 ± 1.0	618.6 ± 0.5	52.0	50	618.7 ± 0.2	50
698.2 ± 1.0	698.4 ± 0.5	31.0	33	698.4 ± 0.3	33
776.8 ± 1.0	777.1 ± 0.9	100.0	100	776.9 ± 0.2	100
827.7 ± 1.0	828.0 ± 1.0	29.1	21	827.6 ± 0.4	30
952.3 ± 1.0					
1010.2 ± 1.0	1012.3 ± 1.0	2.7			
1044.1 ± 1.0	1043.9 ± 1.0	36.3	35.7	1044.0 ± 0.2	35
1085.1 ± 1.0		0.5			
1318.4 ± 1.0	1317.6 ± 1.0	33.2	30	1317.1 ± 0.2	32
1475.2 ± 1.0	1475.1 ± 1.0	19.9	22	1475.3 ± 0.4	21
1651.6 ± 1.0	1658 ± 10	1.8	2.6		
1782.6 ± 1.0	1777 ± 10	0.1			
1822.6 ± 1.0		0.03			
1875.6 ± 1.0	1872 ± 10	0.07			
1960.6 ± 1.0		0.03			

[a]Energies and intensities were measured by the method of external conversion with a double focusing β-spectrometer. Reference 36.

[b]The low energy measurements with the Ge(Li) detector are not precise because of non-linearity in low channels and the absence of well-known low energy standards.

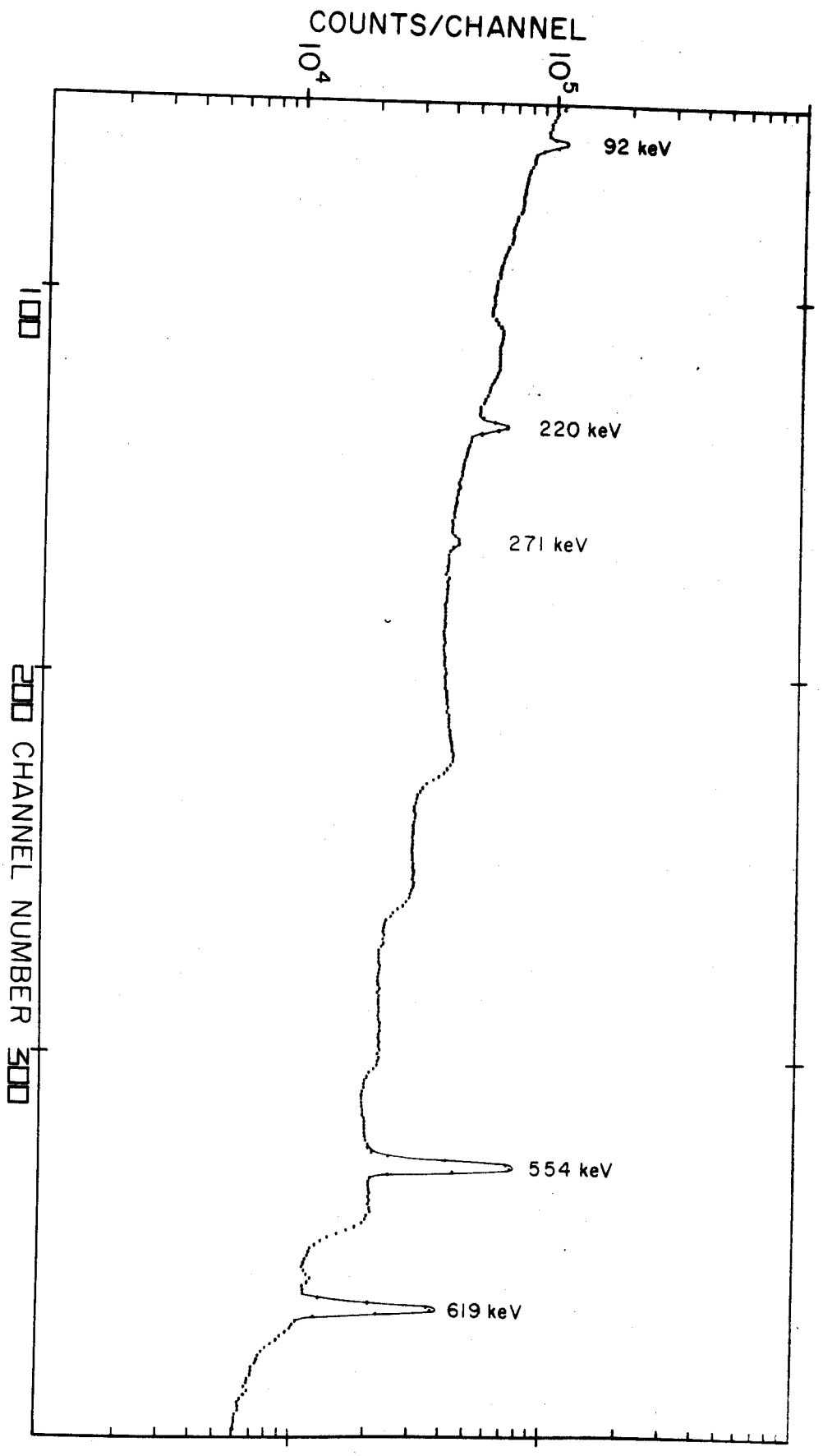

Figure 2a.--Gamma singles spectrum of ^{82}Br taken with a 3 cm^2 x 4 mm Ge(Li) detector. Low energy region.

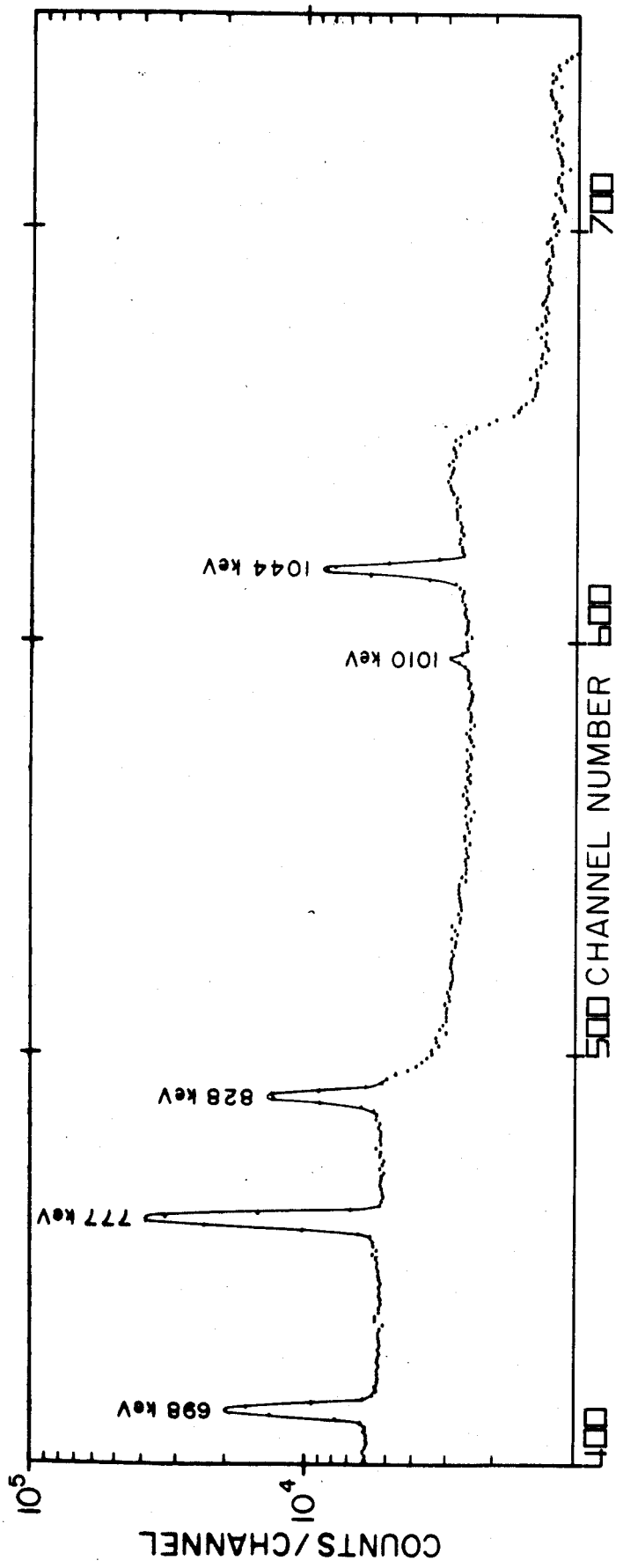

Figure 2b.--Gamma singles spectrum of ^{82}Br taken with the Ge(Li) detector. Intermediate energies.

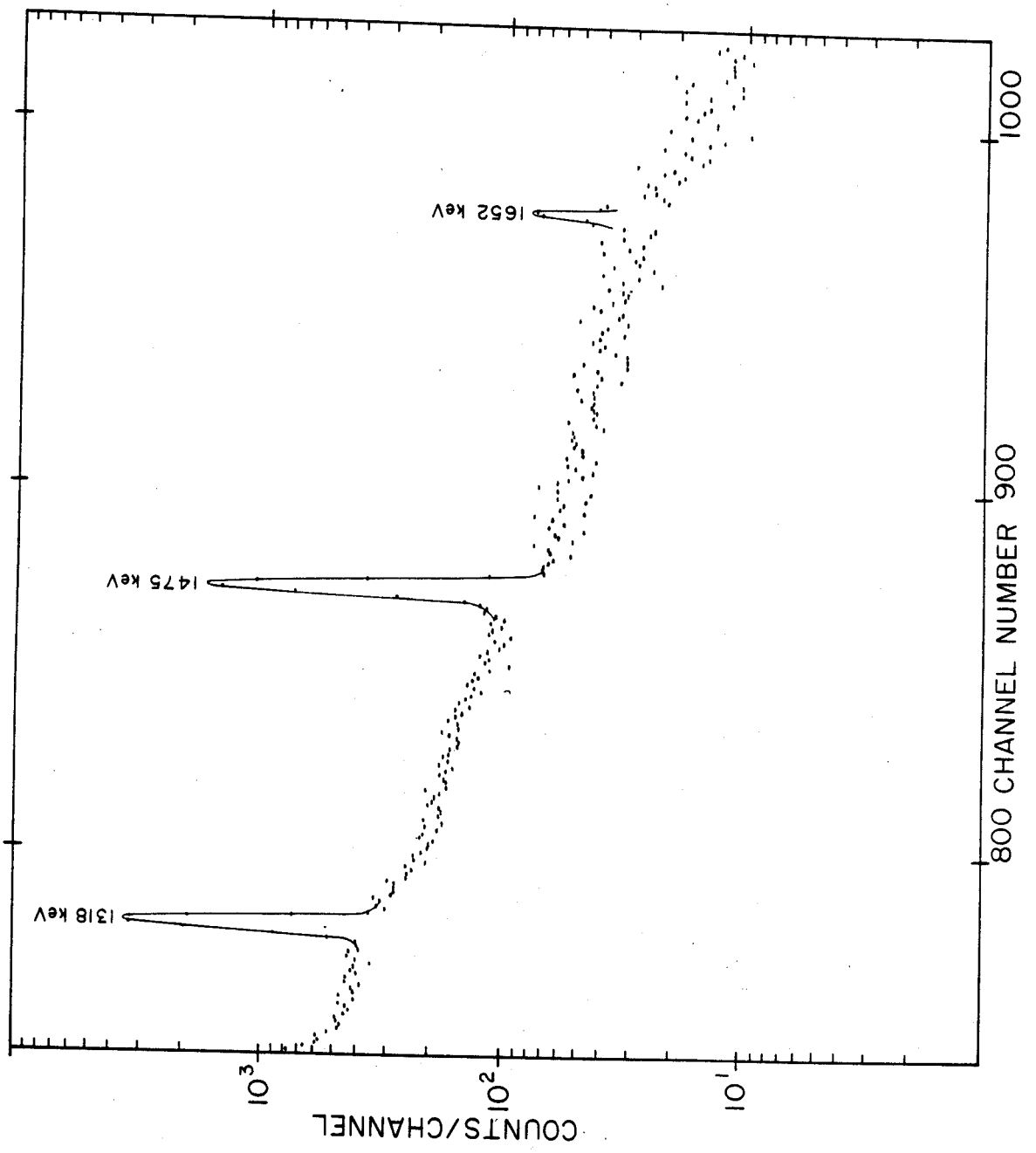

Figure 2c.--Gamma singles spectrum of ^{82}Br taken with the Ge(Li) detector. High energy region.

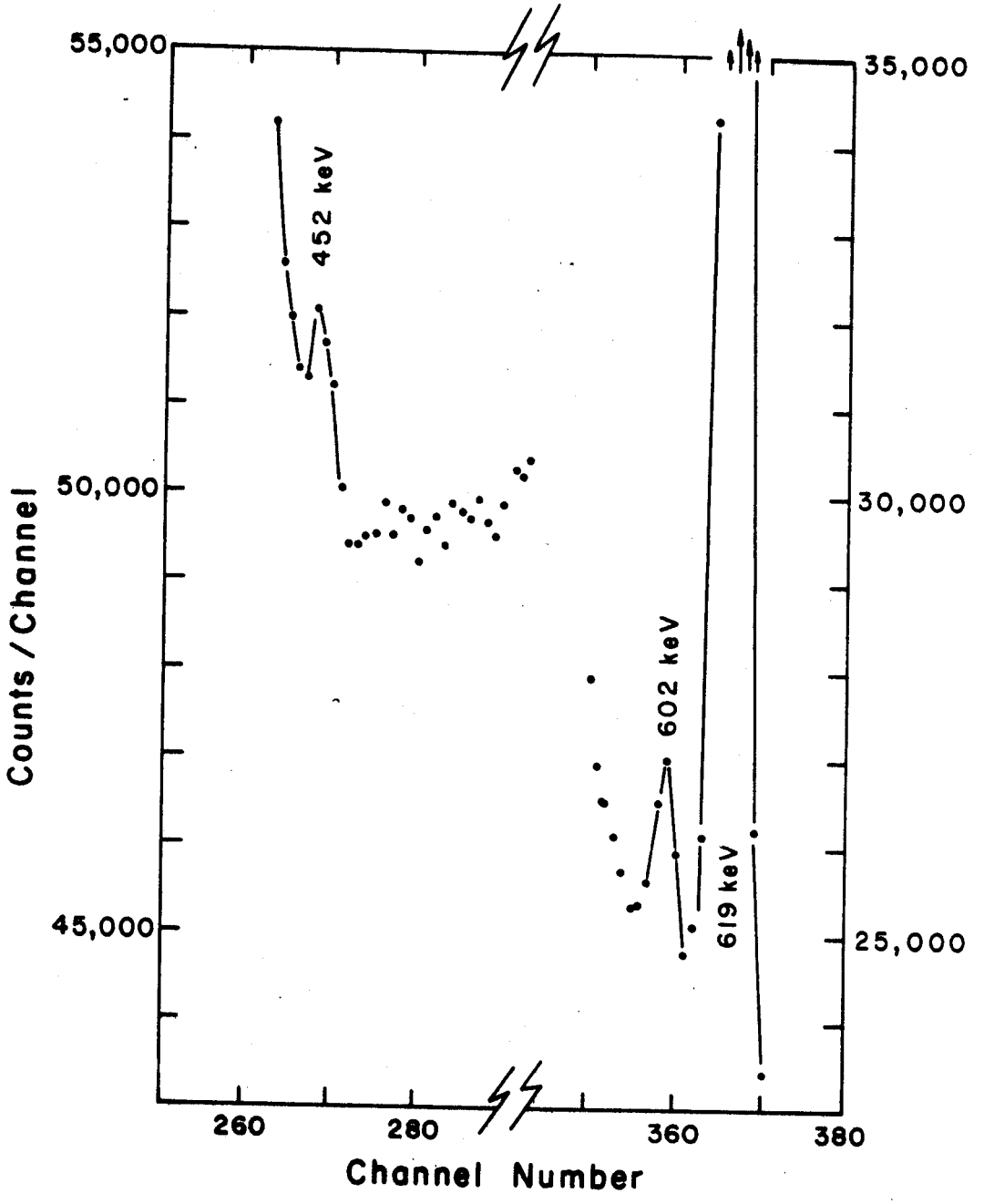

Figure 3a.--Weak gamma transitions observed with the Ge(Li) detector: 425-630 keV. Note the scale breaks for both coordinate axes.

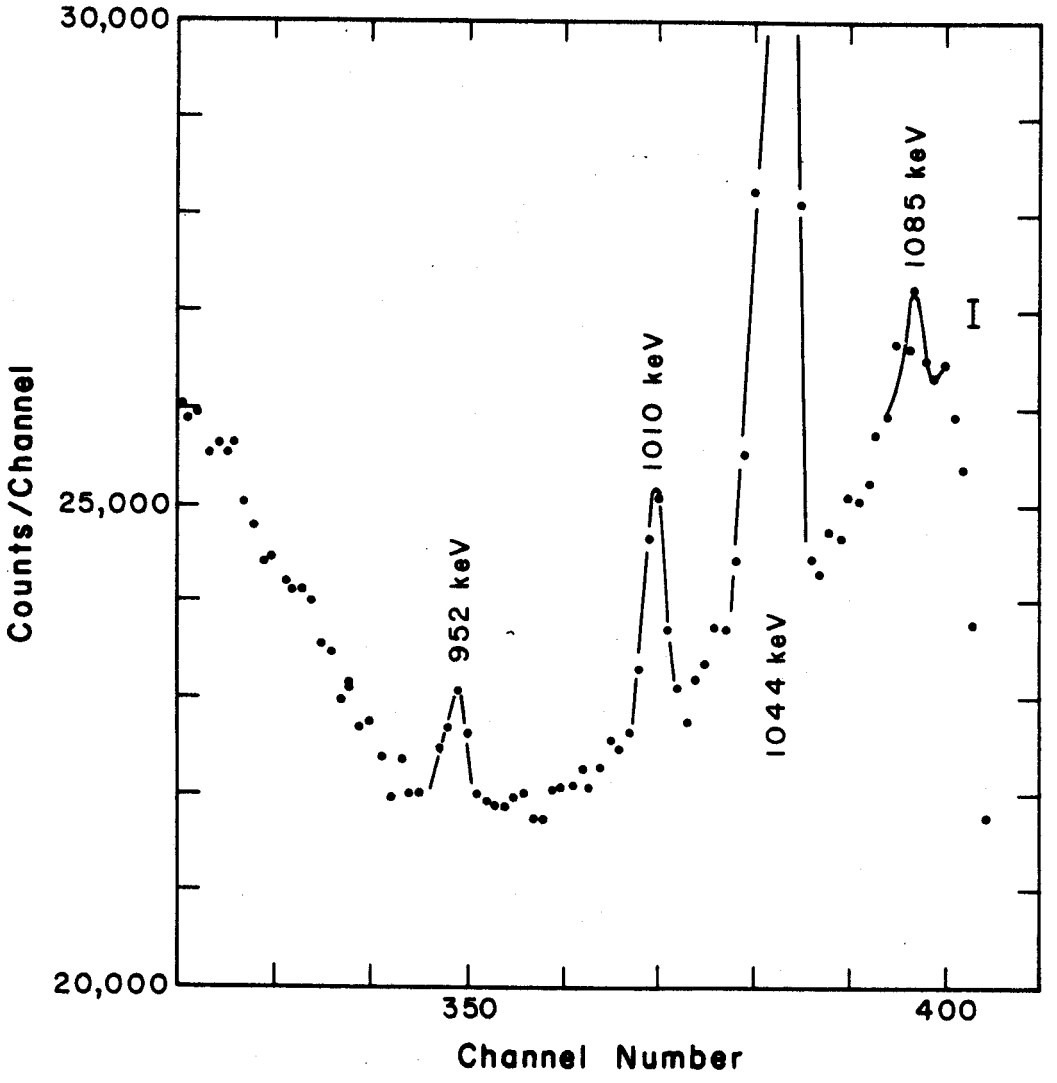

Figure 3b.--Weak gamma transitions observed with the Ge(Li) detector: 850-1100 keV.

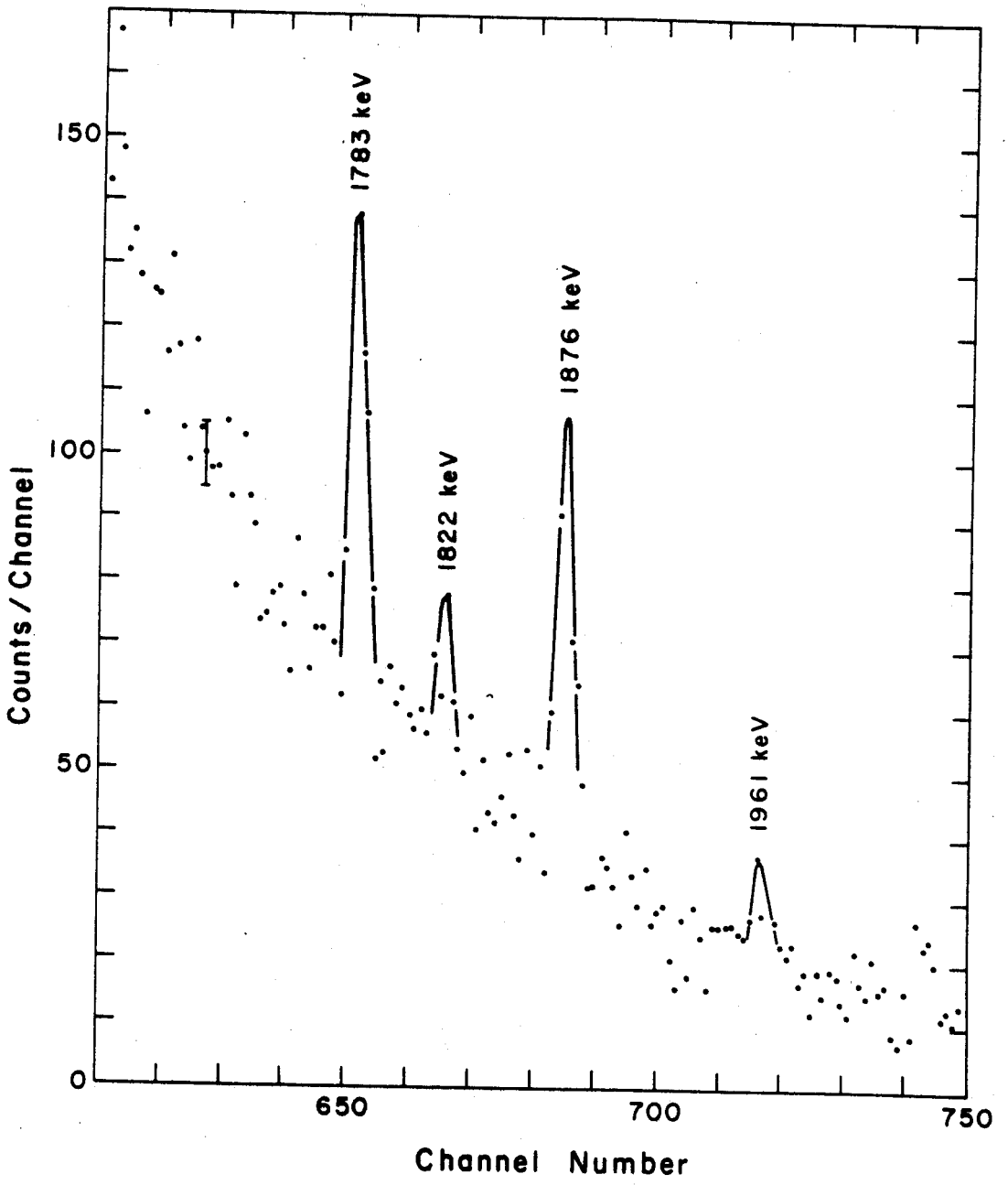

Figure 3c.--Weak gamma transitions observed with the Ge(Li) detector: 1675-2050 keV.

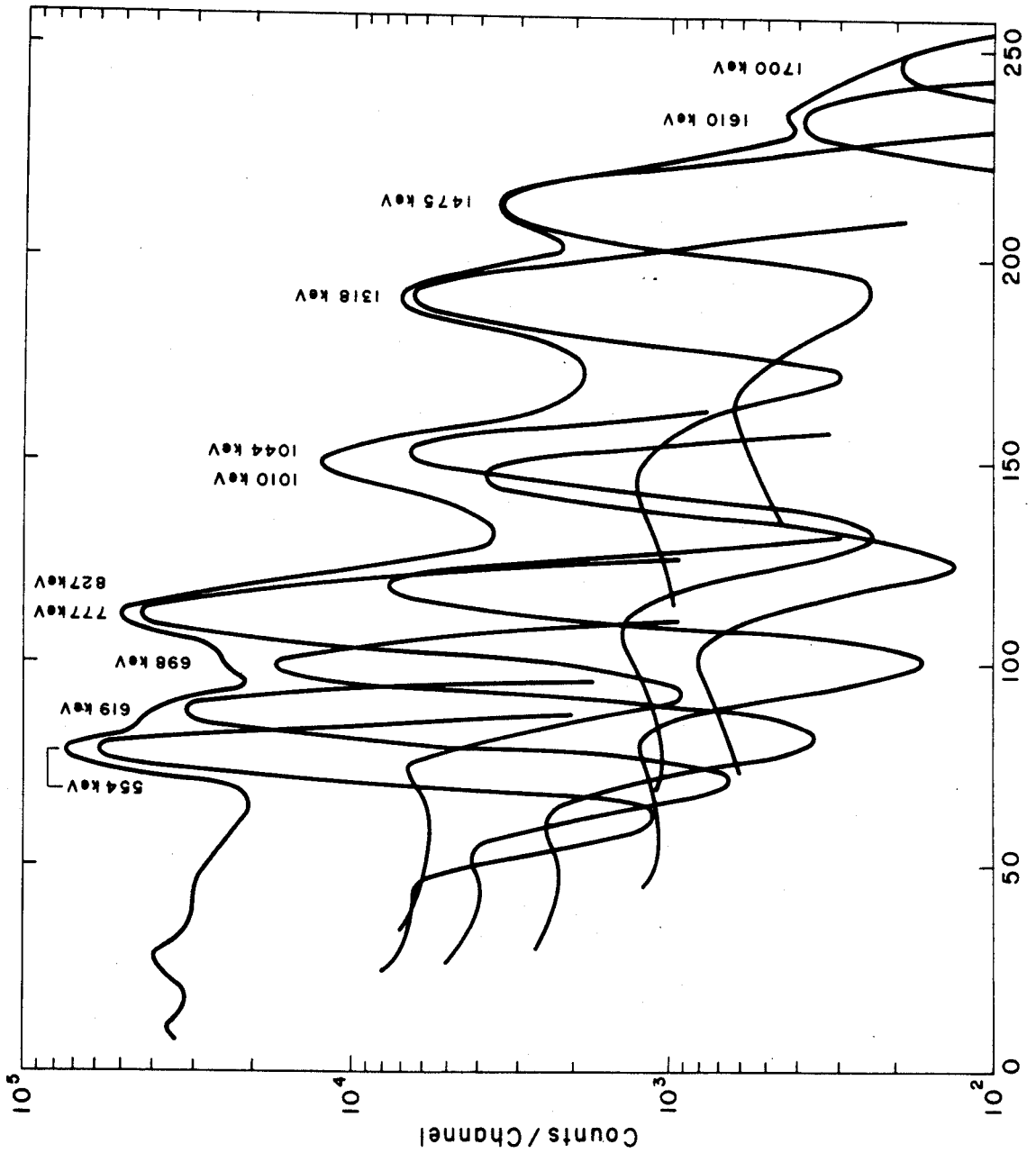

Figure 4.--Gamma singles spectra of ^{82}Br taken with 7.6 cm by 7.6 cm NaI(Tl) detector.

The gamma-ray intensities, relative to the 777 keV photon, were determined using photo-efficiency curves measured by Auble for the Ge(Li) detector (28) and by Heath for the NaI(Tl) detectors (42). The energies and relative intensities are also summarized in Table 3. Also listed in Table 3, for comparison, are the energies and relative intensities of the transitions reported by Hultberg and Hedgran (38). The results of the present measurements are in excellent agreement with the earlier data.

The gamma-ray energies determined from the Ge(Li) detector are considered to be more accurate than the energies determined from the internal conversion electron spectrometers. This is especially the case for the high energy transitions since the electron spectrometer had not been calibrated beyond 1500 keV and an extrapolation of the calibration curve was used there. The energies of the gammas that were determined with the Ge(Li) detector were obtained from a calibration curve determined from the well-known gamma-rays in ^{22}Na, ^{137}Cs, ^{60}Co, and ThC'' in separate experiments. The calibration curve was obtained by a least squares fit of a quadratic curve to the positions of peak centroids as described in Chapter 2. The energies determined in this way were consistent to well within one keV for the strong transitions for several different amplifier gain settings.

3.1.2. Gamma-gamma Coincidence

The gamma-gamma coincidence studies were made with NaI(Tl) detectors. It was not feasible to use the Ge(Li) detector because of the poor efficiency of the small volume Ge(Li) detector available at the time.

All of the previously reported coincidences between the strong gamma-rays (34-35) were observed in addition to coincidences for some of the weak transitions. Only the coincidences between the previously unobserved transitions will be discussed here.

3.1.2.A. Gamma Coincidences with the 1652 keV Gamma-ray.--The gamma spectrum in coincidence with the 1652 keV photopeak is shown in Figure 5. This spectrum has been corrected for chance coincidences. The 1652 keV gamma-ray is seen to be in coincidence with the 221 keV photon and possibly with the 777 keV photon. The peaks at 554, 619, and 1044 keV are the result of coincidences with the sum of the 777 keV photon with Compton scattered photons from the 1318, and 1475 keV gamma-rays and with the 828 keV photopeak. Multi-parameter coincidence spectra of the 1500-1800 keV region with the 400-850, and 650-1200 keV regions verify these assertions. In these measurements, the 554 and 1044 keV peaks were enhanced relative to the 777 keV peak in the coincidence spectra obtained when gating between 1550 and 1600 keV while the 777 keV peak was enhanced relative to the 554

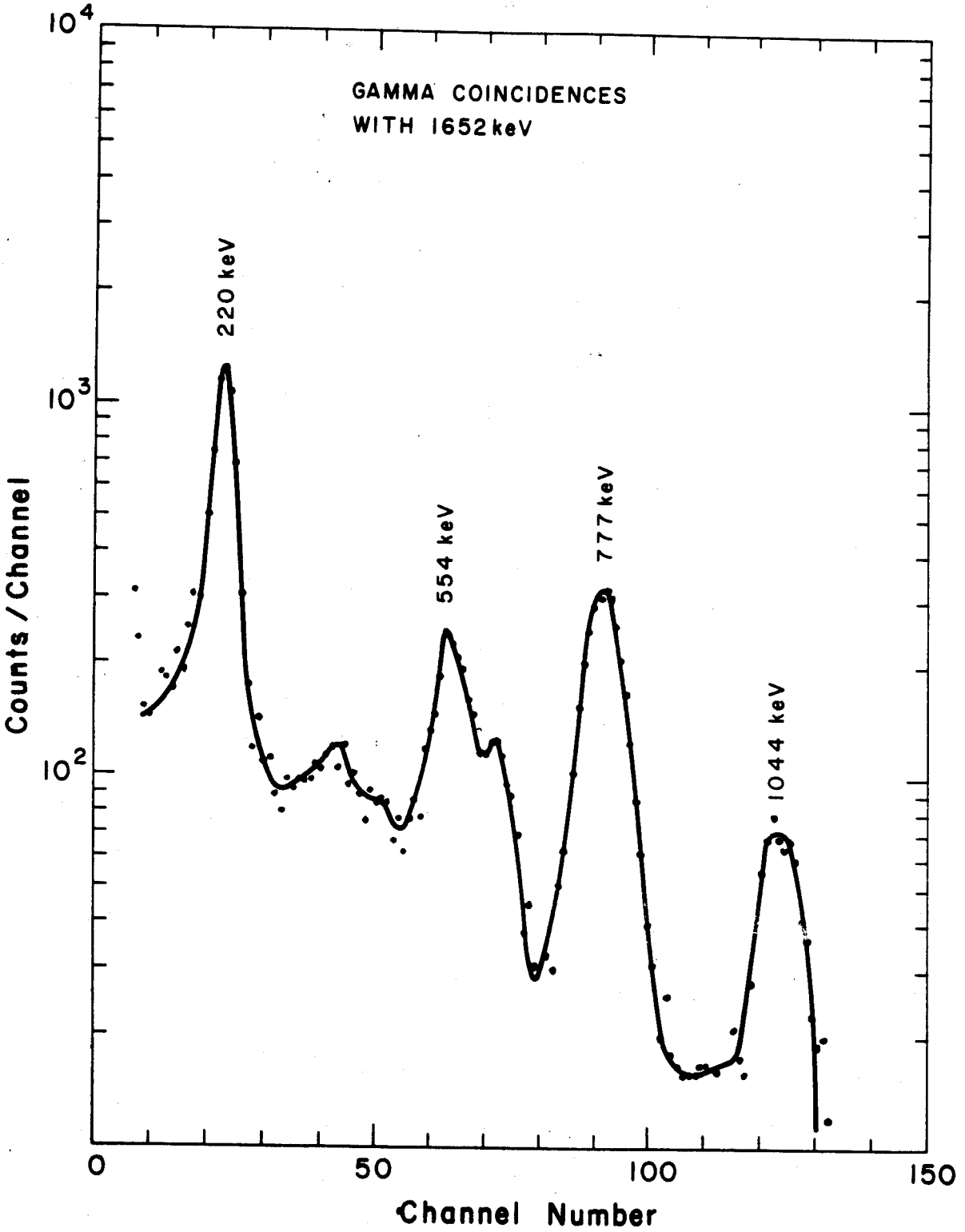

Figure 5.--Gamma spectrum in coincidence with the 1652 keV gamma ray. Both detectors were 7.6 cm by 7.6 cm NaI(Tl) crystals.

and 1044 keV peaks in the coincidence spectrum obtained when gating with the 1652 keV photopeak. It is therefore concluded that the 1652 keV gamma-ray is in coincidence with the 221 and 777 keV gamma-rays.

3.1.2.B. Coincidences with the 650 to 1200 keV Region.--Coincidences in this energy region were also studied in the two parameter mode of the 1024 channel analyzer. The spectrum obtained with coincidences between the 1044 keV photopeak and the 650-1200 keV region is shown in Figure 6A. The 1044 keV gamma-ray is seen to be in coincidence with the 1010 keV photons in addition to being in coincidence with the previously reported strong 777 and 828 keV transitions.

The coincidence spectrum measured between the 274 keV photopeak and the 800-1200 keV region is shown in Figure 6B and, for comparison, the coincidence spectrum between the 221 keV photopeak and the 800-1200 keV region is shown in Figure 6C. The 1044 keV gamma-ray is seen to be in coincidence with the 274 keV gamma-ray and the 221 keV gamma ray with that at 952 keV.

3.1.2.C. Coincidences with the 92 keV Gamma-ray.--The gamma spectrum in coincidence with the 92 keV gamma-ray is complicated because of the presence of interfering coincidences with the underlying Compton background. These interfering coincidences were minimized by subtracting

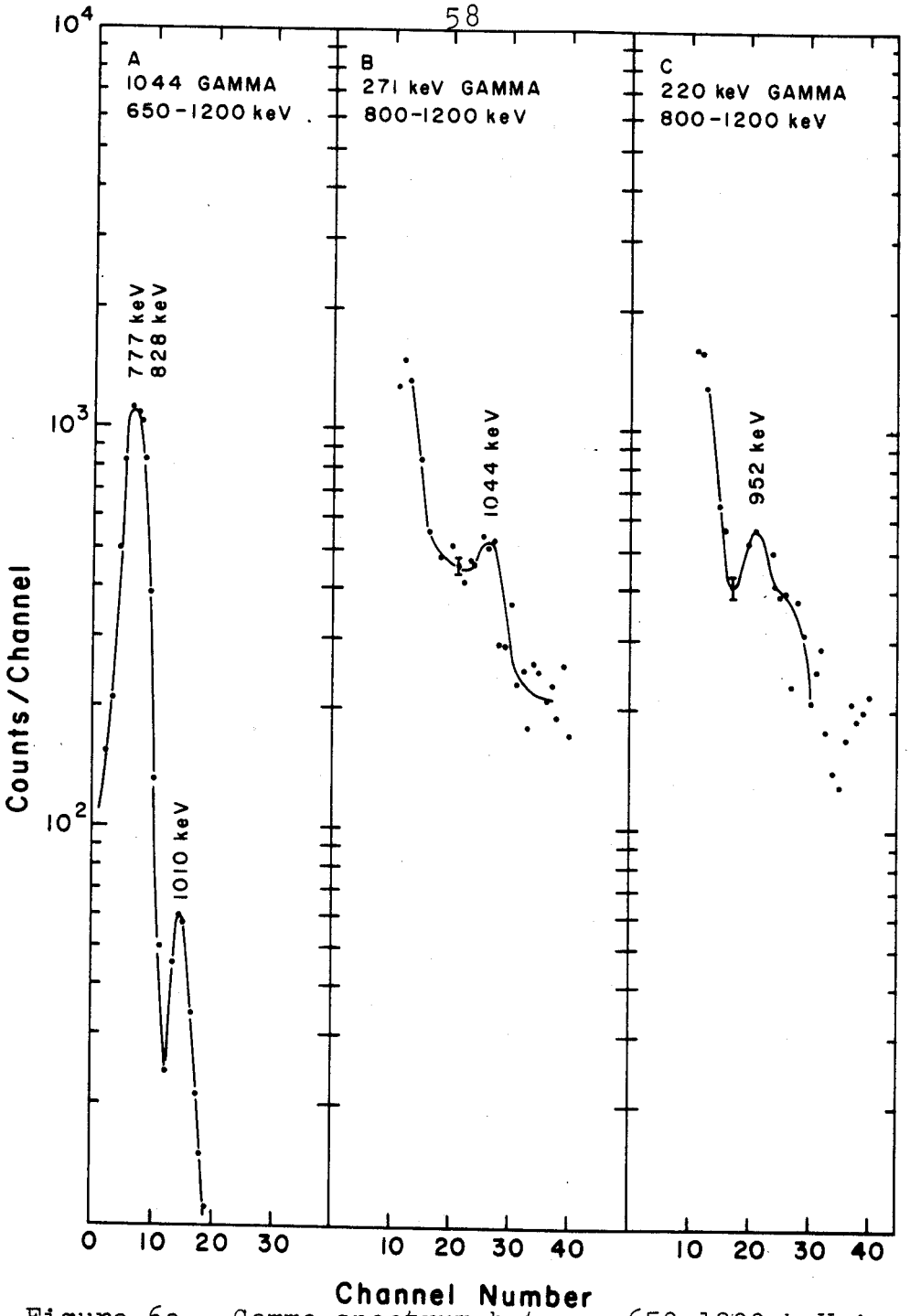

Figure 6a.--Gamma spectrum between 650-1200 keV in coincidence with 1044 keV photopeak. Both detectors were 7.6 cm by 7.6 cm NaI(Tl) crystals.

Figure 6b.--Gamma spectrum between 800-1200 keV in coincidence with 274 keV photopeak. Both detectors were 7.6 cm by 7.6 cm NaI(Tl) crystals.

Figure 6c.--Gamma spectrum between 800-1200 keV in coincidence with 221 keV photopeak. Both detectors were 7.6 cm by 7.6 cm NaI(Tl) crystals.

from the 92 keV coincidence spectrum a second coincidence spectrum. This second spectrum was taken under identical conditions except that 0.635 cm of copper was placed over the face of the NaI(Tl) crystal detecting the 92 keV gamma. The difference spectrum is shown in Figure 7. The 92 keV photon is thus seen to be in coincidence with the 1783, 1475, 1085, 777, and 698 keV gamma-rays. The excess of counts in the regions of 1318 keV is due to an incomplete subtraction of a large 1318 keV peak that was in coincidence with the underlying Compton background and a small gain shift that occurred between the two runs.

3.2. The Decay Scheme of ^{82}Br

The proposed decay scheme for ^{82}Br is presented in Figure 8. The previously reported states (34-38) at 777, 1475, 1821, 2094, 2429, and 2648 keV are consistent with the results of the present investigations. New states have been placed at 2832, 2652, and 2560 keV. The spin assignments shown in the figure are based on angular correlation experiments that will be described later.

The coincidences observed between the 1010-1044 keV gamma-rays are good evidence for the placing of a state at 2832 keV. This placement is supported by the 184 keV transition that was observed in the internal conversion electron spectrum.

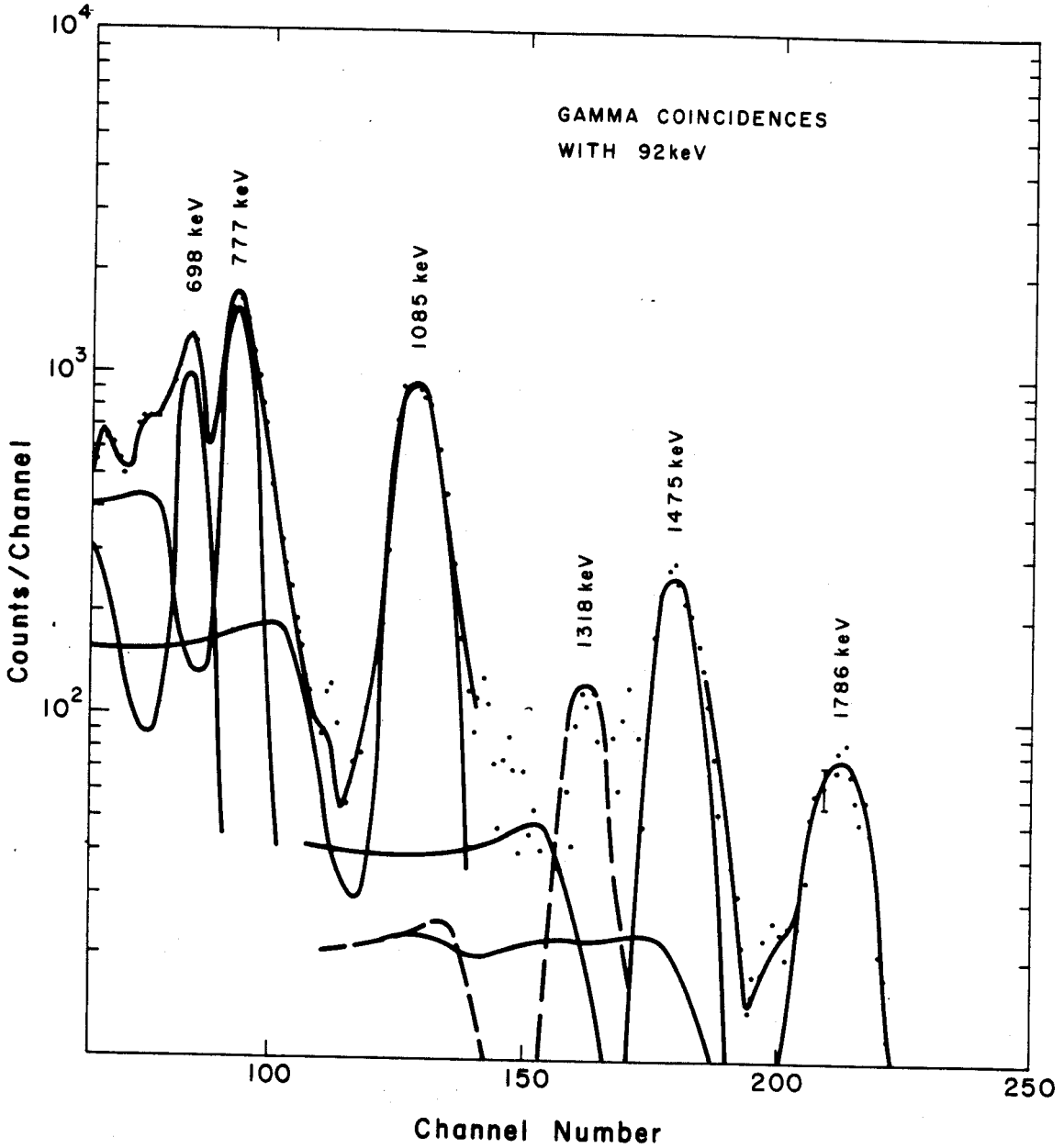

Figure 7.--Gamma spectrum in coincidence with 92 keV photopeak. This spectrum is the difference between the spectra obtained without and with a copper absorber over the 92 keV detector. The detector used to obtain this spectrum was a 7.6 cm by 7.6 cm NaI(Tl) crystal. The detector used for the 92 keV gamma was a 3.8 cm diam by 6 mm thick NaI(Tl) crystal.

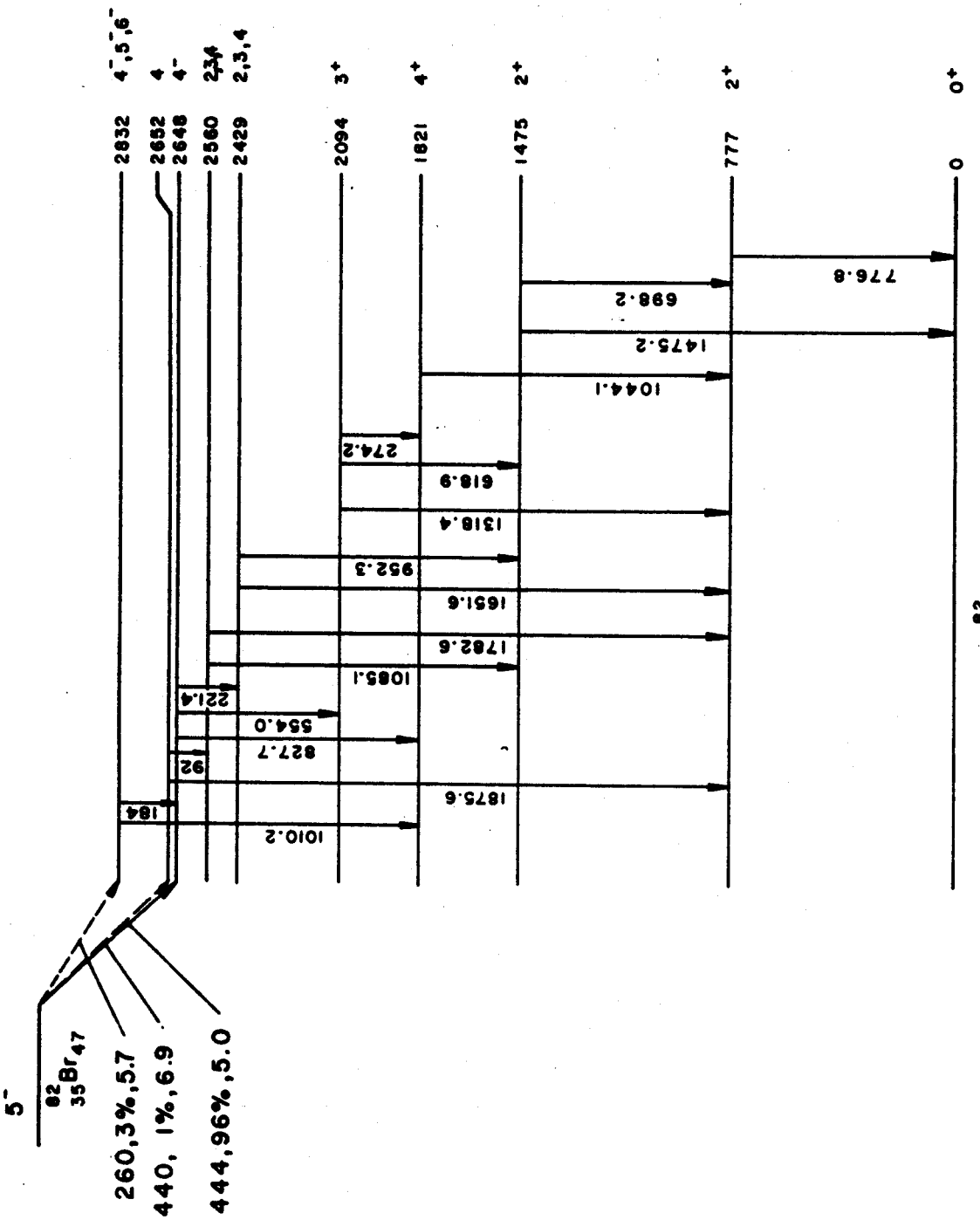

Figure 8.--Proposed decay scheme for ^{82}Br.

States are placed at 2652 and 2560 keV on the basis of energy sums and the coincidence spectrum with the 92 keV transition shown in Figure 7. The intensities of the photons in this coincidence spectrum support the proposed level scheme. The energy difference of 4 keV between the 2652 and 2648 keV states is considered to be outside the precision of the energy measurements of the gamma rays.

The state at 2429 keV, originally proposed by Kennett et al., (41) is consistent with the coincidences observed between the 221-1652 and 221-952 keV gamma rays.

The weak 452, 602, 1823, and 1961 keV gamma rays that were observed in the Ge(Li) detector could not be placed in the decay scheme with any consistency. It is possible, however, that the 452 keV photon is a transition between the 2648 keV state and one at 2196 keV that has been observed (43) in the decay of ^{82}Rb. The 1823 keV gamma could conceivably arise from summing of the 1044.1 and 776.8 keV gamma rays in the detector as the source was in contact with the Ge(Li) detector.

3.3. Directional Correlation Measurements

Directional correlations were measured for eight of the prominent gamma-ray cascades. The experimental procedures used for these measurements are described in Chapter 2.

Since most of the gamma rays were not resolved in the sodium iodide detectors, the coincidence spectra were

taken in the two parameter mode of the 1024 channel analyzer to facilitate the analysis of the data. The 32 x 32 channel mode enabled all eight correlation combinations to be taken in a series of three successive runs. The equivalent chance coincidence spectra were taken simultaneously as described in Chapter 2.

Table 4 lists the energy intervals to which the 32 x 32 channels were set for each run. The last column is the energy interval used in the data analysis to obtain the coincidence counting rate for each cascade.

3.3.1. Analyses of Directional Correlation Data

All of the correlation functions were obtained by fitting the data by least squares and were corrected for the finite geometry of the crystal using the corrections calculated by Yates (44).

In the analyses of the correlation functions to obtain the spin sequences and mixing ratios, the tables of Taylor and McPherson were used whenever one of the transitions was known to be pure (25). For the cases of double mixtures the method of Arns and Wiedenbeck was used (45). For the transitions of mixed multipole order with unobserved intermediate transitions, the method described by Fagg and Hanna was used (24).

The errors quoted include both statistical errors and those resulting from corrections for interfering

Table 4.--Energy intervals used for the analyses of the two parameter angular correlation data.

	32 x 32 channel multiparameter energy intervals		Energy intervals	
Cascade (in keV)	Detector 1 (in keV)	Detector 2 (in keV)	Detector 1 (in keV)	Detector 2 (in keV)
619-1475	1210-1510	425-715	1458-1491	618-636
554-1475			1458-1491	528-555
554-1318			1300-1333	528-575
828-1044	900-1410	650-950	1028-1060	827-845
1044-777			1028-1060	750-780
1318-777			1295-1337	750-780
698-777	625-930	675-950	760-780	670-690
828-777			760-780	830-850

coincidences. These errors were determined using a pessimistic ± 20% error in the relative intensities listed in Table 1.

3.3.1.A. The 1318-777 keV Correlation.--The 1318-777 keV gamma cascade is the only one for which there are no interferences from Compton background or unresolved photopeaks. The measured correlation function is

$$W_{1318-777}(\theta) = 1 - (0.027 \pm 0.007)\, P_2(\theta) - (0.079 \pm 0.014)\, P_4(\theta) \quad (1)$$

The interpretation here is simplified because the first excited state has been shown to be at 777 keV by Coulomb excitation (39) and nuclear resonance fluorescence (46). The spins and parities of the ground and first excited states of even nuclei are assumed to be 0^+ and 2^+, respectively. The values for A_2 and A_4 in equation (1) are consistent with the spin sequence* of 3(1,2)2(2)0 with a mixing ratio $\delta_{1318} = -4.40 \pm 0.9$. This is the only reasonable spin sequence that agrees with the correlation data.

3.3.1.B. The 698-777 keV and 828-777 keV Correlations.--The photopeaks for the 698, 777, and 828 keV gamma rays are not resolved. However, according to

*The numbers in the parentheses are the multipole orders, L, of the gamma transitions.

the decay scheme, the 698 keV gamma-ray is not in coincidence with the 828 keV gamma-ray. For these reasons, the two parameter spectrum was analyzed by dividing the "gating channels" into three regions: (a) the low energy side of the 698 keV photopeak, (b) the 777 keV photopeak, and (c) the high energy side of the 828 keV photopeak. The fraction of the 777 keV photons present in the spectra coincident with regions (a) and (c) can easily be subtracted after normalizing the high energy side of the 828 keV photopeak in the spectrum coincident with the 777 keV photopeak region, (b), to the high energy side of the 828 keV photopeak in the spectra coincident with regions (a) and (c). A small portion of the 828-777 and 698-777 keV coincidences are subtracted with this procedure. However, these will be subtracted in the same ratio as their respective correlation functions. The results will then be the same as multiplying the correlation function by a constant.

The resulting correlation function for the 698-777 keV cascade is

$$W(\theta)_{698\text{-}777} = 1 - (0.265 \pm 0.025)\, P_2(\theta) + (0.249 \pm 0.038)\, P_4(\theta) \quad (2)$$

The only spin sequence that agrees with these data is 2(1,2)2(2)0 with a mixing ratio of $\delta_{698} = -3.0 \pm 0.7$.

For the 828-777 keV cascade

$$W(\theta)_{828-777} = 1 + (0.149 \pm 0.029)\, P_2(\theta) + (0.002 \pm 0.044)\, P_4(\theta) \quad (3)$$

The analysis of this correlation function will be discussed with those of the 1044-777 keV and 828-1044 keV correlation functions (section 3.3.1.C.) since the ordering of these transitions is uncertain. A number of spin sequences are possible for the 828-777 cascade depending upon this order.

3.3.1.C. The 828-1044 keV and 1044-777 keV Correlations.--A technique similar to that described in section 3.3.1.B. can be used to obtain the 828-1044 keV correlation function. Both the 828 and 777 keV transitions are in coincidence with the 1044 keV gamma-ray. In addition, the 777 keV gamma-ray is in coincidence with the 1318 keV transition. The removal of interfering 777 keV coincidence in the 828 keV photopeak coincidence spectrum can be achieved by normalizing the 1318 keV photopeak in the 777 keV photopeak coincidence spectrum to the 1318 keV photopeak in the 828 keV photopeak coincidence spectrum and subtracting. The resulting correlation function for the 828-1044 keV cascade is

$$W(\theta)_{828-1044} = 1 + (0.190 \pm 0.027)\, P_2(\theta) - (0.028 \pm 0.047)\, P_4(\theta) \quad (4)$$

The 1044-777 keV correlation function can now be obtained from the spectrum coincident with the 1044 keV photopeak. The measured total angular correlation function has the form

$$W(\theta) = aW(\theta)_{1044-777} + bW(\theta)_{828-1044} + cW(\theta)_{1318-777} \quad (5)$$

where a, b, and c are constants which can be determined from the decay scheme in terms of the relative intensities given in Table 3. The correlation function for the 1318-777 keV cascade is included since the Compton component under the 1044 keV photopeak will contribute to the total 777 keV coincidences. The solution for the 1044-777 keV cascade is

$$W(\theta)_{1044-777} = 1 + (0.095 \pm 0.018)\, P_2(\theta) + (0.042 \pm 0.044)\, P_4(\theta) \quad (6)$$

Since the order of the 828-1044 keV gamma rays are, at this point, uncertain, the analyses of the correlation functions given by equations (3), (4), and (6) were made with the order of emission of the gamma rays arranged in two successive orders: (a) 828-1044-777 keV and (b) 1044-828-777 keV. The possible arrangements are shown in Figure 9. It is to be noted that in either case, one of the three correlation functions will involve an unobserved transition.

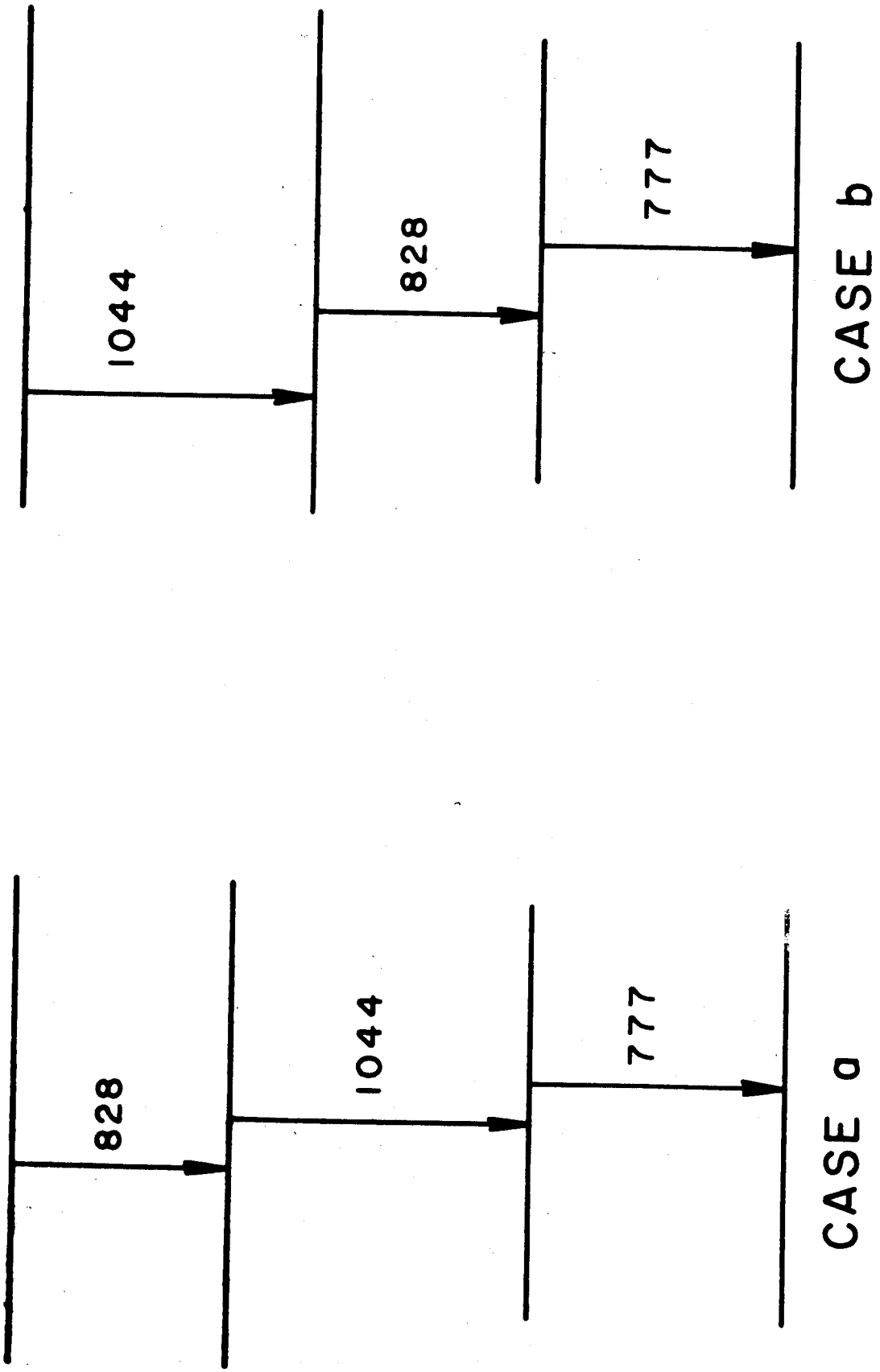

Figure 9.--Possible orders of 828-1044-777 keV transitions.

For case (a), the correlation function for the 1044-777 keV cascade, equation (6), yields possible spin sequences 4(2,3)2(2)0, with a mixing ratio δ_{1044} = 0.02 $\pm$ 0.03, and 5(3,4)2(2)0, with a mixing ratio of δ_{1044} = 0.2 $\pm$ 0.3.

The correlation function for the 828-777 keV cascade, equation (3), is consistent with a spin sequence of 4(1,2)4[(2)]2(2)0 with a mixing ratio δ_{828} = -0.1 $\pm$ 0.1. The notation [(2)] indicates the multipole order of the unobserved 1044 keV transition.

The spin sequence 5(3,4)2(2)0 for the 1044-777 keV cascade was found to be inconsistent with the 828-777 keV correlation function.

The correlation function for the 828-1044 keV cascade, equation (4), yields a spin sequence of 4(1,2)4(2,3)2 with a mixing ratio $\delta_{828} = -0.02\ ^{+0.09}_{-0.03}$ and δ_{1044} = -0.1 $\pm$ 0.1. This is the only spin sequence consistent with the correlation function. This function is independent of the order of emission of these successive gamma rays.

Case (b) was found to give inconsistent results. The 828-777 keV correlation coefficients satisfy spin sequences of 2(1,2)2(2)0, with a mixing ratio δ_{828} = -0.13 $\pm$ 0.2, and 3(1,2)2(2)0, with a mixing ratio δ_{828} = -0.33 $\pm$ 0.03; however, the 1044-777 keV and 828-1044 keV correlation functions cannot be satisfied for

any possible combination of spins based upon the 828-777 keV cascade results. It is therefore concluded that the ordering of the transitions is 828-1044-777 keV successively, namely case (a).

3.3.1.D. The 554-1318 keV Correlation.--The 554-1318 keV correlation measurements contain coincidences with the Compton background from the 777 and 1475 keV photons. Corrections for these were made in the same manner as in section 3.3.1.C. for the 1044-777 keV correlation function. The correlation function for the 554-1318 keV cascade is found to be

$$W(\theta)_{554-1318} = 1 - (0.065 \pm 0.012)\, P_2(\theta) - (0.007 \pm 0.024)\, P_4(\theta) \quad (7)$$

The correlation data are consistent with the spin sequence of 4(1,2)3(1,2)2 with $\delta_{554} = 0 \pm 0.1$ and $\delta_{1318} = 5.4\ ^{+2.1}_{-1.4}$ or $\delta_{1318} = 0.45 \pm 0.07$. The sign of δ_{1318} is now changed since the 1318 keV gamma-ray is now the second transition in the cascade (47). The mixing ratio $\delta_{1318} = 0.45 \pm 0.07$ may be discarded since it is not consistent with the mixing ratio for the 1318 transition obtained from the 1318-777 keV cascade. This is the only possible spin sequence that satisfies the correlation function.

3.3.1.E. The 554-1475 and the 619-1475 keV Correlations.--The photopeaks of the 554 and 619 keV gamma-rays are not resolved in the spectrum obtained in

coincidence with the 1475 keV photons. However, there are no underlying Compton coincidences contributing. Taking slices on the high energy side of the 619 keV and the low energy side of the 554 keV photopeaks in the multi-parameter spectrum, the coincidence data can be expressed with the equations.

$$W(\theta)_{554\ \text{slice}} = a_1 W(\theta)_{554\text{-}1475} + b_1 W(\theta)_{619\text{-}1475}$$

and

$$W(\theta)_{619\ \text{slice}} = a_2 W(\theta)_{554\text{-}1475} + b_2 W(\theta)_{619\text{-}1475}$$

The coefficients a_1, a_2, b_1, and b_2 can be determined from the relative intensities listed in Table 3. The coefficients a_2 and b_1 are made relatively small by the choice of the gating regions.

The results for the 619-1475 keV cascade is

$$W(\theta)_{619\text{-}1475} = 1 + (0.138 \pm 0.031)P_2(\theta) - (0.094 \pm 0.033)P_4(\theta) \quad (8)$$

This correlation function is consistent with possible spin sequences of 3(1,2)2(2)0 with a mixing ratio $\delta_{619} = -2.0 \pm 0.3$ and 4(2,3)2(2)0, with the mixing ratio $\delta_{619} = -1.4 \pm 0.1$.

For the 554-1475 keV cascade, the result is

$$W(\theta)_{554\text{-}1475} = 1 - (0.031 \pm 0.017)P_2(\theta) + (0.028 \pm 0.029)P_4(\theta) \quad (9)$$

If the mixing ratio is taken to be $\delta_{619} = -2.0 \pm 0.03$ for the unobserved 619 keV photons, then the spin sequences consistent with the 554-1475 keV correlation function is 4(1,2)3[(1,2)]2(2)0, with mixing ratio $\delta_{554} = 0.0 \pm 0.2$. This spin sequence is in good agreement with the results obtained in section 3.3.1.D.

3.3.1.F. The Remaining Correlation Functions.--A brief attempt was made to measure the four angular correlations of the 554-619, 554[619]698, 619-698, 619[698]777 keV cascades. The resolution of the detectors and the presence of the underlying Compton backgrounds from the higher energy cascades did not allow an accurate determination of the correlation functions. Therefore, these results are not reported here.

3.3.2. Summary of Angular Correlation Measurements and the Resulting Spin Assignments

The present results are summarized in Table 5 along with the correlation functions reported by other investigators for some of the cascades (34, 35, 40). The A_2 and A_4 coefficients are listed with the spin sequences and mixing ratios. The sequences and ratios listed here are only those that give a consistent decay scheme.

Comparisons of the correlation functions obtained in this work with those reported by other investigators, show that agreement, in general, is good to within the reported errors.

Table 5.--Summary of ^{82}Kr angular correlation data.

Cascade Energies, keV	Correlation Coefficients A_2	A_4	Assigned Spin Sequence	Mixing Ratios[d]
1318 - 777	-0.027 ± 0.007	-0.079 ± 0.014[a]	3(1,2)2(2)0	$\delta_{1318} = -4.40 \pm 0.9$
	-0.020 ± 0.008[a]	-0.085 ± 0.018[a]		
	-0.011 ± 0.008[b]	-0.074 ± 0.013[b]		
698 - 777	-0.265 ± 0.025	+0.249 ± 0.38	2(1,2)2(2)0	$\delta_{698} = -3.0 \pm 0.7$
	-0.27 ± 0.06[c]	0.25 ± 0.08[c]		
828[1044]777	+0.149 ± 0.029	+0.002 ± 0.044	4(1,2)4[(2)]2(2)0	$\delta_{828} = -0.1 \pm 0.1$
	+0.18 ± 0.03[b]	+0.018 ± 0.048[c]		$\delta_{1044} = 0 \pm 0.1$
828 - 1044	+0.190 ± 0.027	-0.028 ± 0.047	4(1,2)4(2,3)2	$\delta_{828} = -0.02\ ^{+0.09}_{-0.03}$
	+0.17 ± 0.01[b]	+0.009 ± 0.019[c]		$\delta_{1044} = -0.1 \pm 0.1$
1044 - 777	0.095 ± 0.018	+0.042 ± 0.044	4(2,3)2(2)0	$\delta_{1044} = 0.02 \pm 0.03$
	0.088 ± 0.019	+0.007 ± 0.028[c]		
554 - 1318	-0.065 ± 0.012	-0.007 ± 0.024	4(1,2)3(1,2)2	$\delta_{554} = 0 \pm 0.1$
	-0.064 ± 0.006[a]	-0.005 ± 0.013		
	-0.08 ± 0.03[b]	+0.01 ± 0.01[b]		if $\delta_{1318} = +5.4\ ^{+2.1}_{-1.4}$
619 - 1475	0.138 ± 0.031	-0.094 ± 0.033	3(1,2)2(2)0	$\delta_{619} = -2.0 \pm 0.3$
	0.128 ± 0.007[a]	-0.031 ± 0.017[a]		
	0.106 ± 0.003[b]	-0.052 ± 0.010[b]		
554[619]1475	-0.031 ± 0.017	+0.028 ± 0.029	4(1,2)3[(1,2)]2(2)0	$\delta_{554} = 0.0 \pm 0.2$
	-0.010 ± 0.021[a]	+0.028 ± 0.038[a]		$\delta_{619} - 2.0 \pm 0.3$
	-0.039 ± 0.008[b]			

[a]Reference 34. [b]Reference 35. [c]Reference 40.

[d]The mixing ratios are those that were obtained from the corresponding correlation coefficients that are reported in this work. Only those yielding a consistent decay scheme are given here.

Table 6 lists the internal conversion coefficients that have been reported by other investigators (34, 35, 37) and the multipole orders determined from the correlation functions and internal conversion data.

From these data, unique spin assignments for each state can be made:

(a) The 777 keV State. The spin of this state was assumed to be 2^+ because it is the first excited state of an even-even nucleus. All of the correlation data are consistent with this spin assignment. The internal conversion coefficient for the 777 keV transition (34, 35, 37) is in agreement with the theoretical conversion coefficient for an E2 transition.

(b) The 1475 keV State. The angular correlation functions obtained from the 619-1475, 554-1475, and 698-777 keV cascades are all consistent for a spin assignment of 2 for this state. On the basis of the internal conversion coefficients (34, 35, 37) for the 1475 keV and 698 keV transitions, the assigned parity is positive.

(c) The 1821 keV State. The correlation functions for the 828-1044, 1044-777, and 828-777 keV cascades are consistent with a spin assignment of 4 for the 1821 keV state. The possible spin sequence of 5(3,4)2(2)0, determined from the 1044-777 keV correlation that was discussed in section 3.3.1.C. can be eliminated since it does not lead to any possible spin states that will

Table 6.--Summary of ^{82}Kr internal conversion coefficients, mixing ratios, and multipole order.

Transition Energy	$\alpha_K \times 10^3$ Experimental	$\alpha_K \times 10^3$ Theoretical[a]	δ	Multipole Order
554 keV	0.68 ± 14%[b] 0.70 ± 0.10[c] 0.673[d]	0.676	0.0 ± 0.1	E1
619 keV	1.60 ± 11%[b] 1.3 ± 0.2[c] 1.23[d]	1.40	2.0 ± 0.3	0.2M1 + 0.8E2
698 keV	1.1 ± 15%[b] 0.81 ± 0.11[c] 1.08[d]	1.046	3.0 ± 0.7	0.1M1 + 0.9E2
777 keV	1.00 ± 20%[b] 0.81 ± 0.10[c]	0.822	∞[e]	E^2
828 keV	0.32 ± 30%[b] 0.29 ± 0.04[c] 0.356[d]	0.282	0.0 ± 0.1	E1
1318 keV	0.18 ± 11%[b] 0.24 ± 0.03[c] 0.302[d]	0.245	4.4 ± 0.9	0.05M1 + 0.95E2
1475 keV	0.18[b] 0.21 ± 0.3[c] 0.137[d]	0.188	∞[e]	E2

[a]The theoretical conversion coefficients are those calculated using the multipole order and mixing ratios listed for each transition. The multipole orders and mixing ratios are from the angular correlation data.

[b]Reference 34.

[c]Reference 35.

[d]Reference 37.

[e]Assumed value.

satisfy the 828-777 and 828-1044 keV correlation functions. In addition, the life-time for such a transition would be much longer than the limit of 0.06 nsec reported by Flanger and Schneider (48). The internal conversion coefficient (34, 35, 37) of the 1044 keV transition indicates that the parity is positive.

(d) The 2094 keV State. On the basis of the possible spin sequences determined from the 554-1318, 1318-777, and 619-1475 keV correlation functions, a spin of 3 is assigned to the 2094 keV state. The possible spin of 4 for the 2094 keV state determined from the 619-1475 keV correlation function, discussed in section 3.3.1.E., can be eliminated since it is not consistent with the other correlation functions. Also, the mixing ratio for the 619 keV transition for this case would give approximately 70% octupole radiation which would be inconsistent with the lifetime and internal conversion coefficient (34, 35, 37). The internal conversion coefficients of the 1318 and 619 keV transitions indicate the parity of this state is positive.

(e) The 2648 keV State. All of the correlation functions for transitions from the 2648 keV state are consistent with a spin assignment of 4. The internal conversion coefficients of the 554 and 828 keV transitions indicate that the 2648 keV state has negative parity (34, 35, 37).

3.4. Other Recently Reported Works

Since the completion of the above experimental studies of ^{82}Br in 1965 and the publication of a report on the results (49), a number of papers have appeared on the same activity. These results are discussed briefly below.

Reidy and Wiedenbeck (50) used a 2m Ge curved-crystal spectrometer to accurately measure a number of the gamma ray energies. They report the energies: 92.19, 221.5, 273.5, 554.3, 619.2, 698.3, 776.6, 827.8, 1044.3, 1317.5, and 1474.3. The agreement is seen to be excellent except for that with the 1474 keV transition. In general, Ge(Li) detectors are thought to be more accurate in this energy region than are bent crystal spectrometers.

S. Raman (51), using a 0.22 cm^3 Ge(Li) detector with a 2.2 mm depletion depth, has studied the decay of ^{82}Br. He reports gamma rays at 94 $\pm$ 2, 138 $\pm$ 4, 222 $\pm$ 2, 274 $\pm$ 2, 554 $\pm$ 0.6, 617.9 $\pm$ 0.8, 697.7 $\pm$ 1, 775.6 $\pm$ 0.8, 951 $\pm$ 2, 1008 $\pm$ 2, 1043.3 $\pm$ 0.8, 1317.8 $\pm$ 0.7, 1473.1 $\pm$ 0.9, 1649.5 $\pm$ 2.5, 1778 $\pm$ 3, 1868 $\pm$ 2, 1953 $\pm$ 2, and 2057 $\pm$ 5. Agreement is seen to be fair except for the high energy gamma rays. Unfortunately, Raman does not report any details as to how the energies were determined or that he considered the existence of non-linearities in his apparatus. Such non-linearities have since been found to be common place (52). Raman proposes a decay scheme with states at 0,776, 1474, 1820, 1953, 2093, 2426,

2554, 2647, and 2828 keV. Some of the differences between this decay scheme and the one reported in this thesis can be attributed to the discrepancies in the reported energies.

Gfirtner, Reiser and Schneider have reported some similar Ge(Li) measurements (53) on ^{82}Br. The scheme they report is similar to that of Raman. However, they also do not give any details as to the method of calibration which makes comparisons difficult.

Most recently, Hsu and Wu have reported their work (54) with a 1cm^3 Ge(Li) detector. They report gammas at 93, 138, 222, 274, 553, 606, 619, 698, 777, 827, 951, 1008, 1044, 1081, 1318, 1475, 1650, 1778, and 1955 keV and place states at 0, 777, 1475, 1820, 1955, 2095, 2426, 2555, 2648, and 2828 keV. Again no details are given as to the energy measurements and calibrations.

In the present measurements, non-linearities were carefully accounted for by calibrating the counting system with sources of gamma rays with well-known energies. The non-linearities were found to be large enough to easily account for the discrepancies between the measurements reported in this thesis and those listed above. Non-linearities of this size are fairly common in the field.

3.5. Discussion of the Decay Scheme of ^{82}Br

It is interesting that the 2648 keV state has an even spin and odd parity. The ground state spin of ^{82}Br has been reported (55) to be 5^- with the negative parity assignment based upon the log ft value for the beta decay and the negative parity of the 2648 keV state. The ground state spin of ^{82}Br can be described by a $g_{9/2}$ neutron coupling to a $p_{3/2}$ proton hole state and is consistent with the weak Nordheim rule. The even spin and odd parity of the 2648 keV state can be accounted for if, in the beta decay, the $g_{9/2}$ neutron is converted to a $g_{9/2}$ proton which then couples to the $p_{3/2}$ proton hole. A similar 4^- state has recently been observed by Hendrie and Farwell (56) and by Day, Blair, and Armstrong (57) in ^{90}Zr at 2.74 MeV. They interpret this state as arising from coupling $p_{1/2}$ and $g_{9/2}$ proton states.

It has been observed that the beta decay of ^{82}Br is nearly 100% to the 2648 keV state in ^{82}Kr. An upper limit of 0.6% has been placed (35) upon the beta decay to states lower than 2648 keV. However, on the basis of a calculated log ft for a first forbidden beta decay to the 4^+, 1821 keV state, the branching ratio to this state should be approximately 40%. The branching ratio to the 3^+, 2094 keV state is similarly estimated to be less than 0.5%. The fact that no branching has been observed to the 1821 keV state could indicate that this state is not a simple shell model state.

The characters of the 2832, 2652, 2560, and 2429 keV states are uncertain since the spins and other properties of these states are unknown. However, limits may be placed upon their spins based upon the transitions involving them. The spin and parity assignments of 4^-, 5^-, or 6^- for the 2832 keV state are based upon the log ft = 5.7 for the beta decay to this state and on the fact that this state gamma decays to the 4^-, 2648 keV and 4^+, 1821 keV states. Similarly, a spin assignment of 4, for the 2652 keV state is consistent with the log ft = 6.8 for the beta decay to this state. The spin assignments of 2, 3, or 4 for the 2560 keV state are based upon the gamma decays from this state to the 2^+ states at 1475 keV and 777 keV. The spin assignments of 2, 3, or 4 for the 2429 keV state are based upon the gamma decay of this state to the 1475 keV and 777 keV states and upon the fact that the spin 4^-, 2648 keV state gamma decays to the 2429 keV state.

The ordering and spacings of the strongly excited states in ^{82}Kr are quite similar to those predicted by the non-axial rotator model of Davydov and coworkers (4, 6). It is interesting to compare some of the relative transition probabilities that were determined in this and other recent work (46) with the predictions of this model (4, 6). This is done by comparing the "non-axiality" parameter γ calculated from the transition probabilities

with that calculated from the energies of the states (18).

Davydov and Chaban have considered the interaction of rotation and vibration in non-axial even-even nuclei and have shown that when the "non-adiabaticity" parameter $\mu \lesssim 0.5$ the reduced E2 transition probabilities are very nearly equal to those predicted by Davydov and Filippov who did not take this interaction into account (5). To first order, the effect of the "non-adiabaticity" is to cause a change in the "non-axiality" parameter γ and thereby change the reduced E2 transition probabilities, B(E2). Klema, Mallmann and Day (17) have shown that the energy of the 4^+ state at 1821 keV can be described in terms of the ratio of the energies of the spin 2' and 2 states and the parameters $\gamma = 27.7° \pm 0.2°$ and $\mu = 0.450 \pm 0.002$ and that of the 3^+ state at 2094 keV by $\gamma = 29.0° \pm 0.1°$ and $\mu = 0.38 \pm 0.02$. Thus, the Davydov-Filippov transition probabilities are expected to be applicable.

The ratio of the B(E2) for the 698 keV and 1475 keV transitions from the second 2^+ state is

$$\frac{B(E2;\ 2' \rightarrow 2)}{B(E2;\ 2' \rightarrow 0)} = 60 \pm 10$$

This corresponds to a $\gamma = 27.1° \pm 0.1°$ which is in fair agreement with the values obtained by Klema et al, (17)

for the 1821 and 2094 keV states that were quoted above. Using the B(E2) that was recently measured for the 777 keV first excited state in a nuclear resonance fluorescence experiment by Beard (46) and the non-axiality parameter γ one can estimate (4) the intrinsic quadrupole moment Q_o, and, thereby, the deformation parameter β. For $\gamma = 27.1°$, $Q_o = 1.5 \times 10^{-24} cm^2$ and $\beta = 0.2$. A nuclear radius of $R = 1.2 \times 10^{-13} A^{1/3} cm$ was used. These are in reasonable agreement with the Q_o and β values obtained for other nuclei in this mass region (4, 58).

The results of Davydov and Filippov can also be used to calculate the ratio of the reduced E2 transition probabilities for the transitions from the 2094 keV 3^+ state to the 1475 keV $2'^+$ and 777 keV 2^+ states (4). The transitions involved are the 619 and 1318 keV gammas. The experimental ratio

$$\frac{B(E2;\ 3\rightarrow 2)}{B(E2;\ 3\rightarrow 2')} = 0.017 \pm 0.005$$

which corresponds to $\gamma = 27.3° \pm 0.2°$. This is somewhat lower than 29.0° obtained for the 2094 keV state by Klema et al., from energetics.

CHAPTER IV

THE DECAY SCHEME OF ^{83}Sr

Talmi and Unna, using shell model configurations with the assumption that the nuclear potential is due to two-body effective interactions between nucleons, have made calculations (7) to predict the characters of the ground and first excited states of several strontium isotopes. At the same time, these authors noted the lack of experimental data for isotopes in this mass region. The present work was motivated by a desire to extend the data, as well as to test some of the results of their calculations for ^{83}Sr.

The first investigation reported only three transitions of 40, 385, and 755 keV in addition to positrons (59) as belonging to the decay of ^{83}Sr. Preliminary investigations by Maxia, Kelly, and Horen (60) have indicated that the decay of ^{83}Sr is somewhat more complex with observed transitions at 40, 375, 408, 770, 1160, 1560, and 1960 keV. Later, Reddy, Johnston, and Jha (61) presented data in agreement with Maxia et al., and placed levels at 40, 380, 480, 1160, 1560, 1960, and 2120 keV for ^{83}Rb. These data were all recorded with NaI(Tl) detectors.

It was soon evident from our early gamma-gamma coincidence data taken with NaI(Tl) detectors that the decay scheme was much more complex. We have used high resolution Ge(Li) detectors in singles and coincidence configurations in order to perform a more complete investigation. Some sixty transitions have been identified as belonging to ^{83}Sr decay and fitted into a complex decay scheme.

4.1. Source Preparation

The strontium-83 activities were produced from stable isotopes by means of two different nuclear reactions. The early gamma ray measurements were made using sources produced by bombarding arsenic metal with 10.4 MeV/nucleon ^{12}C ions in the Lawrence Radiation Laboratory HILAC. Later sources were produced by bombarding rubidium chloride with 37 to 42 MeV protons from the Michigan State University cyclotron.

In both cases the strontium activities were separated chemically by precipitating the strontium with $SrCl_2$ carrier in chilled fuming nitric acid. Small amounts of ^{82}Sr and ^{85}Sr were present in the sources from the HILAC bombardment, whereas only the ^{85}Sr contaminant was present in the sources prepared with the cyclotron bombardments.

The ^{83}Sr gamma spectra obtained from the sources produced from the two different nuclear reactions appeared to be identical.

4.2. Experimental Results

4.2.1. The Gamma-Ray Singles Spectrum

The gamma-ray singles spectrum taken with a Ge(Li) detector of 3 cm^3 sensitive volume and resolution of 3 keV for the 662 keV ^{137}Cs photon is shown in Figure 10A and 10B. The low energy part of the spectrum, taken with an expanded gain, is shown in Figure 10A while the high energy portion is shown in Figure 10B.

The energies of the observed transitions are listed in Table 7 along with their relative intensities. The energies of the more intense transitions were determined from spectra taken with ^{83}Sr sources mixed with photon emitters containing transitions of well known energies (21). These energies are listed in Table 2, in Chapter 2. The technique used to determine the energy calibration curve was to least squares fit the peak centroids of the well-known transitions to a quadratic equation after the background had been subtracted from under the peaks as described in Chapter 2. The deviations of the energies of the calibration transitions from the quadratic fit were never greater than 0.1 keV. The energies of the low intensity gamma-rays were similarly determined using the

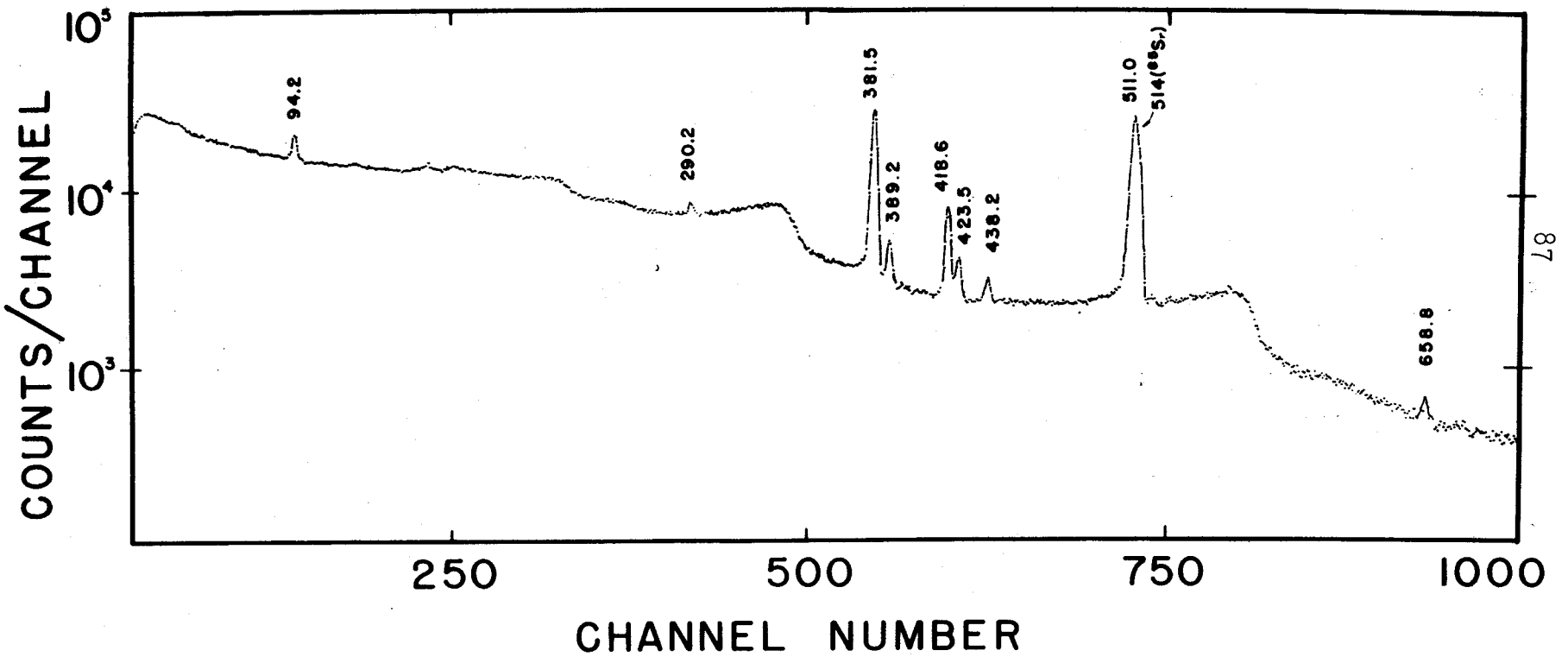

Figure 10a.--Gamma singles spectrum of ^{83}Sr taken with a 3 cm^3 Ge(Li) detector. Low energy portion.

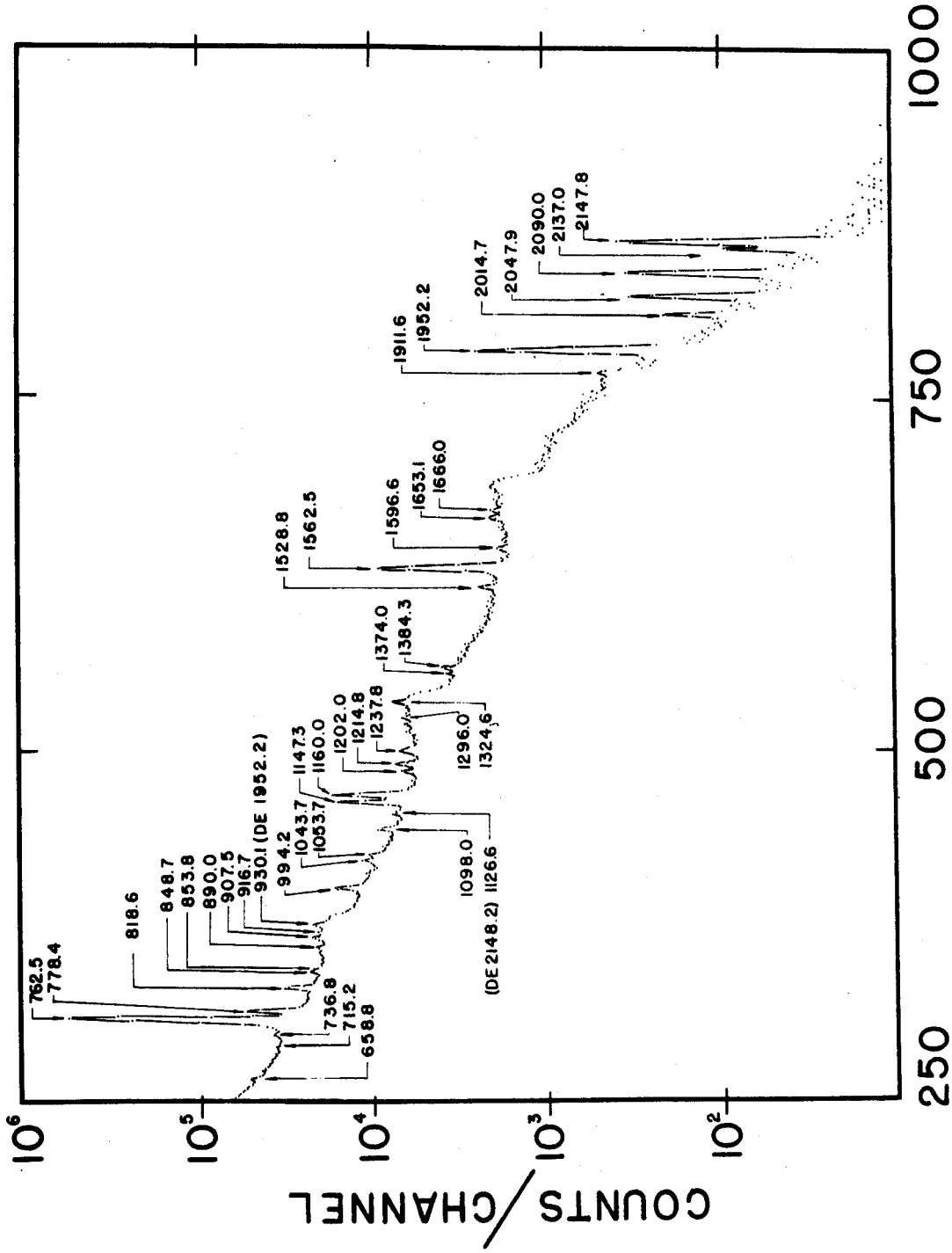

Figure 10b.--Gamma singles spectrum of ^{85}Sr taken with a 3 cm^3 Ge(Li) detector. High energy portion.

Table 7.--Energies and relative intensities of transitions from the decay of ^{83}Sr.

Energy (keV)	Relative Photon Intensity[a] Ge(Li)	NaI(Tl)
42.3 ± 0.1[b]		5.2
94.2 ± 0.5	1.0	1.0
290.2 ± 0.5	1.2	1.0
381.5 ± 0.5[c]	60)	53
389.2 ± 0.5	4.0)	
418.6 ± 0.5	17.8	18
423.5 ± 0.7	4.6	
438.2 ± 0.5	2.7	
511.0	163.2	
540.2 ± 1.0[d]	0.1	
652.8 ± 1.0[d]	0.1	
658.6 ± 1.0	0.4	
714.2 ± 1.0	0.2	
732.0 ± 1.0	0.2	
736.8 ± 0.5	0.5	
753 ± 2.0[d]	0.1)	
762.5 ± 0.5	≡ 100)	≡ 100
778.4 ± 0.5	5.5)	
805 ± 2.0[e]	0.1	
818.6 ± 0.5	2.4	
848.7 ± 1.0	0.4	
853.8 ± 1.0	0.4	
889.2 ± 0.5	0.4	
907.5 ± 0.5	0.5	
916.7 ± 1.0	0.1	
944.2 ± 1.0	0.1	
994.2 ± 0.5	1.5	
1020.1 ± 1.0[d]	0.1	
1036.6 ± 1.0	0.2	
1043.7 ± 1.0	0.5	
1053.7 ± 0.7	0.6	
1098.0 ± 0.5	0.6	
1147.3 ± 0.5	3.8)	7.8
1160.0 ± 0.5	4.5)	
1202.0 ± 0.5	0.4	
1214.8 ± 0.5	0.4	
1237.6 ± 1.0	0.5	
1242.6 ± 1.0	0.3	
1296.0 ± 1.0	0.4	
1324.6 ± 1.0	0.5	
1374.0 ± 1.0	0.2	
1384.0 ± 1.0[e]	0.5	
1528.8 ± 1.0	0.2	
1562.5 ± 1.0	5.5	4.5
1596 ± 2.0[e]	0.1	
1653.1 ± 1.0	0.3	
1666.0 ± 1.0	0.1	
1710 ± 2.0[e]	0.3	
1722 ± 2.0[e]	0.2	
1749 ± 2.0[e]	0.1	
1757 ± 2.0[e]	0.1	
1778 ± 2.0[e]	0.08	
1796 ± 2.0[e]	0.14	
1874 ± 2.0[e]	0.1	
1911.6 ± 1.0	0.1	
1947 ± 1.0[e]	0.1)	2.7
1952.2 ± 0.5	2.6)	
2014.7 ± 0.7	0.1	
2047.9 ± 0.7	0.3	
2090.0 ± 0.7	0.3	
2137.0 ± 1.0	0.1	
2147.8 ± 0.7	0.5	

[a] A 10% error in relative intensities is estimated.

[b] $\pi\sqrt{2}$ beta-ray spectrometer measurement.

[c] Doublet. [d] Seen in coincidence only.

[e] Seen in anti-Compton spectrum only.

strong transitions in ^{83}Sr as standards. The energies thus obtained were consistent at various gain settings. The RMS deviations from the average energies for the strong transitions listed in Table 7 ranged from $\pm$ 0.1 to $\pm$ 0.2 keV. The errors quoted in Table 7 include an estimate of $\pm$ 0.3 keV to account for any systematic errors that may have been present.

The relative intensities were obtained using experimentally determined efficiency curves (28). For comparison, the relative intensities of the strong transitions measured with NaI(Tl) detectors are also listed in Table 7. In general, the agreement of the two measurements was quite good.

Several very weak transitions were observed in spectra obtained using the anti-Compton spectrometer. These spectra were obtained from two different source geometries with respect to the Ge(Li) and NaI(Tl) split annulus detectors, and are shown in Figure 11A and 11B. In one case, the source was placed outside the annulus and the gamma rays collimated into the Ge(Li) detector. In the second case, the source was inserted into the well of the annulus and a 5.1 cm by 5.1 NaI(Tl) detector was mounted in the tunnel above the source to increase the total solid angle subtended by the NaI(Tl) detectors. In this second case, more real coincidences due to gamma cascades in the source were subtracted from the spectrum

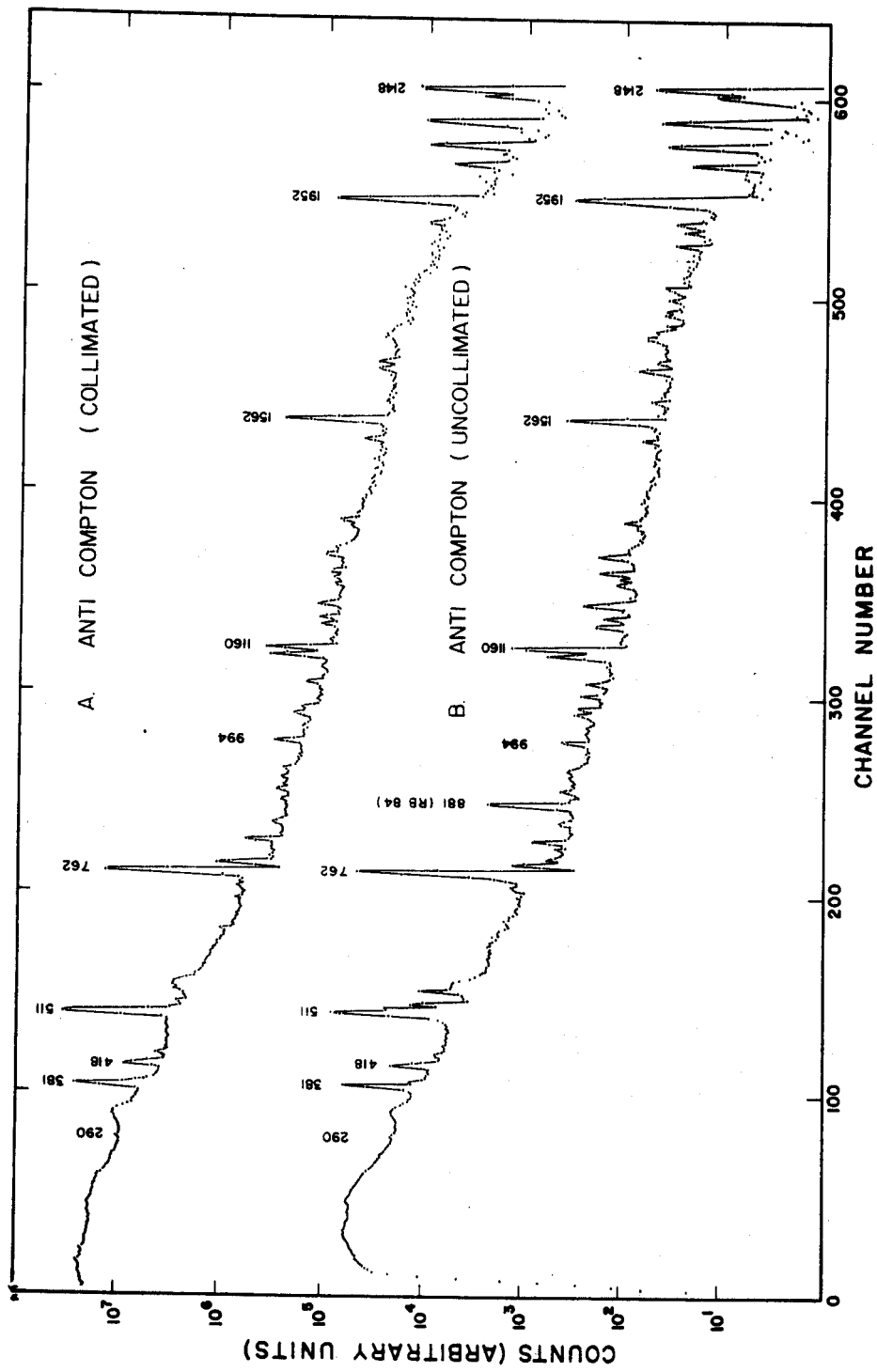

Figure 11.--Anti-Compton gamma spectra of ^{83}Sr obtained with a 7 cm^3 Ge(Li) counter and the NaI(Tl) annulus detector. Spectra A was recorded with the gamma rays collimated into the Ge(Li) detector from an external source. Spectra B was recorded with the source in the tunnel of the annulus. The energies of the weak transitions are listed in Table 8.

than in the first case. Therefore, in addition to improving peak to Compton ratios, those transitions involved in strong coincidence cascades can also be determined easily. The energies and relative intensities of the gamma rays observed in these anti-Compton spectra are listed in Table 8. These intensities are given relative to the intensity of 1952.2 keV transition which, as it will be seen later, is not in coincidence with any gamma ray.

4.2.2. Gamma-Gamma Coincidence Studies

Gamma-gamma coincidence experiments were made for all of the strong transitions and many of the weak ones. Initially, these were made using two 7.6 by 7.6 cm NaI(Tl) gamma detectors. The energy resolutions of these detectors were approximately 9 percent for the 662 keV gamma of ^{137}Cs. Later, the coincidence experiments were repeated using either a 7.6 cm by 7.6 cm NaI(Tl) crystal or the split annulus NaI(Tl) crystal as the gate detector and a 7 cm^3 Ge(Li) detector for display on the 1024 channel analyser. The energy resolution of the 7 cm^3 Ge(Li) detector was 4.5 keV for the 662 keV gamma of ^{137}Cs. The results of both studies were consistent, and only those data taken with the germanium detector will be discussed here.

In order to complement the anti-Compton data, a coincidence spectrum with the NaI(Tl) annulus-Ge(Li)

Table 8.--Energies and relative intensities of gamma-rays in the decay of ^{83}Sr observed in the anti-Compton and "Any Gamma-Gamma" Coincidence Experiments.

Energy (keV)	Relative Intensity: Anti-Compton Collimated[a]	Anti-Compton Uncollimated[b]	"Any Gamma-Gamma"
290.2	1.1		
381.5	48.0	24.2	210
389.2	3.9	1.3	27.5
418.6	13.7	6.8	50.3
423.5	3.7	1.8	12.8
438.0	2.3	0.3	7.5
511.0			256
658.6	0.33		5.8
714.2	0.15		2.2
732.0	0.16		3.0
736.8	0.48	0.2	6.6
762.5	90.0	63.9	≡ 100
778.4	4.5	1.2	31.8
805		0.1	
818.6	1.8	0.67	15.5
848.7	0.34	0.1	5.5
853.8	0.44	0.2	2.6
889.2	0.38		3.5
907.5	0.57	0.29	11.4
916.7	0.24		8.8
944.2	0.55	0.1	6.8
994.2	1.3	0.43	12.5
1036.6	0.14	0.06	2.7
1043.7	0.86	0.37	6.8
1053.7	0.5	0.33	5.7
1098.0	0.63	0.22	4.0
1147.3	3.3	1.2	34.3
1160.0	3.9	3.9	3.2
1202.0	0.56	0.42	
1214.8	0.7	0.2	6.8
1237.6	0.46	0.45	
1242.6	0.26	0.29	
1296.0	0.3	0.4	3.5
1324.6	0.73	0.37	7.5
1374.0	0.20	0.04	
1384.0	0.57	0.14	5.4
1528.8	0.30	0.05	3.0
1562.5	5.0	1.7	39.3
1596		0.07	
1653.1	0.21	0.22	
1666.0	0.16	0.05	2.3
1710		0.26	
1722		0.18	
1749		0.10	
1757		0.10	
1778		0.08	
1796		0.14	
1874	0.05	0.08	
1911.6	0.14	0.14	
1947		0.1	
1952.2	≡ 2.6[c]	≡ 2.6[c]	
2014.7	0.11	0.14	
2047.9	0.34	0.31	
2090.0	0.41	0.37	
2137.0	0.11	0.09	
2147.8	0.57	0.55	

[a]Source outside annulus tunnel.

[b]Source inside annulus tunnel, immediately adjacent to the Ge(Li).

[c]Adjusted to equal relative intensity of the 1952.2 photon in singles.

system was recorded using an integral gate. This is called the "any gamma-gamma coincidence experiment." For this measurement, the source was sandwiched between 0.35 cm of copper to produce total annihilation and then placed 2 cm above the Ge(Li) detector. A 2.2 cm thick cylindrical iron shield was placed around the Ge(Li) detector to reduce crystal to crystal scattering. The coincidence spectrum recorded from this configuration is shown in Figure 12. The energies and relative intensities of the gamma rays observed in this coincidence spectrum are also listed in Table 8. Almost all of the gamma rays were noticeably enhanced relative to the 762.5 keV gamma ray, indicating that this gamma-ray is not in so strong coincidence as the others.

Additional coincidence spectra were recorded in separate experiments with the gates set on the peaks with energies of 94.2, 381.5, 418.6, 762.5, 1147.3, 1160.0, and 1562.5 keV. For comparison, coincidence spectra were also recorded for coincidence gates set on the Compton regions below and above these peaks. Also, the 600-735 keV and 800-1100 keV regions of the spectra were divided into six segments of 50 to 100 keV width and coincidence gates set on each segment.

Three different NaI(Tl) detectors were used to provide the coincidence gates. A 3.8 cm by 2.5 cm NaI(Tl) detector with a 0.013 cm beryllium window was used for

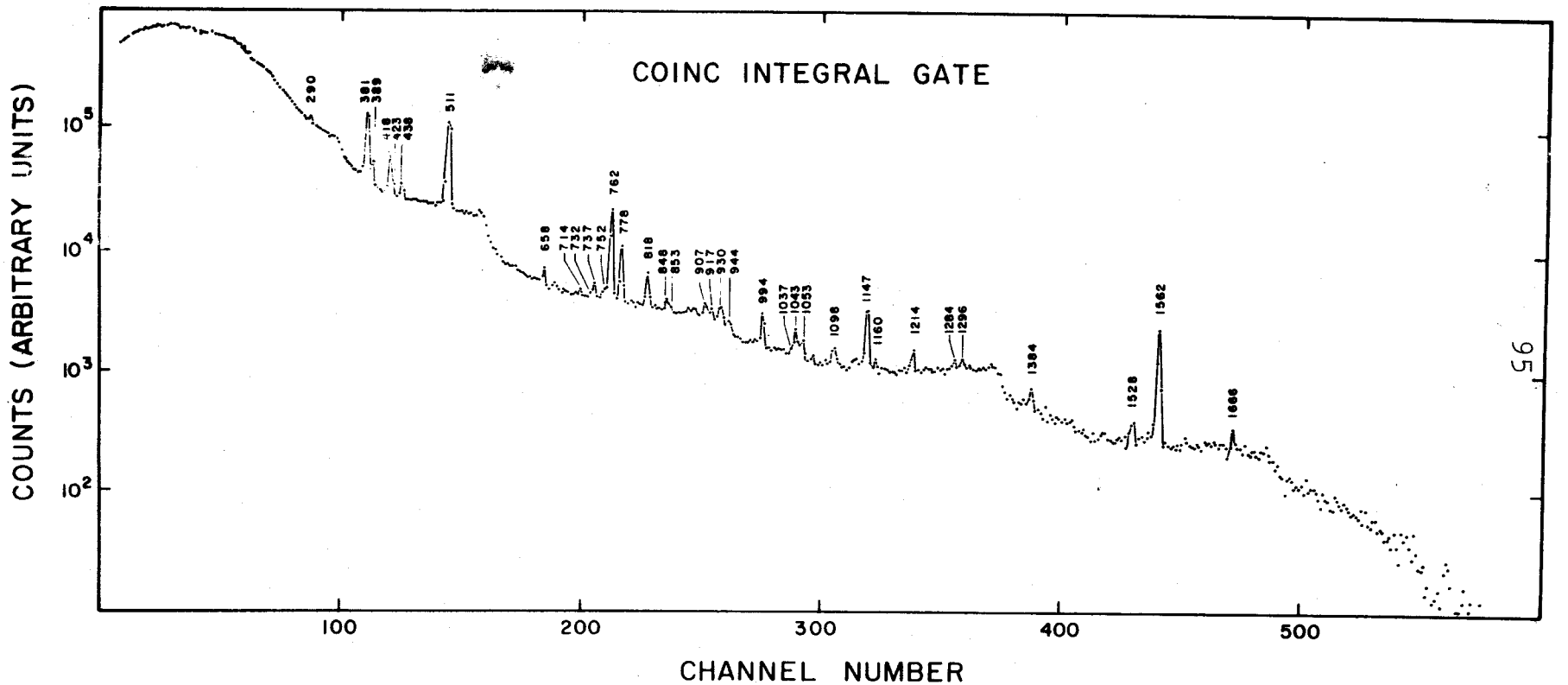

Figure 12.--"Any gamma-gamma coincidence" spectrum of ^{83}Sr taken with the 7 cm^3 Ge(Li) and NaI(Tl) annulus detectors.

the coincidence gates set on the 94.2 keV peak and the Compton region directly above it. A 7.6 cm by 7.6 cm NaI(Tl) detector was used for the coincidence gates set on the 381.5, 762.5, and 1562.5 keV photopeaks. The split annulus NaI(Tl) detector was used for all of the other coincidence gates. The results of all these measurements are shown in Figures 13-20, inclusive. Many of the spectra have been gain shifted by the computer for ease of comparison and presentation. These spectra have not been corrected for chance coincidence; however, the gross true to chance ratio was monitored and in every experiment it was 25 to 1 or greater.

In order to identify the states populated by positron decay, a triple-coincidence experiment was performed using the NaI(Tl) split-annulus and the 7 cm^3 Ge(Li) detectors. The source was placed into the well of the split annulus and above the Ge(Li) detector. The pulses from each half of the split annulus were used to provide a coincidence gate on the 511 keV photo-peak. The coincidence spectrum recorded from this configuration is shown in Figure 21B. In order to distinguish those gamma rays depopulating the states fed by the positron decay from the double escape peaks of the high energy gamma rays, the experiment was repeated with the source placed external to the split annulus detector and the gamma rays collimated into the Ge(Li) detector. This spectrum

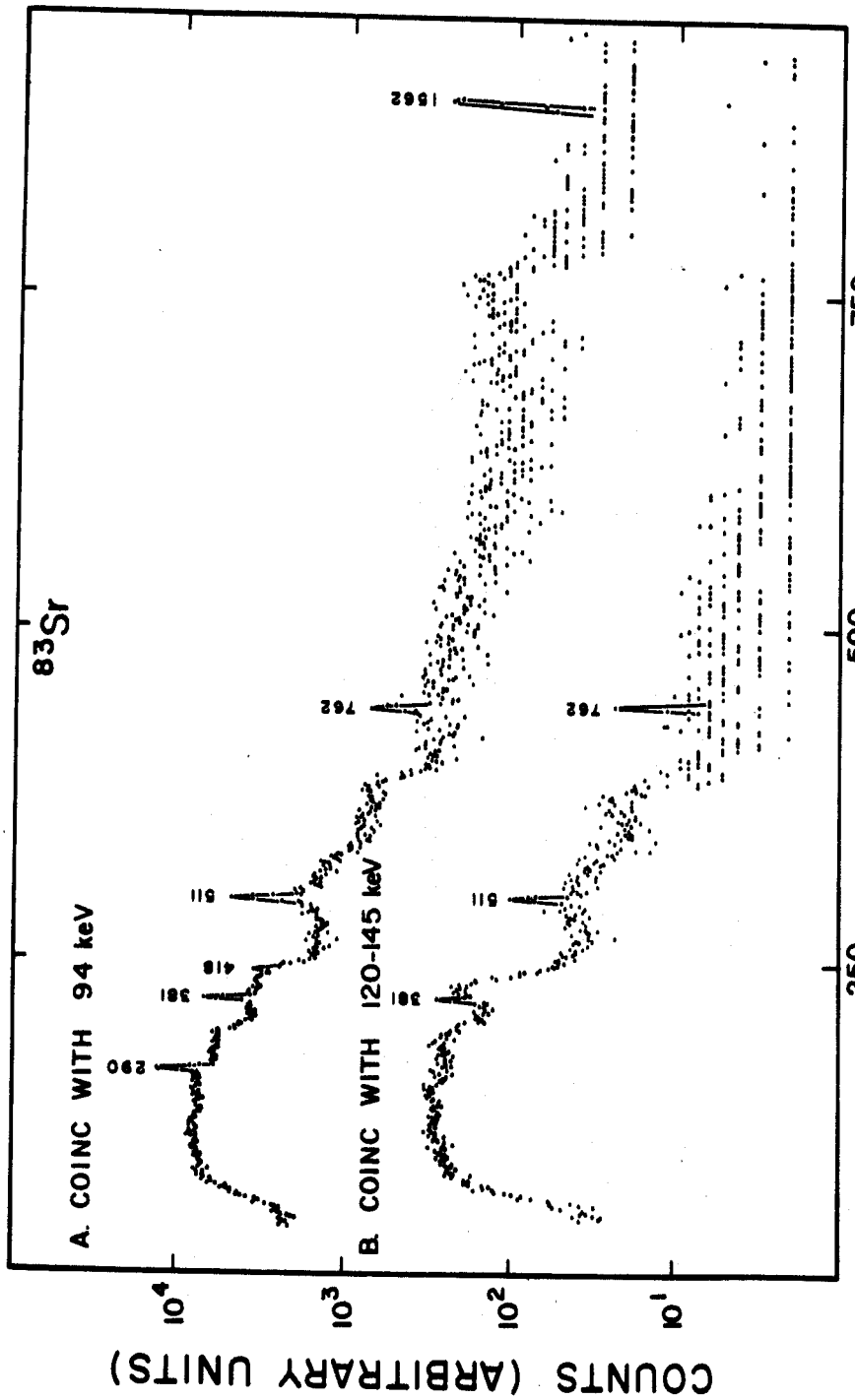

Figure 13.--Gamma spectrum in coincidence with the 94.2 keV gamma taken with the 7 cm3 Ge(Li) counter. The coincidence gate detector was a 3.8 cm by 2.5 cm NaI(Tl) crystal with a 0.013 cm beryllium window. For comparison, spectrum B was recorded with the NaI(Tl) detector gated on the region above the 94.2 gamma ray.

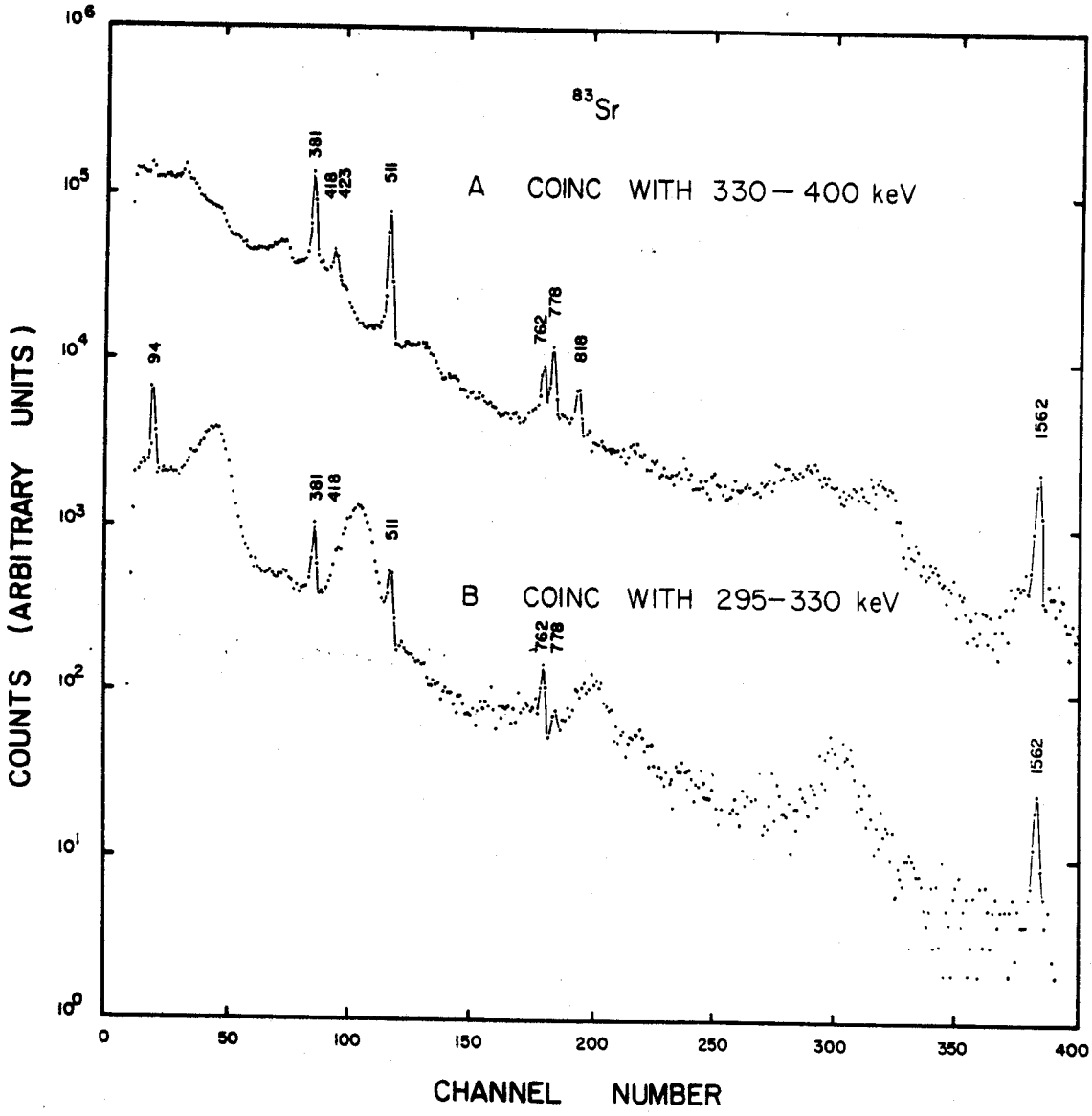

Figure 14.--Gamma spectrum in coincidence with segments of 295-400 keV region taken with the 7 cm^3 Ge(Li) counter and a 7.6 cm by 7.6 cm NaI(Tl) detector. Spectrum A was recorded with the NaI(Tl) detector gated on 295-330 keV. Spectrum B was recorded with the NaI(Tl) detector gated on the low energy side of the 381, 418, 423 keV peaks.

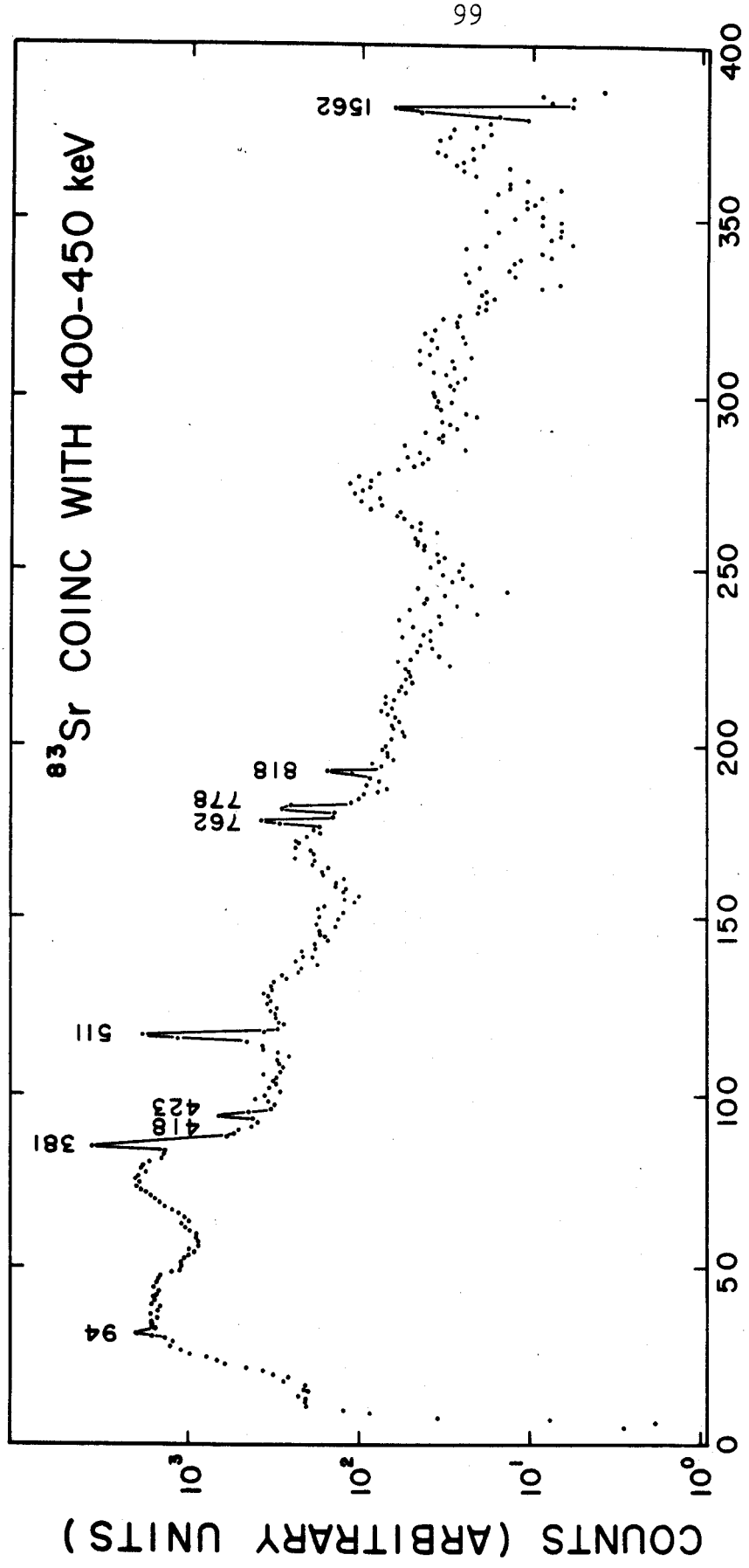

Figure 15.--Gamma spectrum in coincidence with the 400-450 keV region taken with the 7 cm^3 Ge(Li) counter and the NaI(Tl) split annulus detector.

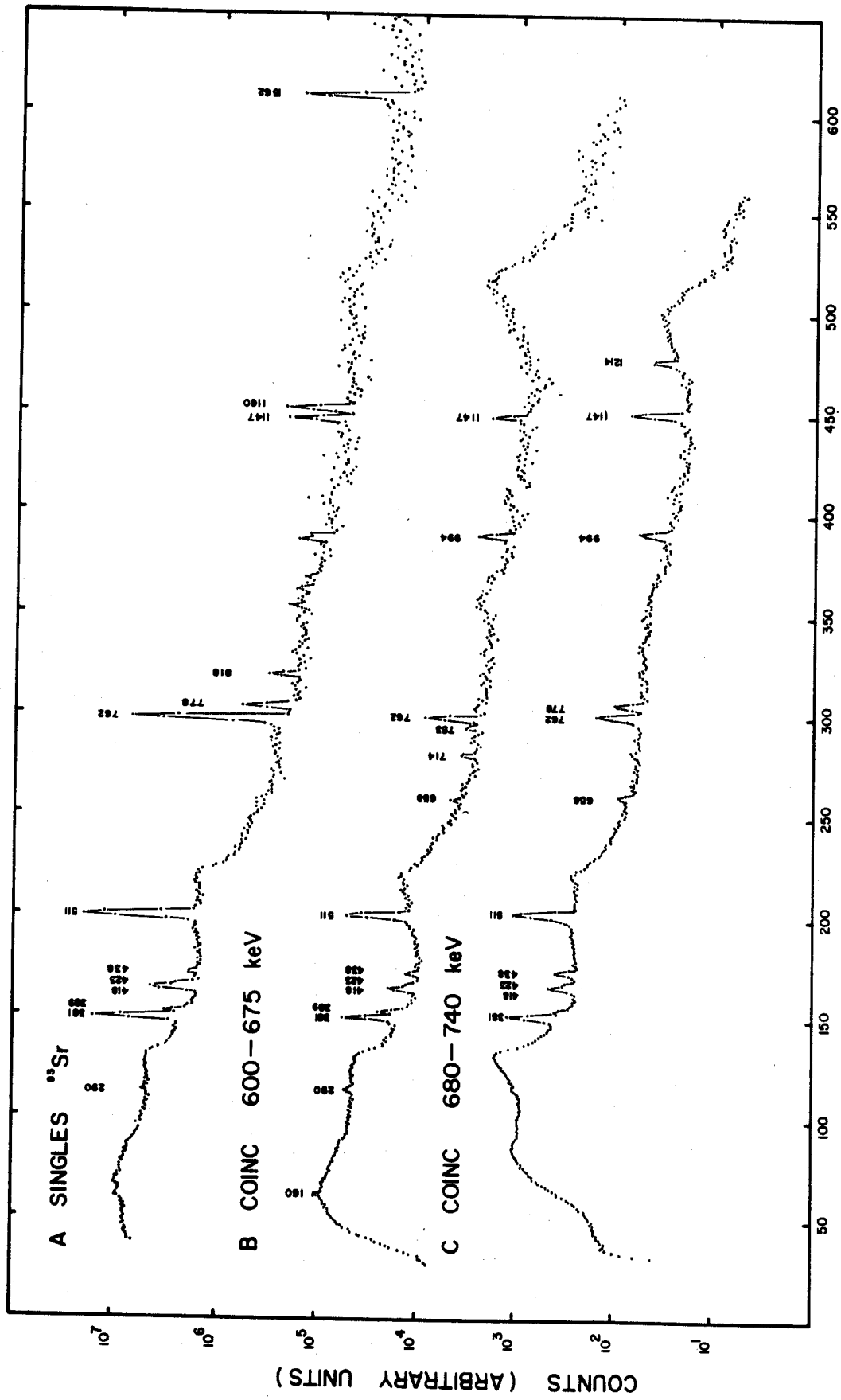

Figure 16.--Gamma spectra in coincidence with segments of the 600-740 keV reion taken with the same detectors as for Figure 15. A singles spectrum is given for reference. The spectra have been arbitrarily displaced vertically for ease of presentation. The energy scales have been adjusted to be equal with the MSU CDC 3600 computer.

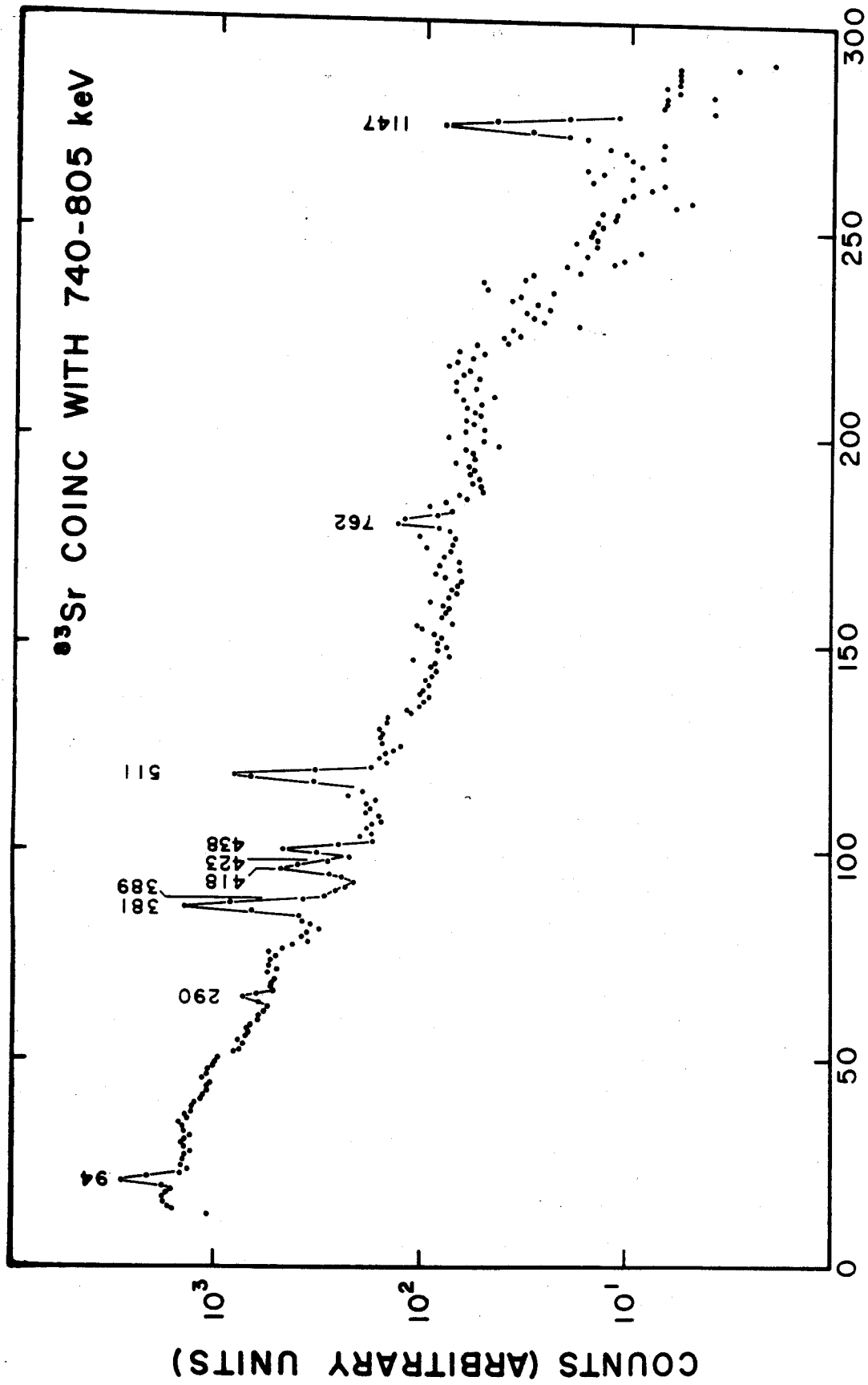

Figure 17.--Gamma spectrum in coincidence with the 762 keV photopeak taken with the same detectors as in Figure 14.

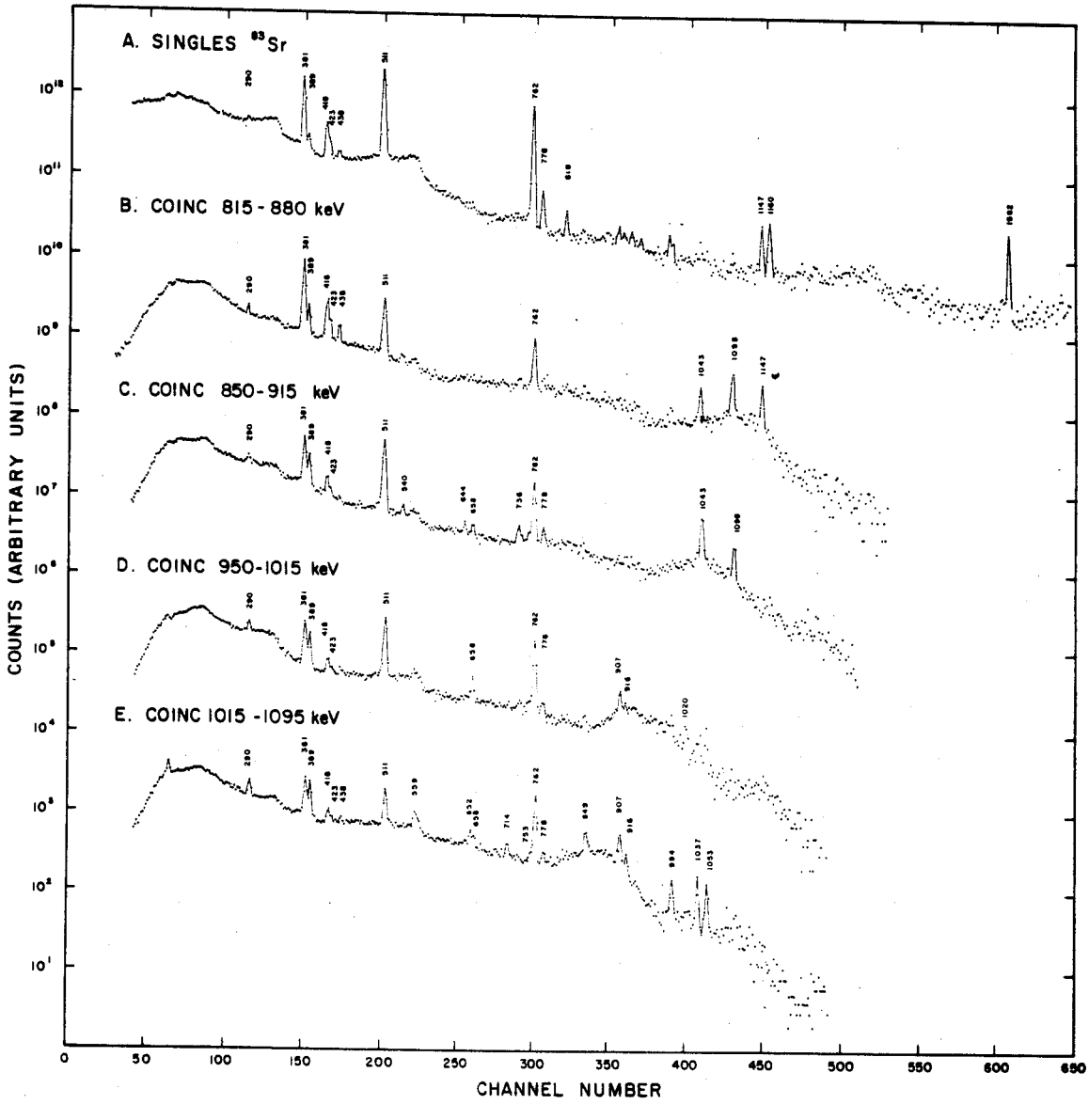

Figure 18.--Gamma spectrum in coincidence with various segments of the 800-1100 keV region. Spectrum A is a singles spectrum for reference. The detectors were the same as for Figure 15. The scales have been adjusted the same as in Figure 16.

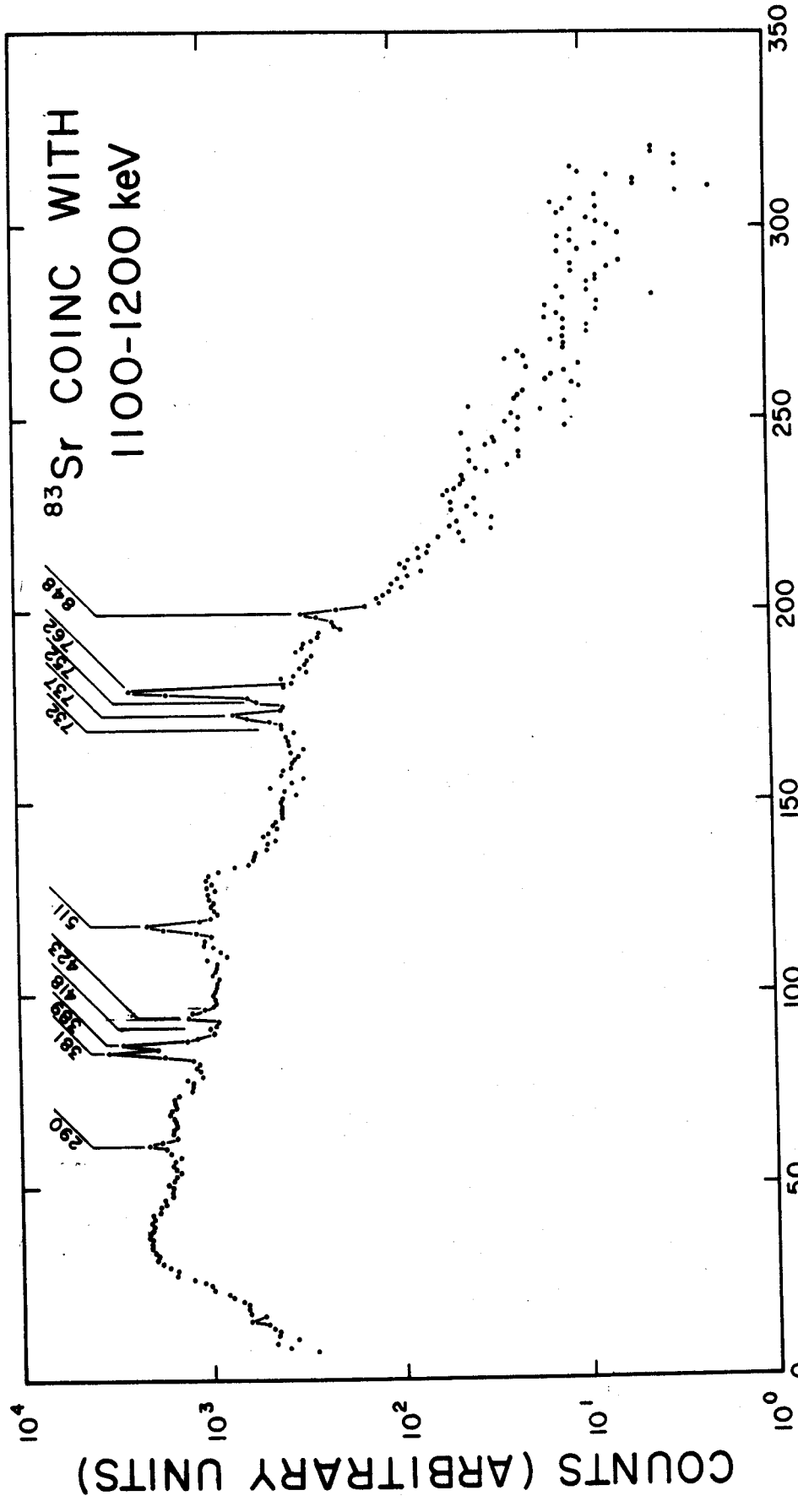

Figure 19.--Gamma spectrum in coincidence with the 1147-1160 keV doublet. The detectors were the same as in Figure 14.

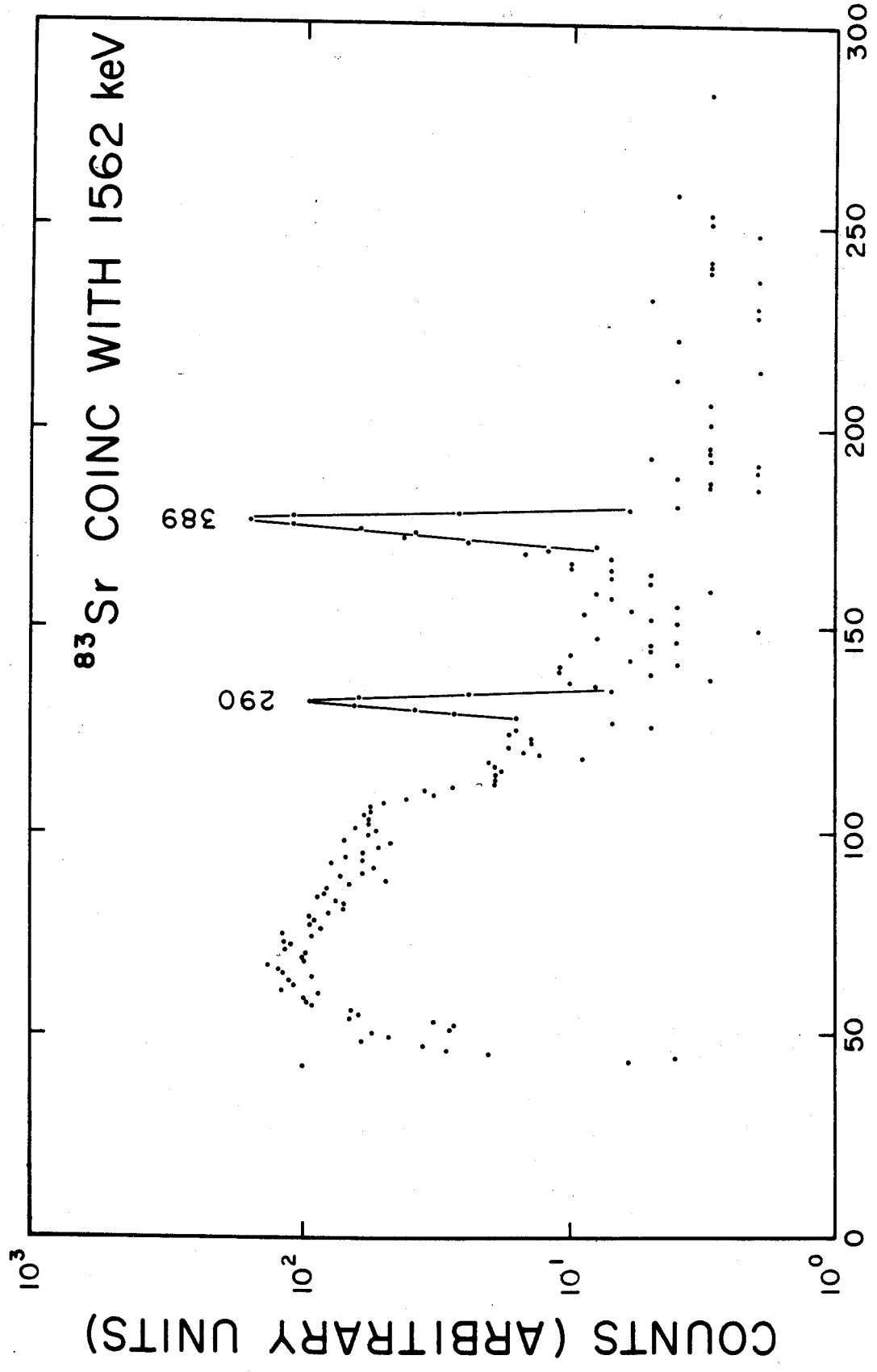

Figure 20.--Gamma spectrum in coincidence with the 1562.5 keV peak. The detectors were the same as in Figure 14.

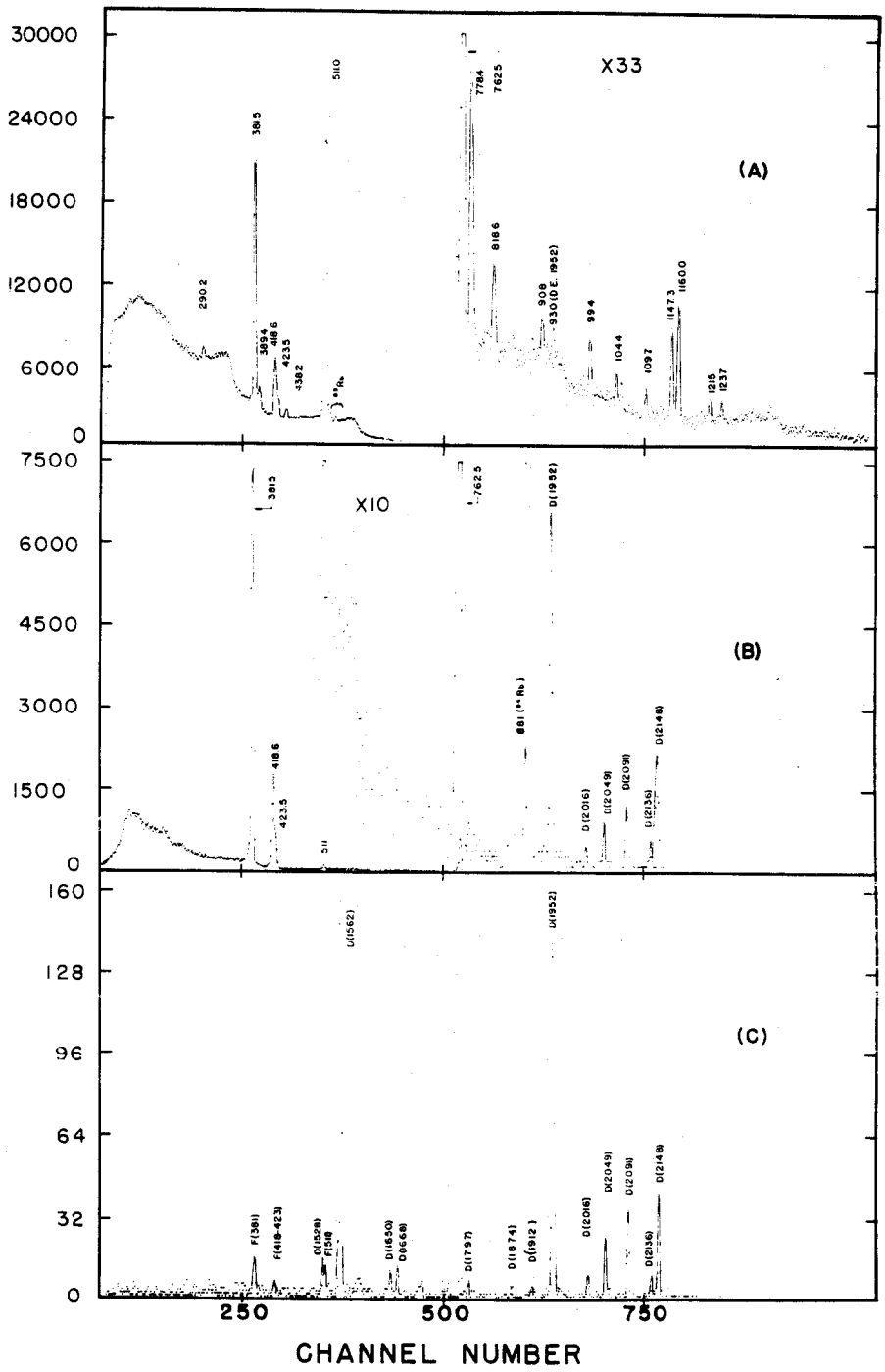

Figure 21.--Positron feeding spectra of ^{83}Sr taken with the 7 cm^3 Ge(Li) counter and the NaI(Tl) split annulus detector. Spectrum A is a singles spectrum for reference. Spectrum B is the positron feeding and double escape spectrum. Spectrum C is the double-escape spectrum obtained with the gamma ray collimated into the Ge(Li) detector from an external source.

which contains only the double escape peaks, is shown in Figure 21C.

Note that the double escape peak of the 1562.5 keV gamma was greatly reduced in the spectrum obtained with the source in the annulus (Figure 21B). This is caused by the 511 keV annihilation quanta from the 1562.5 keV gamma ray summing with the coincident 94.2, 290.2, and 389.2 keV gamma rays. These gammas were very efficiently detected in the split annulus and the summing produced pulses corresponding to energies appreciably greater than 511 keV, and therefore the gate requirement was no longer satisfied. The intensity of gamma rays in cascade that are in coincidence with the positrons will be reduced similarly in the coincidence spectrum.

In almost every case, the coincidence gates necessarily included two or more gamma rays because of their close energy spacings and, in addition, many underlying Compton photons. This makes the interpretation of most of the coincidence data difficult. However, a consistent interpretation can be obtained by quantitative comparison of the different coincidence spectra. A summary of the coincidences seen in these experiments is presented in Table 9. It is possible to establish by the comparison of spectra recorded in the adjacent coincidence gates that some of the peaks appearing in the coincidence spectra are the result of coincidences with Compton photons in the gate interval. These are listed in Table 9 under

Table 9.--Coincidence summary.

Gate Interval in keV	Gammas in Gate in keV	Coincidence with Gammas in keV	Compton or Sum Coincidences	Figure No.
87 - 112	94.2	290.2, 1562.5	381.5, 418.6, 423.5, 511.0, 762.5,	13A
120 - 145	None		381.5, 418.6, 423.5, 511.0, 762.5,	13B
295 - 330	290.2	94.2, 1562.5	381.5, 418.6, 511.0, 762.5, 778.4,	14A
340 - 400	381.5, 389.2, 418.6 423.5	381.5, 418.6, 423.5, 511.0 778.4, 818.6, 1562.5	94.2, 762.5	14B
400 - 450	381.5, 389.2, 418.6 423.5, 438.2	381.5, 418.6, 423.5, 511.0, 762.5 778.4, 818.6, 1562.5	94.2	15
600 - 675	644.5, 652.8, 658.6 674.0	381.5, 418.6, 423.5, 658.6, 714.2 753.2, 762.5, 994.2	290.2, 389.2, 511.0, 1147.3	16B
680 - 740	674.0, 714.2, 732.0 736.8, 753. 762.5	381.5, 418.6, 423.5, 438.2 511.0, 658.6, 714.2, 762.5 778.4, 994.2, 1043.7, 1147.3 1214.8		16C
740 - 805	732.0, 736.8, 753 762.5, 778.4, 818.6	381.5, 418.6, 423.5, 438.2, 511.0 762.5, 778.4, 1147.3		17
815 - 880	818.6, 848.7, 853.8, 889.2	381.5, 418.6, 423.5, 438.2, 762.5 1043.7, 1098.0, 1147.3	290.2, 389.2, 511.0	18B
850 - 915	848.7, 853.8, 889.2 907.5, 916.7	381.5, 418.6, 423.5, 540.2, 644.5, 658.6, 732.0, 736.8, 762.5, 778.4, 1043.7, 1098.0	290.2, 389.2, 511.0	18C
950 - 1015	944.2, 994.2, 1020,	381.5, 418.6, 423.5, 658.6, 762.5, 778.4, 907.5, 994.2, 1020.1, 1052.7	290.2, 389.2, 511.0,	18D
1015 - 1095	1020, 1037.8, 1043.7 1053.7, 1098.0	381.5, 418.6, 423.5, 559, 652, 658 714.2, 753.2, 762.5, 778.4, 848.7 907.5, 916.7, 994.2, 1037.8, 1053.7	290.2, 389.2, 511.0	18E
1100 - 1200	1098.0, 1147.3, 1160.0 1202.0, 1214.8	381.5, 418.6, 423.5, 732.0, 736.8, 753.2, 762.5, 848.7	290.2, 389.2, 511.0	19
1525 - 1600	1528.8, 1562.5	94.2, 290.2, 389.2		20

the heading Compton or Sum Coincidences. The appearance of the 511 keV peak in all of the coincidence spectra of the coincidence gates between 800-1200 keV can be accounted for by sum coincidences. These arise from one of the 511 keV annihilation quanta summing with any of the coincident 381.5, 418.6, 423.5 or 762.5 keV gamma rays or their Compton photons in the NaI(Tl) annulus detector.

Comparison of the coincidence spectra obtained from gates at 680-740 keV, 740-805 keV, 815-880 keV and 1100-1200 keV (Figures 16C, 17, 18B, and 19) reveals that the 762.5 keV transition is in coincidence with the 1147.3 keV gamma ray. Further, the peak at 438.2 keV is concluded to be in coincidence with the 762.5 keV gamma since the 762.5 keV peak is observed to grow as the coincidence gate is moved from 330-400 keV to 400-500 keV (Figures 14B and 15).

The ratio of intensity of the 381.5 keV gamma ray to the combined intensities of the 418.6 and 423.5 keV gammas recorded in the coincidence spectra obtained with the coincidence gates at 340-400, 400-450, 740-805, and 1100-1200 keV (Figures 14B, 15, 17, and 19) were very informative and were crucial in the construction of the decay scheme. These ratios were 4.2, 5.2, 2.3, and 4.0, respectively, in comparison to 2.7 in the singles spectrum. Furthermore, the 418.6 and 423.5 keV gamma rays always

appeared in the coincidence spectra together and in the same intensity ratio as in singles. These ratios can be explained only with the conclusion that the 381.5 keV peak actually consists of two gamma rays very close in energy with one of them in coincidence with the other as well as with the 418.6 and 423.5 keV gamma rays. The relative intensities of the two 381.5 keV gamma rays have been calculated from the coincidence data to be 23.5 for the one in coincidence with the 418.6 and 423.5 keV gamma rays and 36.5 for the other. No noticeable broadening of the 381.5 keV peak was observed. An upper limit of 0.2 keV is placed for the energy difference of the doublet.

The 42.3 keV transition was not observed to be in prompt coincidence with any of the gamma rays, X-rays or positrons.

4.2.3. The Internal Conversion Coefficient for the 42.3 keV Transition

An attempt was made to measure the K internal conversion coefficient for the 42.3 keV transition. For this purpose, a continuous flow argon-methane proportional counter was used. The source, which was evaporated onto an aluminized Mylar film 3mg/cm^2 thick, was mounted internal to the proportional counter. The recorded electron spectrum obtained is shown in Figure 22.

The K internal conversion coefficient was calculated from electron coincidences with the X-ray in the following manner. The number of K conversion electrons, $N_{K\varepsilon}$, in coincidence with the X-ray is given by

$$N_{K\varepsilon} = \frac{N\alpha_K \omega_K \Omega_X \varepsilon_X \Omega_\varepsilon \varepsilon_\varepsilon (1 - e^{-\lambda \Delta T_c})}{1 + \alpha_T}$$

where ω_K is the K X-ray fluorescent yield, $\Omega_X \varepsilon_X$ is the solid angle and detector efficiency for the X-ray, $\Omega_\varepsilon \varepsilon_\varepsilon$ is the solid angle and detector efficiency for the electron, and ΔT_c is the coincidence counting time. The number of 42 keV gamma rays for an equivalent counting time is given by

$$N_{42} = \frac{N \Omega_{42} \varepsilon_{42} P_{es}^{-\lambda t_s} (1 - e^{-\lambda \Delta t_s})}{1 + \alpha_T}$$

where $\Omega_{42} \varepsilon_{42}$ is the solid angle and detector efficiency for the 42 keV gamma ray, P_{es} is the X-ray escape ratio, t_s is the time of which the gamma ray singles spectrum was taken after the start of the coincidence measurement, and Δt_s is the singles counting time. Solving these two equations for α_K gives

$$\alpha_K = \frac{N_{K\varepsilon}}{N_{42}} \frac{\Omega_{42} \varepsilon_{42} P_{es}}{\omega_K \Omega_X \varepsilon_X \Omega_\varepsilon \varepsilon_\varepsilon} \frac{e^{-\lambda t_s} (1 - e^{-\lambda \Delta t_s})}{(1 - e^{-\lambda \Delta t_c})}$$

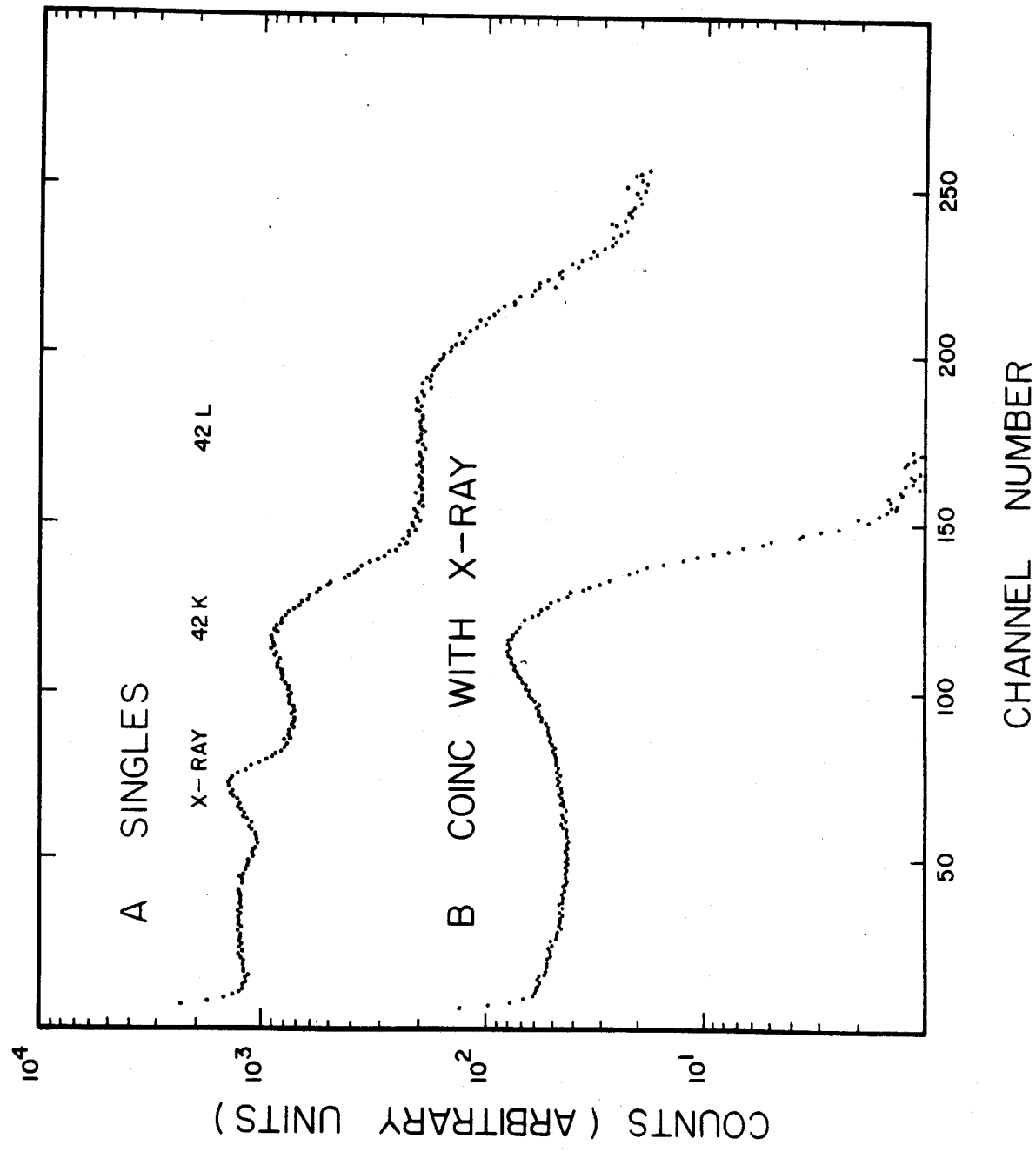

Figure 22.--Electron spectra obtained with an argon-methane continuous flow proportional counter. Spectrum A is the singles spectrum. Spectrum B is the electron spectra in coincidence with the x-ray.

For these experiments a 6 mm NaI(Tl) detector with a 0.012 cm beryllium window was used to detect the X-ray and 42 keV gamma ray. The values of ω_K and P_{es} were taken from nuclear spectroscopy tables (21). The ratio of

$$\frac{\varepsilon_X \Omega_X}{\varepsilon_{42} \Omega_{42}}$$

was measured to be 0.85 in an absorption experiment using ^{85}Sr and ^{137}Cs x-γ ray sources. The detector efficiency solid angle product for the electrons is very difficult to determine because of the geometry of the source mount on the proportional counter. The source did not present a full 2π steradians solid angle to the proportional counter. This resulted from the relationship of the source diameter to the diameter and wall thickness of the orfice of the source mounting on the proportional counter. The source diameter was 0.5 inch compared to 0.75 inch for the orifice. In addition, the wall thickness was not uniform but varied from 0.04 to 0.16 inches. This made the calculation of the effective solid angle difficult. However, limits upon the solid angle were determined from these dimensions. The solid angle subtended by the disk source must be between the limits of the solid angle subtended by two point sources, one located at the center of the orifice and the other located outside the counter. These estimates then give $0.25 \leq \varepsilon_\varepsilon \Omega_\varepsilon \leq 0.5$ assuming 100%

detection efficiency for the conversion electrons by the proportional counter. The internal conversion coefficient, α_K, was calculated to be $19 \leq \alpha_K \leq 38$.

L. M. Beyer has since measured (62) the α_K conversion coefficient to be 29.3 ± 3.5 using the MSU "Orange" electron spectrometer. He has also shown from energy differences of the K and L internal conversion electrons of the 42.3 keV transition that this transition is in ^{83}Rb and not in ^{83}Sr.

In addition to the 42.3 keV transition, Beyer has measured (62) the internal conversion coefficients for the 94.2, 290.2, 381.5, 418.6, 423.5, 438.2, 762.5, 778.4, and 818.6 keV transitions. His data are summarized in Table 10 since the multipolarities of the transitions will be useful to determine the characters of the excited states.

4.2.4. Half-life Measurements of the 42.3 keV Transition

Since the 42.3 keV gamma ray was not found to be in prompt coincidence with any of the radiations, a delayed coincidence experiment was performed to measure its half-life. A block diagram of the delayed coincidence spectrometer is shown in Figure 23. The delay circuit used here was the delayed-trigger circuit of a Tektronix 545 oscilloscope which provided a variable time delay from 2 to 500 microseconds. The delay circuit was adjusted to provide a 20 microsecond delay. The linear gate circuit

Table 10.--Summary of internal conversion coefficients[a] and multipole order[a] of some of the transitions in ^{83}Rb.

E_γ	α_K	K/L + M	Multipole Order
42.3	29.3 ± 3.5		M2
94.2	2.2 ± 0.2 (-1)[b]		M1 ≤ 10% E2
290.2	1.4 ± 0.2 (-2)	10 ± 2	35% M1, 65% E2
381.5	7.1 ± 0.3 (-3)	7.4	E3, ≤ 10% M1
389.2	6.5 ± 0.5 (-3)	8 ± 2	E2, ≤ 20% M1
418.6	1.4 ± 0.2 (-3)		E1
423.5	1.6 ± 0.4 (-3)		E1
438.2	2.7 ± 0.4 (-3)		M1
762.5	9.5 ± 0.5 (-4)		E2
778.4	9.6 ± 2 (-4)		M1, E2
818.6	1.1 ± 0.4 (-3)		M1, E2

[a]Reference 62.

[b]The number in the parenthesis is the appropriate power of 10, i.e., 2.2 ± 0.2 (-1) means (2.2 ± 0.2) x 10^{-1}.

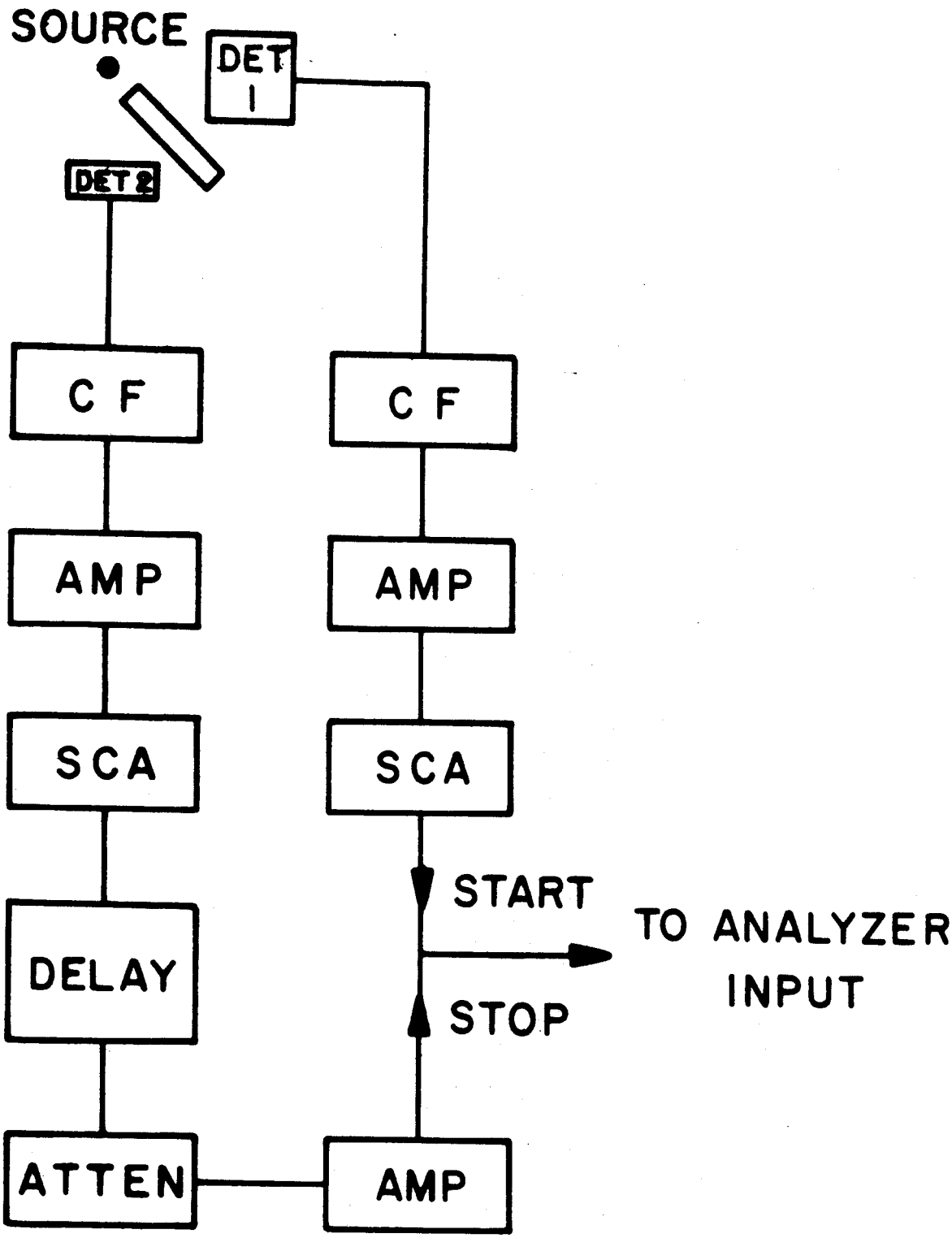

Figure 23.--Block diagram of the delayed coincidence spectrometer.

in the analog to digital converter of a 256 channel vacuum tube RIDL model 52 analyser was purposely disabled by clipping the pins of the vacuum tube that controlled the circuit so that the gate would not close. When a gamma ray is detected in the first detector, a pulse from the single channel analyser (SCA) starts the address scaler in the 256 channel analyser which counts at 2 M Hertz. When a gamma ray is detected in the second detector the pulse from the SCA is delayed by approximately 20 μsecs and then amplified. After amplification it is also sent into the input of the 256 channel analyser. This second pulse has sufficient amplitude to cause the upper level discriminator in the converter to act as the gate to stop the conversion process and, hence, stop the address scaler where it is at the instant of the second pulse. A count is then stored in the appropriate channel. The resulting spectrum gives the time decay curve of the transition. The spectrometer was tested by measuring the half-life of the 514 keV state in ^{85}Sr. The half-life of this state was measured to be (0.9 ± 0.2) μsecs, in excellent agreement with that measured by Sunyar et al., (63).

The source strength must be very weak in order to keep the chance coincidence rate low. This weak source strength required long counting times in order to achieve reasonable statistics. In addition, the spectrometer is fixed by the frequency of the oscillator in the converter

(0.5 μ sec/channel in this case). This limits the useful range here to approximately 0.75 to 50 μ secs.

To measure the life-time of the 42.3 keV state, the single channel analyzers were set to the 42.3 keV photopeak and the X-ray, the 511, 381.5, and 762.5 keV photopeaks in separate experiments. The results were inconclusive, either $T_{1/2} < 0.5$ μsec, or $T_{1/2} > 50$ μsecs. The latter is consistent with the M2 character of the 42.3 keV transition for which the life-time would be approximately 1 m sec, well beyond the range of this spectrometer.

4.3. The Proposed Decay Scheme for ^{83}Sr

A decay scheme consistent with all the data has been constructed from the results of the coincidence studies, energy sums and relative intensities of the transitions and is shown in Figure 24. The log ft values listed on the decay scheme were determined from the relative intensities into and out of each state and from the X-ray and positron intensities. The positron branching ratios were determined from the Fermi plots (62) of the positron spectrum and from the triple-coincidence experiments between the gamma rays and two 511 keV annihilation quanta.

A summary of the energies of the states in comparison with the energy sums of the transitions in cascade depopulating them are listed in Table 11. Those transitions that were crossovers to the ground state were not included in

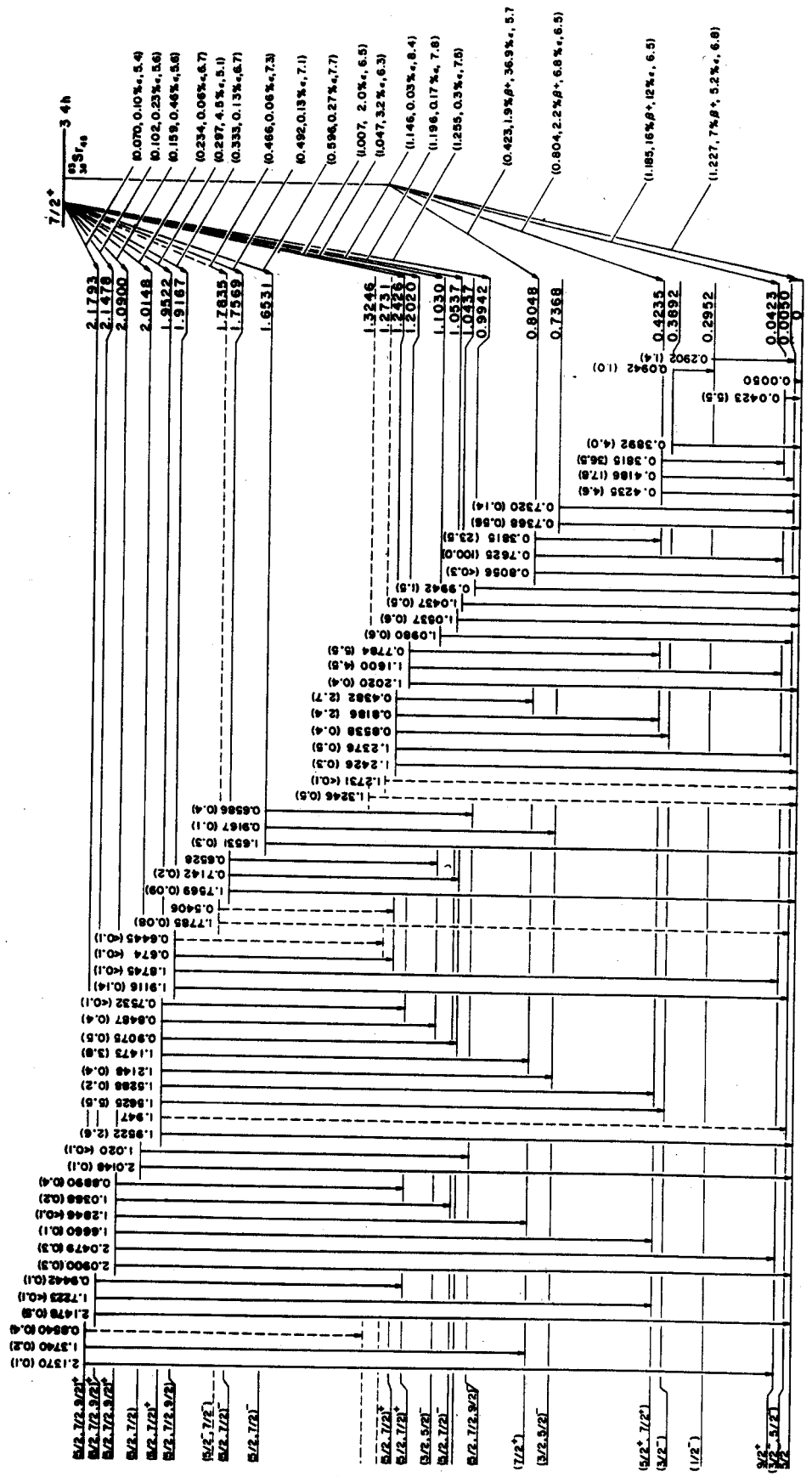

Figure 24.--Proposed decay scheme of ^{83}Sr.

Table 11.--Summary of gamma cascade energy sums.

State in KeV	Cascade Sum in keV	Deviation in keV	Coin Spectrum Figure No.
5.0			
42.3			
295.2[a]	295.2 = 5.0 + 290.2		
389.2	389.4 = 5.0 + 94.2 + 290.2	+0.2	13A, 14A
423.5	423.6 = 5.0 + 418.6	+0.1	
	423.8 = 42.3 + 381.5	+0.3	
736.8	737.0 = 5.0 + 732.0	+0.2	
804.8[b]	804.8 = 42.3 + 762.5		
	805.0 = 381.5 + 423.5	+0.2	14B, 15
	805.3 = 42.3 + 381.5 + 381.5	+0.5	14B
994.2			
1043.7			
1053.7			
1103.0[a]	1103.0 = 5.0 + 1098.0		
1202.0	1202.3 = 42.3 + 1160.0	+0.3	
	1201.9 = 423.5 + 778.4	-0.1	14B, 15, 17
1242.6	1242.6 = 5.0 + 1237.6		
	1243.0 = 389.2 + 853.8	+0.4	18B
	1242.1 = 423.5 + 818.6	-0.5	14B, 15, 17
	1243.0 = 42.3 + 438.2 + 762.5	+0.4	15, 17
1273.1			
1324.6			
1653.1	1653.5 = 736.8 + 916.7	+0.4	18C
	1652.8 = 658.6 + 994.2	-0.3	16B, 18D
1756.9	1757.9 = 714.2 + 1043.7	+1.0	16C, 18E
	1755.8 = 652.8 + 1098.0 + 5.0	-1.1	18E
1783.5[a]	1783.5 = 5.0 + 1778.5		
	1783.2 = 540.6 + 1242.6	-0.3	
	1783.4 = 389.2 + 540.6 + 853.8	-0.1	18C
1916.7[a]	1916.6 = 5.0 + 1911.6	-0.1	
	1916.8 = 42.3 + 1874.5	+0.1	
	1916.6 = 674.0 + 1242.6	-0.1	
	1917.6 = 644.5 + 1273.1	-1.1	
1952.2	1952 = 5.0 + 1947		
	1951.9 = 5.0 + 94.2 + 290.2 + 1562.5	-0.3	13A, 14A, 20
	1951.7 = 389.2 + 1562.5	-0.5	14B, 20
	1952.3 = 423.5 + 1528.8	+0.1	12
	1951.6 = 736.8 + 1214.8	-0.6	16C, 19
	1952.1 = 42.3 + 762.5 + 1147.3	-0.1	17, 19
	1951.2 = 907.5 + 1043.7	-1.0	18C, 18E
	1951.7 = 5.0 + 1098.0 + 848.7	-0.5	18C, 18E
	1955 = 753 + 1202.0	-3	19
2014.8	2014.2 = 1020.0 + 994.2	-0.6	18D
2090.0	2090.2 = 42.3 + 2047.9	+0.2	
	2089.5 = 423.5 + 1666.0	-0.5	12
	2089.5 = 42.3 + 762.5 + 1284.6	-0.6	
	2090.3 = 1036.7 + 1053.7	+0.3	18E
	2091.0 = 889.0 + 1202.0	+1.0	
2147.8	2145.8 = 423.5 + 1722.3	-2.0	
	2146.2 = 944.2 + 1202.0	-1.6	
2179.3[a]	2179.3 = 42.3 + 2137.0		
	2178.8 = 42.3 + 762.5 + 1374.0	-0.5	
	2178.6 = 854.0 + 1324.6	-0.6	

[a]No gamma ray was seen at this energy.

[b]The energy of this state was taken to be the sum of the 42.3 and 762.5 keV gammas.

the table because the energies and the state energies are the same, except for the 804.8 keV state. In Table 11 the column labeled "Coinc Spectrum Fig. No." refers to the coincidence spectra that support the placement of the transition.

4.3.1. Evidence for the 42.3 keV state

The placement of a state at 42.3 keV was dictated by the relative intensity of the 42.3 keV transition and its long life-time. The total internal conversion coefficient, α_T, has been measured to be 33 which gives a total of 188 units for this transition (relative to 100 for the 762.5 keV gamma ray) making the 42.3 keV transition the strongest in the decay scheme.

4.3.2. Evidence for the 423.5, keV, 804.8 keV and the 5.0 keV states

A state was placed at 423.5 keV as a result of the relationships of the 381.5 and 423.5 keV gamma rays in the coincidence spectrum. It is supported by several observed coincidence cascades that are listed in Table 9.

It was not possible to account for the relative intensity of the 42.3 keV transition without having the 762.5 keV gamma ray feeding the 42.3 keV state. Furthermore, a very low intensity gamma ray of about 805 keV was observed in the anti-Compton spectrum described in section 4.2.1. Therefore, a state was placed at 804.8

keV, which is the energy sum of the 42.3 and 762.5 keV transitions.

The 381.5 keV peak was shown in section 4.2.2. to consist of two gamma rays very close in energy in coincidence with each other. The second 381.5 keV gamma ray is therefore placed as depopulating the 804.5 keV state to the 423.5 keV state.

At this point, it was not possible to complete the construction of the decay scheme, consistent with the coincidence data, without postulating a state at 5.0 keV. The previously mentioned intensity ratios of the 418.6 and 423.5 keV doublet imply that these transitions originate from the same state. In addition, there were several other doublets 5 keV apart, namely 732.0-736.8, 1237.6-1242.6, and 1947-1952.2 keV pairs. The 732.0-736 keV doublet also always occured together and in the same intensity ratio in both the single and the coincidence spectra.

An effort was made to look for a gamma ray at 5 keV with a proportional counter and with a thin window, high resolution Si(Li) detector*; but, because of the highly converted nature of low energy transitions, the results were inconclusive.

A search was made in both the gamma ray and in the internal conversion spectra by Beyer (62) for a transition

*We are grateful to Dr. George Beard, Wayne State University, for the use of his detector.

of 37 keV which would fit between the 42.3 and 5.0 keV states. The data limited the intensity for such a 37 keV transition to an upper limit of 1%, relative to the intensity of the 42.3 keV gamma ray.

The triple coincidence spectra (Figure 21) support the placement of these states. Only the 381.5, 418.6, 423.5, and 762.5 keV transitions are seen to be in prompt coincidence with the positrons. The positron branching ratios calculated from early triple coincidence data obtained from NaI(Tl) detectors were, in units relative to the 762.5 keV gamma ray, 4.0 $\pm$ 0.8 for the 804.7 keV state, and 7.2 $\pm$ 1.5 for the 423.5 keV state and agree within the experimental error with those obtained by Beyer from Fermi plots (62) which were 5.2 $\pm$ 1.0 for the 804.7 keV state and 7.9 $\pm$ 1.5 for the 423.5. These values are consistent with those calculated using the proposed decay scheme, relative intensities, and theoretical K/β^+ and $\varepsilon_K/\varepsilon_L$ ratios (21, 64).

4.3.3. Evidence for States at 295.2 and 389.2 keV

The coincidence spectra show that the 1562.5 keV gamma ray is in coincidence with the 94.2, 290.2, and 389.2 keV transitions and that the 94.2 keV gamma ray is in coincidence with the 290.2 keV gamma. The 389.2 keV gamma ray was not observed to be in coincidence with either the 94.2 or 290.2 keV gamma rays. The energy

difference of 4.8 keV between the 389.2 ± 0.5 keV, and the sum of the 94.2 ± 0.5 and the 290.2 ± 0.5 keV gamma rays is too large to be accounted for by experimental error of the energy measurements of these three gamma rays; therefore, the 389.2 keV gamma ray cannot be a crossover transition for just the 94.2 and 290.2 keV gamma rays alone. These coincidence data can easily be explained with the inclusion of the unobserved 5.0 keV transition in cascade with the 94.2 and 290.2 keV gammas. Hence, states were placed at 295.2 and 389.2 keV.

The evidence for the placement of the state at 295.2 instead of 99.2 keV is weak. It consists of the fact that the 290.2 keV gamma ray is slightly more intense than the 94.2 keV gamma. According to the energy sum, the very weak 1796 keV transition fits very nicely between the states at 2090.0 and 295.2 keV. However, the 1796 keV gamma ray was seen only once and then in an anti-coincidence spectrum that was taken over a long period of time. Therefore, this transition was not placed in the decay scheme.

4.3.4. Evidence for States at 1202.0, 1242.6 and 1952.2 keV

The anti-Compton and the "any gamma-gamma" coincidence spectra indicate that the 1160.0, 1202.0, 1237.6, 1242.6, 1947 and 1952.2 keV transitions are not in prompt coincidence with any of the other gammas. Therefore, they probably populate the 42.3 keV, 5.0 keV, or the ground state.

Numerous coincidence relationships and energy sums support the placements of states at 1202.0, 1242.6, and 1952.2 keV. These are listed in Table 11.

4.3.5. The Remaining States

The remaining states account for a very small fraction of the decays of ^{83}Sr and were placed on the basis of the coincidence data and, in a few cases, upon the existence of an energy sum alone. These are summarized in Table 11. Those transitions not observed in coincidence and not satisfying an energy sum were left out of the decay scheme. These were the 1296.0, 1384.3, 1596.0, 1710, 1749, and 1796 keV gamma rays.

4.3.6. Spin and Parity Assignments

Hobson et al., (65) and Hubbs et al., (66) have measured the ground state spin and parity of ^{83}Rb to be $5/2^-$ by atomic beam methods. Beyer has determined (62) the spins and parities of the 5.0, 99.4, 389.2, 423.5, 804.8, 1202.0 and 1242.3 keV states on the basis of his internal conversion coefficients measurements. His results are listed in Table 12. These assignments, and the log ft values for the decay of ^{83}Sr to the excited states in ^{83}Rb,imply that the ground state spin of ^{83}Sr is 7/2+.

The spins (and parities) of the higher excited states are shown on the decay scheme and are assigned on the basis of the log ft values and gamma-ray branching to the lower excited states.

Table 12.--Spin and parity assignments.

State Energy, keV	Spin and Parity[a]
0	$5/2^{-}$[b]
5.0	$3/2^{-}$, $5/2^{-}$[c]
42.3	$9/2^{+}$
295.2	$1/2^{-}$
389.2	$3/2^{-}$
423.5	$5/2^{+}$
804.8	$7/2^{+}$

[a]Reference 62. [b]Reference 65 and 66.

[c]$3/2^{-}$ is preferred.

4.4. Discussion of the Decay Scheme of ^{83}Sr

Talmi and Unna predict ^{83}Sr to have a ground state spin of $9/2^{+}$. Excited states of spin and parity $1/2^{-}$ and $7/2^{+}$ are predicted at 170 keV and 320 keV, respectively (7). Their proposed level structure is similar to those proposed for other odd mass strontium isotopes (1), namely ^{85}Sr and ^{87}Sr. The $7/2^{+}$ ground state assignment from the present data disagrees with their predictions. However, the predicted $7/2^{+}$ state does lie relatively low in energy. The observation has been made that the Talmi-Unna calculations are the only ones in this mass region in which the energy of the $7/2^{+}$ state is depressed so low (67).

It is interesting to note that the other odd mass nuclei with 45 neutrons, i.e., ^{77}Ge, ^{79}Se, and ^{81}Kr, all have $7/2^{+}$ ground state spins (1). Thus, the $7/2^{+}$ spin

and parity assignment for ^{83}Sr are consistent with the systematics in this region. This $7/2^+$ spin and parity could be achieved from the shell model configuration of $(g_{9/2})^{-3}_{7/2}$.

The level diagram for odd mass rubidium isotopes is shown in Figure 25. It is apparent that the level diagram for ^{83}Rb is consistent with those of the other odd mass rubidium isotopes. The ground state ($5/2^-$), the 5.0 ($3/2^-$), and the 42.3 ($9/2^+$) keV states in ^{83}Rb can be explained qualitatively by shell model proton configurations of $(f_{5/2})^{-1}$, $(p_{3/2})^{-1}$, and $(g_{9/2})^1$ respectively. As can be seen from Figure 25, the $(p_{3/2})^{-1}$ and $(f_{5/2})^{-1}$ configuration are in competition for the ground state of the rubidium isotopes. Hence, it is not unusual for ^{83}Rb to have a low lying $3/2^-$ state, though the data do not rule out the possibility that the spin of the 5.0 keV state is $5/2^-$.

The higher excited states cannot be explained so easily as they probably arise from more complicated shell model configurations as well as collective excitations. Beyer has suggested that the 423.5 and 804.6 keV states may be vibrational states built upon the $9/2^+$ level or as arising from the coupling of the 2^+ core excitation with the $9/2^+$ particle state (62). However, both of these interpretations have difficulties associated with them.

In the first case, the crossover to cascade ratio is too strong by about a factor of 7 when compared to the

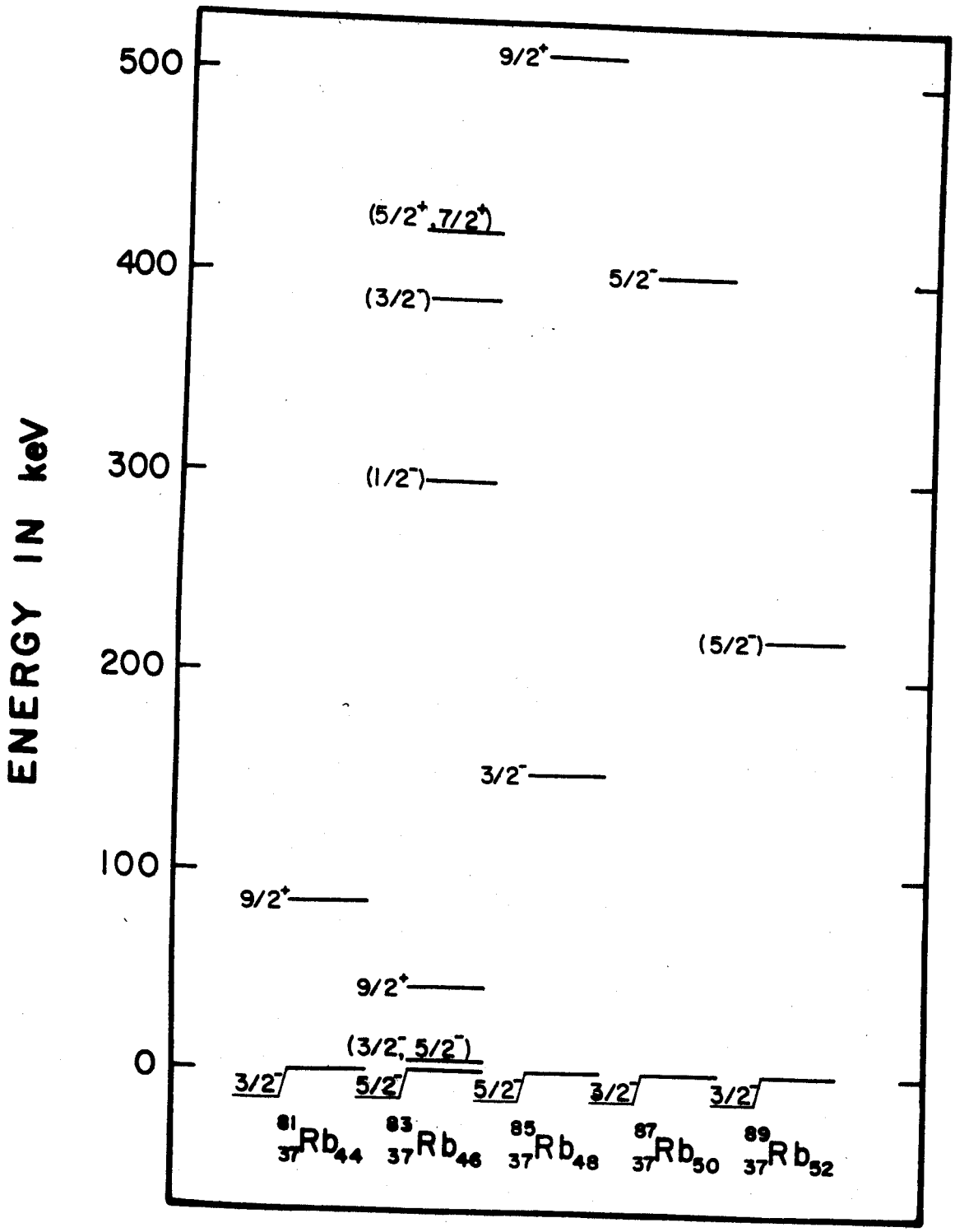

Figure 25.--Comparison of the energy levels of the odd-mass strontium isotopes.

neighboring ^{82}Kr even-even nucleus. In the second interpretation, the 381.5 keV transition would be expected (19) to be M1, whereas Beyer has shown (62) that the transition is probably E2.

CHAPTER V

SUMMARY AND CONCLUSIONS

The high resolution spectroscopic study of the decay of ^{82}Br has identified the location of several weakly populated states as well as confirmed some of the previous results for the strongly excited states. The gamma-gamma angular correlation measurements have enabled the unique assignments of the spins to the strongly excited states and the multipolarities of the transitions from them. Transitions from the new weakly populated states and log ft values were used to place limits upon the spins and parities for these states.

The level structure of ^{82}Kr was used to test the asymmetric rotor model of Davydov and coworkers (4, 6). The distortion parameters computed from the relative reduced transition probabilities obtained in this work and from the lifetime measurements by Beard (46) were in fair agreement with those calculated from energetics (17) for the strongly excited states. However, the D-F model is unable to account for the new weakly excited states. Even so, because of the fair agreement for the strong transitions of this nucleus, and for other nuclei in this mass region which were discussed in the Introduction, it may be possible

to use the D-F model as an indicator for nuclei approaching permanent deformation. At least in these cases, it corroborates the calculations of Marshalek et al. (5).

A consistent decay scheme for ^{83}Sr was constructed from coincidence data (recorded with high resolution Ge(Li) detectors), energy sums and relative intensities. The level structure of ^{83}Rb was found to be very complex with many closely spaced excited states. An isomeric M2 transition was discovered at 42.3 keV. The level structure is incomplete in that it is not possible to make unique spin assignments to most of the known states. This makes comparisons of this decay scheme with any theoretical model difficult.

Since ^{82}Kr and ^{83}Rb differ by the addition of a single proton to an even-even core, it was originally anticipated that the states in the two nuclei might be simply related via the core-coupling model. However, no simple relationship was found to exist between the level schemes. For example, it was not possible reliably to determine the center of gravity of the positive parity core-particle multiplets which would be built upon the $9/2^+$, 42.3 keV state. This determination and others were hampered by the uncertainties in the spin assignments, particularly for the high energy states. Likewise, the determination of the core-particle multiplets which would be built upon the $5/2^-$ ground state is complicated because

of the very close $3/2^-$, 5.0 keV state. Since both of these nuclei are several protons and neutrons from closed shells, the coupling between core excitation and particle states might be considerably stronger than that normally considered as valid for the simple core-coupling model.

The ground state of ^{83}Sr has been inferred to be $7/2^+$ from the data presented in this thesis. This assignment is consistent with other odd-mass nuclei with 45 neutrons. Although this assignment did not agree completely with the predictions of Talmi and Unna (7), their calculations appear to explain in part some of the properties of odd-mass nuclei in this region of the periodic table. Their calculations are the only ones for which the energy of the $7/2^+$ state is brought down so low.

BIBLIOGRAPHY

1. Nuclear Data Sheets. Washington, D. C.: The National Academy of Sciences--National Research Council.

2. M. A. Preston. Physics of the Nucleus. Reading Massachusetts: Addison-Wesley Publishing Co., Inc. 1962.

3. O. Nathan and S. G. Nilsson. Collective Nuclear Motion and the Unified Model, in α-β-γ Ray Spectroscopy, edited by Kai Siegbahn. Amsterdam: North-Holland Publishing Co., 1965. Chapter 10.

4. A. S. Davydov and G. F. Filippov. JETP 33(1957), 555.

   A. S. Davydov and G. F. Filippov. JETP (Sov. Phys.) 8 (1959), 303.

   A. S. Davydov and G. F. Filippov. Nucl. Phys. 8 (1958), 237, and References cited therein.

5. E. Marshalek, L. W. Pearson, and R. K. Sheline. Rev. Mod. Phys. 35 (1963), 108.

6. A. S. Davydov and A. A. Chaban. Nucl. Phys. 20 (1960), 449, and References cited therein.

7. I. Talmi and I. Unna. Nucl. Phys. 19 (1960), 225.

8. A. Bohr and B. R. Mattleson. Matt. Fys. Medd. Dan. Vid. Selsk. 27 no. 16 (1953).

9. M. Goeppert Mayer. Phys. Rev. 75 (1949), 1966.

10. O. Haxel, J. H. D. Jensen, and H. E. Suess. Phys. Rev. 75 (1949), 1766.

11. M. G. Mayer and J. H. D. Jensen. Elementary Theory of Nuclear Shell Structure. New York: John Wiley & Sons, Inc., 1955.

12. D. Kurath. Phys. Rev. 101 (1956), 216.

13. R. F. Sweet, K. H. Bhatt, and J. B. Ball. Phys. Lett. 8 (1964), 131.

14. J. P. Elliott and B. H. Flowers. Proc. Ray. Soc. (London) A 229 (1955), 536.

15. D. J. Horen and W. H. Kelly. Phys. Rev. 145 (1966), 988.

16. A. Bohr. Matt. Fys. Medd. Dan. Vid. Selsk. 26 no. 14 (1952).

17. E. D. Klema, C. A. Mallmann, and P. Day. Nucl. Phys. 25 (1961), 266.

18. R. D. Lawson and J. L. Uretsky. Phys. Rev. 108 (1957), 1300.

19. A. DeShalit. Phys. Rev. 122 (1961), 1530.

20. S. G. Nilsson, K. Danske Vidensk. Selsk. Mat. Fys. Medd. 29 no. 16 (1955).

21. A. H. Wapstra, G. J. Nijgh, and R. VanLieshout. Nuclear Spectroscopy Tables. Amsterdam: North-Holland Publishing Co., 1959.

22. Nuclear Data 1 no. 1B. New York: Academic Press, 1966. Edited by K. Way.

23. H. Fraunfelder and R. M. Steffan. Angular Distribution of Nuclear Radiation, in α-β-γ Ray Spectroscopy, edited by Kai Siegbahn. Amsterdam: North-Holland Publishing Co., 1965. Chapter 19.

24. L. W. Fagg and S. S. Hanna. Rev. Mod. Phys. 31 (1959), 711.

25. H. W. Taylor and R. McPherson. Privately circulated tables (September, 1960).

26. M. E. Rose. Internal Conversion Coefficients. New York: Interscience Publishers, Inc., 1958.

27. G. T. Ewan and A. J. Tavendale. AECL no. 2079 (1964). References cited therein.

28. R. L. Auble and G. Berzins. (M.S.U.) private communication (1965).

29. R. L. Auble and W. H. Kelly. Nucl. Phys. 73 (1965), 625.

30. C. W. Reich, J. A. Merrill, and E. D. Klema. Nucl. Instr. 23 (1963), 36.

31. R. L. Auble, D. B. Beery, G. Berzins, L. M. Beyer, R. C. Etherton, W. H. Kelly, and W. C. McHarris. Nucl. Inst. and Meth. 51 (1967), 61.

32. J. M. Cork, J. M. LeBlanc, W. H. Nester and M. K. Brice. Phys. Rev. 90 (1953), 444.

33. D. C. Lu, W. H. Kelly, and M. L. Wiedenbeck. Phys. Rev. 95 (1954), 1533.

34. R. C. Waddell and E. N. Jensen. Phys. Rev. 102 (1956), 816.

35. N. Benczer-Koller. CU-177 (1958).

36. V. S. Dubey, C. E. Mandewille, and M. A. Rothman. Phys. Rev. 103 (1956), 1430.

37. B. S. Dzhelepov, V. A. Eliseev, V. P. Prikhadtseva, and Yu V. Kholnov. Izv. Akad. Nauk SSSR (ser. fiz.) 23 (1959), 207.

38. S. Hultberg and A. Hedgran. Ark. Fys. 11 (1957), 369.

39. N. P. Heydenburg, G. F. Pieper, and C.E. Anderson. Phys. Rev. 108 (1957), 106.

40. L. Simons, S. Bergström, and A. Anttila. Nucl. Phys. 54 (1964), 683.

41. T. J. Kennett, I. B. Webster, and W. V. Prestwich. Nucl. Phys. 58 (1964), 56.

42. R. Heath, S. H. Vegors, and L. L. Marsden. IDO-16880-1 (August, 1964).

43. M. Saki, H. Ikegami and T. Yamazaki. J. Phys. Soc. Japan 17 (1962), 1087.

44. M. J. L. Yates. in α-β-and γ-ray Spectroscopy. ed. by K. Siegbahn, loc. cit., App. 9.

45. R. G. Arns and M. L. Wiedenbeck. Phys. Rev. 111 (1958), 1631.

46. G. B. Beard. Phys. Rev. 145 (1966), 862.

47. S. Ofer. Phys. Rev. 114 (1959), 870.

48. W. Flanger and H. Schneider. Nuclear Physics 55 (1964), 207.

49. R. C. Etherton and W. H. Kelly. Nucl. Phys. 84 (1966), 129.

50. J. Reidy and M. L. Wiendenbeck. Bull. Am. Phys. Soc. 10 (1965), 1131.

51. S. Raman. Nucl. Phys. A90 (1967), 508.

52. W. W. Black, and R. L. Heath. Nucl. Phys. A90 (1967), 650.

R. L. Robinson, et al. Nucl. Phys. 74 (1964), 281.

53. H. Griftner, W. Reiser, and H. Schneider. Z. Naturf. 20a (1965), 1727.

54. F. H. H. Hsu and C. S. Wu. Nucl. Phys. A94 (1967), 205.

55. H. L. Garvin, T. M. Green, and E. Lipworth. Bull. Am. Phys. Soc. 2 (1957), 344H2.

56. D. L. Hendric and G. W. Farwell. Phys. Lett. 9 (1964), 321.

57. R. B. Day, A. G. Blair, and D. D. Armstrong. Phys. Lett, 9 (1964), 327.

58. K. Alder and R. M. Steffen. Am. Rev. Nucl. Sci. 14 (1964), 403.

59. T. Kurayanagi. J. Phys. Soc. Japan 16 (1961), 2363.

60. V. Maxia, W. H. Kelly, and D. J. Horen. J. Inorg. Nucl. Chem. 24 (1962), 1175.

61. K. R. Reddy, A. S. Johnston, and S. Jha. Bull. Am. Phys. Soc. 9 no. 1 (1964), 17.

62. L. M. Beyer. Ph.D. Thesis, Michigan State University (1967), unpublished.

63. A. W. Sunyar, et al. Phys. Rev. 86 (1952), 1023.

64. M. L. Perlman and M. Wolfsberg. BNL 485 (T-110) (1958).

65. J. P. Hobson, et al. Phys. Rev. 104 (1956), 101.

66. J. C. Hubbs, et al. Phys. Rev. 107 (1957), 723.

67. L. S. Kisslinger and R. A. Sorenson. Rev. Mod. Phys. 35 (1963), 853.